

Viscoelastic Characterization of Out-of-Autoclave Composite Laminates:  
Experimental and Finite Element Studies

Mehrnoosh Abedi

A Thesis  
in  
The Department  
of  
Mechanical and Industrial Engineering

Presented in Partial Fulfillment of the Requirements  
for the Degree of Master of Applied Science (Mechanical Engineering)  
at  
Concordia University  
Montreal, Quebec, Canada

April 2016

© Mehrnoosh Abedi, 2016

**CONCORDIA UNIVERSITY**  
**SCHOOL OF GRADUATE STUDIES**

This is to certify that the thesis was prepared

By: Mehrnoosh Abedi

Entitled: Viscoelastic Characterization of Out-of-Autoclave Composite Laminates:  
Experimental and Finite Element Studies

and submitted in partial fulfilment of the requirements for the degree of

**Master of Applied Science (Mechanical Engineering)**

complies with the regulations of the University and meets the accepted standards with respect to originality and quality.

Signed by the final examining committee:

_____	Chair
Dr. A. K. W. Ahmed, MIE	
_____	Examiner
Dr. S. V. Hoa, MIE	
_____	Examiner
Dr. L. Tirca, BCEE	External to the Program
_____	Supervisor
Dr. R. Sedaghati, MIE	
_____	Supervisor
Dr. M. Hojjati, MIE	

Approved by:

\_\_\_\_\_  
Dr. S. Narayanswamy, M.A.Sc. Program Director  
Department of Mechanical and Industrial Engineering

\_\_\_\_\_  
Dr. A. Asif, Dean  
Faculty of Engineering & Computer Science

Date: April 26, 2016

## ABSTRACT

### Viscoelastic Characterization of Out-of-Autoclave Composite Laminates: Experimental and Finite Element Studies

Mehrnoosh Abedi

In the last two decades, the Out-of-Autoclave (OOA) manufacturing process has been mainly established to replace the conventional autoclave curing technology due to the notable techno-economic features. The principal idea of OOA processing is to facilitate fabrication of composites with the same required material performance as autoclave-cure systems, whereas utilizing more economical and light-weight equipment. The present research work aims at application of an unconventional approach to efficiently and effectively identify the viscoelastic material properties (storage and loss moduli) of composite laminates fabricated using OOA manufacturing process. First, the in-plane viscoelastic parameters of a highly directional OOA prepreg system (a high-modulus carbon/epoxy composite material) are identified experimentally using the dynamic mechanical analysis (DMA). DMA testing is performed on unidirectional sample coupons with different thicknesses and using two distinct DMA clamp configurations. To assess the accuracy of the measured properties, a finite element (FE) model based on the first-order shear deformation theory is developed and programmed in the MATLAB environment using DMA test data to evaluate the fundamental damping factors and the first three resonance frequencies of unidirectional laminated beam and plate components. Subsequently, a modal experimental test has been conducted to evaluate the modal characteristics of the fabricated unidirectional beams as well as thin to moderately thick plates clamped at one end (CFFF) in response to an impact excitation. It has been demonstrated that a good agreement exists between modal experimental test results and those obtained from the FE model on the basis of measured material properties using the DMA three-point bending clamp configuration. Using the FE model, the effect of fiber orientation on the fundamental damping factor in a unidirectional beam under CFFF boundary condition has subsequently been investigated and then assessed experimentally for selective fiber orientations. Finally, the developed FE model has been utilized to investigate the effect of lamination sequence, number of layers, structural geometry and boundary conditions of square laminated plates on the natural frequency and loss factor associated with the fundamental mode of flexural free vibration.

The optimal values have also been identified, considering unidirectional, cross-ply, and angle-ply square laminates under combined clamped and free boundary conditions.

*Dedicated to*

***My dear husband, Iman***

*for his everlasting support, patience, and inspiration*

&

***My beloved parents***

*for their unconditional love and encouragement*

&

***My darling brother***

*who is my heart's reverberation, and soul's resonance*

## **Acknowledgment**

First and foremost, I would like to highly appreciate my supervisors, Dr. Ramin Sedaghati and Dr. Mehdi Hojjati for their invaluable guidance from the beginning of the work as well as unwavering support and encouragement throughout the research. I am sincerely grateful to them for giving me the opportunity to get such a precious experience.

It is an honor to extend my gratitude to the committee members who devoted their time for the detailed review of the thesis and provided constructive comments to make this work improved.

My special thanks are cordially extended to my dear friend, Dr. Mehdi Eshaghi, who has always motivated me and devoted his time unconditionally during my studies and experiments. This thesis would not have been possible without his immense support and boundless enthusiasm. I am also privileged to have his pure and faithful friendship.

I would also like to acknowledge Dr. Daniel Rosca for his technical support and practical guidance, which facilitated the research. I wish to express my special thanks to the technical and administrative staff of Mechanical and Industrial Engineering Department, notably Mr. Danius Juras, Ms. Leslie Hosein, Ms. Charlene Wald, Ms. Sophie Mérineau, and Ms. Arlene Zimmerman for their great assistance.

The final recognition goes to my family members, who have truly inspired me and demonstrated care for my success in all aspects of my life. I feel very fortunate to have them in my life and owe them for all sacrifices they have made so far. Their endless love and understanding are always solid supports that keep me moving on throughout the life journey.

Last but not the least, I greatly thank all my dearest friends and officemates, Dr. Farough Mohammadi, Mohammad Razi, Ajinkya Gharapurkar, Amir Mohammad Azimi, and Dina Alizadeh for their constant companionship and establishment of pleasant working atmosphere these years.

# TABLE OF CONTENTS

<b>List of Figures</b> .....	x
<b>List of Tables</b> .....	xiv
<b>Nomenclature</b> .....	xvi
Acronyms.....	xvi
Symbols.....	xvi

## CHAPTER 1

### INTRODUCTION AND SCOPE OF WORK

<b>1.1 Introduction</b> .....	1
<b>1.2 Review of relevant literature</b> .....	2
1.2.1 Characterization of elastic properties.....	2
1.2.1.1 Static testing.....	2
1.2.1.2 Dynamic testing.....	3
1.2.2 Damping mechanism in composite materials.....	5
1.2.2.1 Temperature, frequency, and stress dependency.....	7
1.2.3 Damping analysis and modeling.....	10
1.2.3.1 Macromechanical approach.....	10
1.2.3.1.1 Viscoelastic damping method.....	11
1.2.3.1.2 Modal strain energy method.....	12
1.2.3.2 Micromechanical approach.....	14
1.2.4 Experimental methods- identification of damping properties.....	16
1.2.5 Vibration coupling effect on damping.....	20
<b>1.3 Motivation and objective</b> .....	23
<b>1.4 Organization of thesis</b> .....	25

## CHAPTER 2

### MATERIAL SELECTION AND SAMPLE FABRICATION

<b>2.1 Overview of out-of-autoclave technology</b> .....	27
<b>2.2 Material selection</b> .....	29
2.2.1 CYCOM 5320-1 resin system.....	29
<b>2.3 Fabrication process</b> .....	30
2.3.1 Lamination procedure.....	30
2.3.2 Curing process.....	32
<b>2.4 Quality control</b> .....	34
2.4.1 Void and fiber fraction analysis.....	34
<b>2.5 Summary and conclusions</b> .....	34

## CHAPTER 3

### DYNAMIC MECHANICAL ANALYSIS (DMA)

<b>3.1 Introduction to DMA</b> .....	36
3.1.1 Principles of DMA.....	36
3.1.2 Mathematical representation of storage and loss moduli.....	37
3.1.3 Effects of different parameters on DMA results.....	37
3.1.4 Disagreements between DMA and static results.....	38
<b>3.2 DMA samples</b> .....	40
<b>3.3 Identification of in-plane parameters</b> .....	40
3.3.1 Determination of in-plane storage moduli.....	40
3.3.2 Determination of in-plane loss factors.....	41
<b>3.4 Results and discussion</b> .....	42
3.4.1 DMA experiments.....	42
3.4.2 Identification of in-plane storage parameters.....	42
3.4.2.1 Single-cantilever arrangement.....	42
3.4.2.2 Three-point bending arrangement.....	44
3.4.3 Identification of in-plane damping parameters.....	45
<b>3.5 Summary and conclusions</b> .....	46

## CHAPTER 4

### FINITE ELEMENT FORMULATION AND MODELING

<b>4.1 Introduction</b> .....	48
<b>4.2 FE formulations</b> .....	50
4.2.1 Displacement, strain and stress fields.....	51
4.2.2 FE model of laminated plates.....	55
<b>4.3 Validation of the FE model</b> .....	59
4.3.1 Verification of natural frequencies.....	59
4.3.2 Verification of modal damping parameters.....	62
<b>4.4 Summary and conclusions</b> .....	66

## CHAPTER 5

### EXPERIMENTAL MODAL ANALYSIS AND VALIDATION

<b>5.1 Introduction</b> .....	67
<b>5.2 Experimental setup and samples</b> .....	67
<b>5.3 Modal experiments</b> .....	70
5.3.1 Validation of elastic properties.....	70
5.3.2 Validation of loss factors.....	75
<b>5.4 Parametric study on the fiber angle</b> .....	78
<b>5.5 Summary and conclusions</b> .....	79



## CHAPTER 6

### PARAMETRIC STUDY AND OPTIMUM DESIGN OF LAMINATED PLATES UNDER MIXED BOUNDARY CONDITIONS

<b>6.1 Introduction</b> .....	81
<b>6.2 Assumptions and design parameters</b> .....	82
<b>6.3 Results and discussions</b> .....	84
6.3.1 Effect of boundary condition.....	84
6.3.1.1 Optimal fiber orientation for maximum damping.....	84
6.3.1.2 Optimal fiber orientation for maximum frequency.....	86
6.3.1.3 Optimal fiber orientation for maximum mixed damping and frequency.....	88
6.3.2 Effect of lamination sequence.....	90
6.3.2.1 Optimal fiber orientation for maximum damping.....	90
6.3.2.2 Optimal fiber orientation for maximum frequency.....	91
6.3.3 Effect of laminate thickness.....	92
6.3.4 Effect of laminate aspect ratio.....	97
<b>6.4 Summary and conclusions</b> .....	100

## CHAPTER 7

### CONTRIBUTION, CONCLUSIONS AND FUTUR WORK

<b>7.1 Major contributions</b> .....	102
<b>7.2 Major conclusions</b> .....	103
<b>7.3 Recommendation for the future works</b> .....	105
<b>References</b> .....	107

## LIST OF FIGURES

Figure 1.1. Vibration testing for characterization of elastic constants, (a) plate tested with all edges free [11], (b) plate with all four edges clamped [12].....	4
Figure 1.2. Variation of structural loss factor with fiber orientation for symmetric angle-ply laminates $[n(\pm\theta)]_s$ with different thicknesses/number of layers [30].....	7
Figure 1.3. Schematic view of the experimental setup for evaluation of damping property against temperature [33].....	8
Figure 1.4. Experimental measurements for damping as a function of frequency for various temperatures for glass fiber composite beams, with (a) $0^\circ$ , (b) $45^\circ$ , (c) $90^\circ$ ply angle [33].....	8
Figure 1.5. Variation of SDC ( $\diamond$ ) with temperature for $0^\circ$ composites; thermoplastics (a) PEEK/AS4, (b) HTA/AS4, and thermosets (c) 913C/TS40, (d) 914C/XAS [34].....	9
Figure 1.6. Illustration of on-axis and off-axis coordinate systems.....	11
Figure 1.7. Elliptical hysteresis loop for one cycle.....	13
Figure 1.8. Illustration of a two-phase 3D micromechanical model with elliptical fibers, (a) schematic view, (b) FE model [49].....	14
Figure 1.9. Illustration of the representative volume element (RVE) for a three-phase 2D micromechanical model [50].....	15
Figure 1.10. Measurements (+, $\Delta$ , $\diamond$ , $\times$ , $\bar{x}$ ) and predictions (—) for damping as functions of frequency for glass/epoxy beams with the fiber volume fraction of (a) 35%, (b) 45%, (c) 60% [54].....	16
Figure 1.11. Variation of damping parameter (SDC) with fiber orientation for (a) carbon/epoxy, and (b) glass/epoxy laminate from various methods [62].....	17
Figure 1.12. Schematic view of experimental equipment for damping characterization using (a) the coil/electromagnet drive [58], (b) the impulse excitation [65].....	18
Figure 1.13. Loss factor (a) along fiber direction, (b) normal to fiber direction, (c) of in-plane shear, (d) of a UD laminate, of carbon/epoxy system versus frequency [64].....	20
Figure 1.14. Variation of the fundamental SDC (%) for laminate (a) $\pm 45^\circ$ , (b) $\pm 45/0^\circ$ , (c) cross-ply, (d) all-zero [26].....	22
Figure 1.15. Variation of predicted SDC for as a function of ply angle for simply-supported laminates, (a) a single layer, (b) angle-ply $[-\theta^\circ/\theta^\circ]$ , (c) cross-ply $[0^\circ/90^\circ/0^\circ]$ [77].....	23

Figure 2.1. OOA prepreg generations targeted by Boeing [81].....	28
Figure 2.2. Consolidation stages, (a) tape placement with compaction roller, (b) vacuum compaction or debulking under room temperature, (c) Curing with ideally void-free composition [84].....	29
Figure 2.3. Classification of prepregs before processing, (a) impregnated with dry tows, (b) UD tape with central dry tows, (c) resin film on fabric bed, (d) resin strips on fabric bed [83].....	29
Figure 2.4. Vacuum bag assembly for laminate manufacturing in oven.....	31
Figure 2.5. Sequence of hand layup process.....	32
Figure 2.6. Recommended curing cycles by the material supplier.....	33
Figure 2.7. Thermocouple measurements of temperature at the tool plate surface (Aluminum base plate) during the cure cycle.....	33
Figure 2.8. Microscopy test, (a) specimens for the microscopic test, (b) digital magnification of fibers aligned perpendicular to image plane.....	34
Figure 3.1. Dynamic stress and strain behavior of (a) purely elastic, (b) purely viscos, (c) linear-viscoelastic material [92].....	36
Figure 3.2. Factors playing a role on DMA testing.....	38
Figure 3.3. DMA specimens for single clamp cantilever and three-point bending setups...	40
Figure 3.4. DMA test configurations, (a) single-cantilever clamp, (b) three-point bending clamp.....	42
Figure 4.1. Illustration of (a) the laminated composite element, (b) the coordinate systems.....	51
Figure 4.2. Linear rectangular element and shape functions in non-dimensional coordinate [98].....	52
Figure 4.3. SSSS boundary condition of plates taken from Ref. [126].....	65
Figure 5.1. Samples for modal analysis, (a) Plate $[0/\pm 45/90]_5s$ , (b) Plate $[0/90]_9s$ , (c) Plate $[45]_{12}$ , (d) UD beams.....	67
Figure 5.2. (a) Schematic view, and (b) real image of the experimental setup.....	69

Figure 5.3. Bending modes of cantilever unidirectional beam with fiber angle of $0^\circ$ corresponding to the lower two natural frequencies.....	71
Figure 5.4. Bending modes of cantilever unidirectional beam with fiber angle of $45^\circ$ corresponding to the lower two natural frequencies.....	72
Figure 5.5. Bending modes of cantilever unidirectional beam with fiber angle of $90^\circ$ corresponding to the lower two natural frequencies.....	72
Figure 5.6. First four mode shapes of plate A ( $[45]_{12}$ ).....	73
Figure 5.7. First four mode shapes of plate B ( $[0/\pm 45/90]_{5s}$ ).....	74
Figure 5.8. First four mode shapes of plate C ( $[0/90]_{9s}$ ).....	74
Figure 5.9. Comparison between numerical results ( $\times$ ) and experimental scatter for fundamental modal damping factor.....	77
Figure 5.10. Variation of numerical fundamental loss factor and natural frequency with ply angle.....	78
Figure 5.11. Variation of numerical fundamental loss factor with natural frequency of unidirectional beams with different fiber angles.....	79
Figure 6.1. Combination of clamped and free boundary conditions studied for modal parameters.....	83
Figure 6.2. Variation of objective function ( $w_1 = 1, w_2 = 0$ ) with fiber orientation for 12-ply laminates under combination of clamped and free boundary conditions.....	85
Figure 6.3. Variation of fundamental loss factor with fiber orientation for 12-ply laminates under combination of clamped and free boundary conditions.....	86
Figure 6.4. Variation of objective function ( $w_1 = 0, w_2 = 1$ ) with fiber orientation for 12-ply laminates under combination of clamped and free boundary conditions.....	87
Figure 6.5. Variation of fundamental frequency with fiber orientation for 12-ply laminates under combination of clamped and free boundary conditions.....	87
Figure 6.6. Variation of objective function ( $w_1 = 0.5, w_2 = 0.5$ ) with fiber orientation for 12-ply laminates under combination of clamped and free boundary conditions.....	89
Figure 6.7. Variation of fundamental loss factor with fiber orientation for 12-ply laminates under combination of clamped and free boundary conditions.....	91

Figure 6.8. Variation of fundamental frequency with fiber orientation for 12-ply laminates under combination of clamped and free boundary conditions.....	92
Figure 6.9. Variation of fundamental loss factor with fiber orientation for unidirectional laminates with different thicknesses under mixed free and clamped boundary conditions..	93
Figure 6.10. Variation of fundamental loss factor with fiber orientation for cross-ply laminates with different thicknesses under mixed free and clamped boundary conditions..	94
Figure 6.11. Variation of fundamental loss factor with fiber orientation for angle-ply laminates with different thicknesses under mixed free and clamped boundary conditions..	95
Figure 6.12. Variation of fundamental frequency with fiber orientation for unidirectional laminates with different thicknesses under mixed free and clamped boundary conditions..	96
Figure 6.13. Variation of fundamental frequency with fiber orientation for cross-ply laminates with different thicknesses under mixed free and clamped boundary conditions..	97
Figure 6.14. Variation of fundamental frequency with fiber orientation for angle-ply laminates with different thicknesses under mixed free and clamped boundary conditions..	98
Figure 6.15. (a) Loss factors, (b) frequencies of cantilevered unidirectional laminates with various aspect ratios ( $\alpha$ ) versus the fiber orientation.....	99

## LIST OF TABLES

Table 1.1. Input data and outputs of models for material damping study [31].....	10
Table 1.2. Optimal fundamental loss factor for square and rectangle laminated sandwich plates with viscoelastic core [78].....	23
Table 2.1. Elastic properties from conventional static tests at room temperature.....	30
Table 3.1. Selection of clamp arrangement for DMA testing [91].....	38
Table 3.2. Discrepancies between storage and flexural modulus from DMA and ASTM tests.....	39
Table 3.3. Storage modulus of carbon/epoxy composite using single-cantilever arrangement.....	43
Table 3.4. Storage modulus of carbon/epoxy composite using three-point bending fixture.....	44
Table 3.5. Comparison of DMA storage moduli with elastic properties from static tests...	45
Table 3.6. Loss factors from DMA testing on 12-ply samples undergoing 3-point bending mode.....	46
Table 4.1. Gauss quadrature points, locations, and weights [98].....	54
Table 4.2. Material properties for plates studied in Refs. [118,119].....	60
Table 4.3. Frequency parameter ( $\Omega$ ) of 8-ply clamped square plates, $\Omega = \omega a^2(\rho/(E_T h^2))^{0.5}$ .....	60
Table 4.4. Material properties for plates studied in Ref. [120].....	61
Table 4.5. Dimensionless fundamental frequency parameter ( $\Omega$ ) of four-layered anti-symmetric angle-ply laminated square plate [45/-45/45/-45], material I, $\Omega = \omega a^2(\rho/(E_T h^2))^{0.5}$ .....	61
Table 4.6. Elastic material properties for GFRP studied in Ref. [125].....	62
Table 4.7. Layer damping properties ( $\psi, \eta$ (%)) for plates studied in Ref. [31,125].....	63
Table 4.8. Data for glass/epoxy plates 761 and 734.....	63
Table 4.9. Comparison of damped natural frequencies(Hz) for free plates in Ref. [125]....	63

Table 4.10. Comparison of modal damping ( $\psi$ (%) = $2\pi\eta$ ) for free square plates [31,125].....	64
Table 4.11. Elastic and geometric properties of composite materials taken from Ref. [126].....	64
Table 4.12. Damping properties ( $\psi, \eta$ (%)) for materials in Ref. [126].....	65
Table 4.13. Comparison of fundamental modal damping ( $\psi$ (%)) for four-layered simply-supported rectangular crisscross [ $\theta, -\theta, \theta, -\theta$ ] plates in Refs. [31,126].....	65
Table 5.1. Properties of beam and plate samples for modal analysis.....	68
Table 5.2. First three experimental and numerical flexural natural frequencies (Hz) for unidirectional beams.....	71
Table 5.3. Experimental and numerical natural frequencies (Hz) for laminated plates.....	73
Table 5.4. Fundamental modal damping parameter for unidirectional beams using FE model.....	76
Table 5.5. Fundamental modal damping factor (%) for unidirectional beams of 20 mm × 200 mm obtained experimentally.....	76
Table 5.6. Fundamental modal damping parameter (%) for unidirectional beams of 20 mm × 200 mm obtained experimentally.....	77
Table 6.1. Optimum fiber orientation and maximum loss factors obtained for laminates under mixed clamped and free boundary conditions.....	86
Table 6.2. Optimum fiber orientation and maximum frequencies obtained for laminates under mixed clamped and free boundary conditions.....	88
Table 6.3. Optimum fiber orientation and maximum objectives obtained for laminates under mixed clamped and free boundary conditions.....	89
Table 6.4. Maximum loss factors (%) and frequencies (Hz) of square plates with different thicknesses under combination of clamped and free boundary conditions.....	96
Table 6.5. Influence of the length on frequency and loss factor for beams with the aspect ratio of $\alpha = 10$ at selective fiber angles.....	99

## Nomenclature

ACRONYM	DESCRIPTION
OOA	Out-of-autoclave
ASTM	American Society for Testing and Materials
CLPT	Classical Lamination Plate Theory
FSDT	First-order Shear Deformation Theory
HSDT	Higher-order Shear Deformation Theory
LW	Layerwise
RR	Rayleigh-Ritz
ESL	Equivalent Single Layer
VED	Viscoelastic Damping
SDC	Specific Damping Capacity
GA	Genetic Algorithm
RMVT	Reissner's Mixed Variational Theorem
FE	Finite Element
RVE	Representative Volume Element

SYMBOL	DESCRIPTION
$\delta$	Phase angle
$U$	Maximum strain energy
$\Delta U$	Dissipated energy
$\sigma_0$	Stress amplitude
$\varepsilon_0$	Strain amplitude
$E'$	Storage Young's modulus
$E''$	Loss Young's modulus
$E^*$	Complex Young's modulus
$G'$	Storage shear modulus
$G''$	Loss shear modulus
$G^*$	Complex shear modulus
$L$	Coordinate along fiber direction
$T$	Coordinate transverse to fiber direction
$\hat{T}$	Coordinate through the thickness
$E_{LL}$	Young's modulus along fiber direction
$E_{TT}$	Young's modulus transverse to fiber direction
$G_{LT}$	In-plane shear modulus
$G_{L\hat{T}}, G_{T\hat{T}}$	Transverse shear modulus
$\nu_{LT}$	Major Poisson's ratio
$\nu_{TL}$	Minor Poisson's ratio, $(\nu_L E_T / E_L)$
$\sigma_{LL}, \sigma_{TT}$	On-axis normal stress components
$\tau_{LT}$	On-axis in-plane shear stress component
$\tau_{L\hat{T}}, \tau_{T\hat{T}}$	On-axis transverse shear stress component
$Q_{ij}$	On-axis or principal components of stiffness



$[Q_{ij}], [Q_{ij}^*]$	Real- and complex-valued on-axis stiffness matrix
$\varepsilon_{LL}, \varepsilon_{TT}$	On-axis normal strain components
$\gamma_{LT}$	On-axis in-plane shear strain component
$\gamma_{L\hat{t}}, \gamma_{T\hat{t}}$	On-axis transverse shear strain component
$\theta$	Fiber angle relative to the $x$ -axis in a lamina
$x, y, z$	Off-axis or general or global coordinates
$\sigma_x, \sigma_y$	Off-axis normal stress components
$\tau_{xy}$	Off-axis in-plane shear stress component
$\tau_{xz}, \tau_{yz}$	Off-axis transverse shear stress component
$\overline{Q_{ij}}$	Off-axis components of stiffness
$[\overline{Q_{ij}}], [\overline{Q_{ij}}^*]$	Real- and complex-valued off-axis stiffness matrix
$\varepsilon_x, \varepsilon_y$	Off-axis normal strain components
$\gamma_{xy}$	Off-axis in-plane shear strain component
$\gamma_{xz}, \gamma_{yz}$	Off-axis transverse shear strain component
$\Omega$	Reference plane of laminate structure
$\rho$	Material density
$I_1, I_2, I_3$	Moments of inertia
$[\mathcal{A}], [\mathcal{B}], [\mathcal{D}], [\mathcal{R}]$	Extensional, coupling, bending, and shear rigidity matrix
$[\mathcal{A}^*], [\mathcal{B}^*], [\mathcal{D}^*], [\mathcal{R}^*]$	Complex extensional, coupling, bending, and shear rigidity matrix
$(\xi, \eta, \zeta)$	Normalized coordinate system
$(u, v, w)$	Displacement components
$(u_0, v_0, w_0)$	Displacement components of a point on the mid-plane
$\theta_x, \theta_y$	Rotations of transverse normal about $y$ - and $x$ -axis
$z_k$	Thickness coordinate measured from the mid-plane
$h$	Laminate thickness
$a$	Plate length
$b$	Plate width
$N_i$	Shape function
$[B]$	Matrix of derivatives of shape functions
$[J]$	Jacobian matrix or operator
$\eta$	Material loss factor
$\eta_s$	Structural loss factor
$\eta_i$	Modal loss factor
$\psi_s$	Structural specific damping capacity
$f$	Resonance frequency
$t$	Time
$\{D\}$	Modal shape vector
$\omega$	Angular frequency
$\omega^* = \omega' + i\omega''$	Complex frequency
$\lambda^* = \lambda' + i\lambda''$	Complex eigenvalue
$[K]$	Stiffness matrix
$[K^*]$	Complex-valued stiffness matrix

$[M]$	Mass matrix
$\Delta$	Logarithmic decrement
$\xi$	Damping ratio
$Q$	Quality factor

# CHAPTER 1

## INTRODUCTION AND SCOPE OF WORK

### 1.1 Introduction

As a viable alternative to conventional engineering materials, fiber-reinforced polymer composites are extensively employed in the fabrication of widespread products ranging from high-performance applications in aerospace and defense industries to commercial products such as sports equipment [1]. They have received growing attention owing to their high performance, excellent mechanical properties, and ability to be customized for any application. Analytical and numerical models can be effectively utilized to predict the response behavior of composite structures for design and manufacturing purposes in order to avoid many extensive and expensive experimental tests. However accuracy of these models directly depends on the input elastic and damping material properties. Considering this, to fully exploit advanced inherent features of the fiber-reinforced polymer composites, it is of paramount importance to have comprehensive understanding of their mechanical properties and experimental techniques to accurately assess them [2].

Light-weight composite structures are typically lightly damped and thus sensitive and vulnerable to low frequency resonances under dynamic loading which may cause large amplitude vibration leading to material degradation and failure of composite components [3,4]. Thus besides elastic properties, it is important to correctly assess the damping properties of composite structures in order to accurately evaluate their dynamic responses. Accordingly, extensive research has been conducted and reported in the literature to thoroughly understand not only elastic but also viscoelastic properties of composite structures. Since fiber-reinforced composites are inhomogeneous and anisotropic, characterization of their physical and mechanical properties is much more challenging and complicated than those employed for conventional isotropic materials [5]. Therefore, it is necessary to determine essential properties in each material direction, depending upon analysis requirements. It should be noted that each mechanical identification scheme has also its own limitations and difficulties. The particular challenge is to understand which testing procedure to be properly selected, given required time and involved expenses for

facilities and sample preparation. Thus, it is of interest to explore an experimental method, which can be easier to implement for the evaluation of viscoelastic properties of high-modulus fiber-reinforced composite materials, in particular.

## **1.2 Review of relevant literature**

### *1.2.1 Characterization of elastic properties*

Various identification procedures have been reported in the literature to accurately characterize elastic properties of both isotropic and anisotropic materials. Elastic characteristics are essential for many aspects of structural analysis, namely, static, fatigue, buckling, vibration, etc. Among various identification procedures reported in the literature, the mechanical characterization methods are widely established for obtaining the elastic properties of composite materials and are mostly classified into static and dynamic tests, according to the nature of loading condition. Static tests are the traditional test procedures to describe the stress-strain curves, where the applied load changes smoothly and quasi-statically. Dynamic schemes are, however, considered as indirect alternative techniques for determination of elastic constants, where the material is under free vibration or forced harmonic excitation [6].

#### *1.2.1.1 Static testing*

Owing to their simplicity of application, the static testing is the most common method used to determine elastic constants through direct measurement of the stress-strain relationship. However, this conventional testing procedure may not yield the most stable measurements due to some problems such as inappropriate boundary conditions, inaccuracy in loading rate, incorrect selection of sample shape and dimensions, specimen finishing with low quality as well as difficulty in achieving uniform state of stress and/or strain. According to the international standards, there is also no universal or generally accepted methods for specimen selection and clamping setup.

Many commonly used and applicable static test schemes for the material identification of fiber-reinforced polymer composites, either high- or low-modulus, are conducted as per American Society for Testing and Materials (ASTM) standards. In order to overcome associated malfunctions and limitations of earlier established procedures, testing conditions must be generally re-examined by a careful investigation. In this direction, a number of standard test methods,

differentiating in some aspects, have also been refined, intending the measurement of the same properties. Revised editions of testing methods are mostly established based on proposed modifications in terms of test specimen, testing procedure, fixture geometry and configuration, and data reduction scheme [5]. ASTM D-4762 provides a tabulated list of applied standards sharing the same purpose for material evaluation, inclusive of comments on pros and cons relevant to the modulus of material of testing samples, fixture alignment, and data scatter.

Moreover, there exists a series of non-standard testing techniques considered as industry or company extensions that have been designed and restricted to a specific purpose of evaluation. Many diverse testing procedures are also developed due to the introduction of newly emerged materials whose properties cannot be adequately measured using already defined methods. On the other hand, it is further complicated and costly to progressively evolve testing methods for a broad spectrum of materials such as the class of composites. Although, extensive attempts have been made to design and improve test samples, methods, facilities, or fixtures to either precisely determine more properties, to facilitate measurement, or to better understand uncommon behavior of composite systems. Some reported studies on testing and examination procedures along with associated modifications to the existing standard methods are discussed in [6-8].

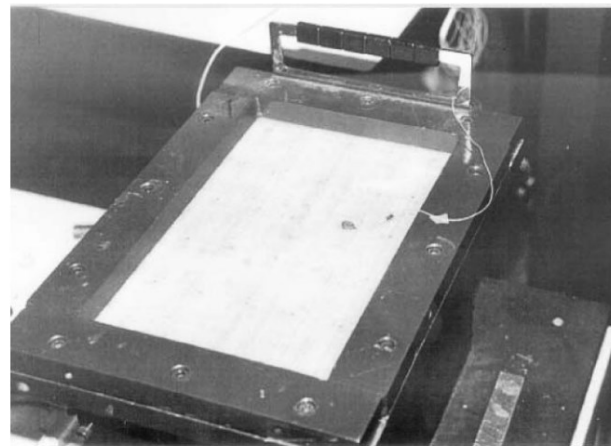
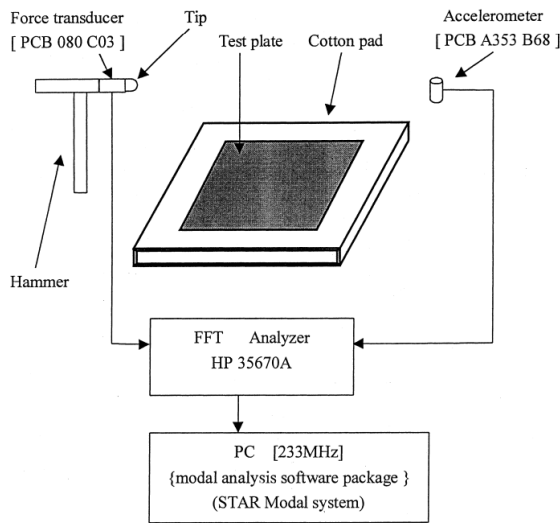
A comprehensive literature review on the static testing is not the focal point of this study as it has been broadly documented and quoted in the open literature and referenced standards as described above.

#### *1.2.1.2 Dynamic testing*

Dynamic tests based on the mixed numerical and experimental vibration analysis have also received increasing attention recently. In this type of characterization approach, the unknown material properties in the numerical model are updated iteratively so that dynamic response or vibration modal parameters evaluated by the model agree well with those obtained experimentally for an existing structure. Vibrating beam specimens only provide two of the elastic constants, i.e.  $E_{LL}$  and  $E_{TT}$ , by testing  $0^\circ$  and  $90^\circ$  specimens. Considering this, evaluating the flexural vibrations of thin and thick plates with different boundary conditions (see Figure 1.1) and stacking sequences may be required to fully estimate the remaining parameters. Examination of thin plates typically provides four independent in-plane elastic constants such as  $E_{LL}$ ,  $E_{TT}$ ,  $G_{LT}$ , and  $\nu_{LT}$ . However, the out-of-plane parameters (moduli and Poison's ratio) are extracted in the case of thick plates with

the aid of advanced theories. This is due to the fact that the vibration behavior of relatively thin plates are quite insensitive to the transverse shear moduli,  $G_{T\hat{f}}$ . For transversely isotropic materials, one of the transverse shear moduli,  $G_{L\hat{f}}$ , can be approximated to  $G_{LT}$ , though. In this regard, the higher frequencies are generally necessary to be measured, which may be difficult under normal testing instruments. Moreover, the numerical equations required to extract the elastic constants may be numerically instable and ill-conditioned [5,9-13].

Indirect identification problems require very large computational efforts to solve an eigenvalue problem in each stage towards the solution. This type of identification method is quite similar to optimization problems, where solutions for unknown material properties are obtained by minimization of the error between desired numerical responses and those obtained experimentally. The choice of optimization algorithm for the purpose of minimization has also a large influence on the accuracy along with the convergence performance of the identification analysis. As another technique, identification of physical parameters characterizing structural behavior is performed using the response function at experimentally design-based reference points to significantly reduce the computational effort [14,15].



(a)

(b)

Figure 1.1. Vibration testing for characterization of elastic constants, (a) plate tested with all edges free [11], (b) plate with all four edges clamped [12].

Note that the Poisson's ratio is the most difficult elastic property to determine by dynamic testing as it has an insignificant effect on the frequency response. Moreover, factors such as the plate aspect ratio, the length-to-thickness ratio and the direction of the orthotropy have great impact

on characterization of the Poisson's ratio. Ragauska and Belevicius [16] found an optimized specimen with the specific orthotropy angle and side-to-thickness ratio for two composite materials so as to estimate the Poisson's factor with a sufficient precision. The problem was addressed using ANSYS integrated with the Genetic Algorithm (GA), considering tuned genetic parameters.

Dynamic mechanical (thermal) analysis (DMA) is another dynamic approach to identify a broad range of properties i.e. mechanical, viscosity, and glass transition with respect to temperature and frequency in a single quick test. The DMA method has been widely used for qualitative studies on composite materials to examine the cure kinetics and the degree of consolidation due to adjustments and modifications in fabrication process for the performance improvement. The method is mostly used for examination of polymers for curing evaluation. However, the application of DMA for material characterization of high-modulus materials has resulted in inaccurate results, compared to those from the flexural static tests [17,18]. The discrepancies on experimentally measured characteristics of high-modulus composites, particularly, in terms of elastic constants have been noticed in a few studies [19]. While, the effect of several measurement parameters, in particular, on the longitudinal elastic modulus has been systematically investigated in few studies [20], the accuracy of other elastic constants, i.e. the transverse and in-plane shear moduli, has not been evaluated.

### *1.2.2 Damping mechanism in composite materials*

Damping, or the energy dissipation parameter, is known as the major contributing factor to vibration and noise attenuation in structures. For light-weight composite materials, damping analysis is also of great importance in terms of structural health monitoring. This is due to the fact that damages or permanent changes result in significant increase in damping rather than stiffness [21]. In structural mechanics, energy dissipation is mainly due to the inherent material damping and the external sources associated with either joints or damping treatments added passively or actively [22,23]. For damping analysis, there exist a number of quantifying factors which specify damping performance or capacity. As a measure of vibration damping, dimensionless quantities such as the damping factor,  $\xi$ , loss factor (tangent),  $\eta$ , logarithmic decrement,  $\Delta$ , specific damping capacity (SDC),  $\psi$  are frequently used.

From an engineering point of view, a trade-off between damping, stiffness and/or strength must be taken into consideration as inherent damping exhibits behavior opposing the stiffness performance. Because of increasing demand for high performance structures, modifications are usually required. In this respect, damping studies relevant to composite structures generally address methods to enhance damping performance by either manipulation of constituent and ply parameters or incorporation of interlaminar or constrained polymer layers in a layup, whether partially or entirely. The latter significantly improves overall damping by observing the optimum in-plane and/or transverse location of embedded viscoelastic layers, laminate configuration (stiffness and number of compliance layers confining damping layers), and proper selection of interleaved material [2]. To analyze a damped composite system even integrated with viscoelastic layers, the contribution of energy dissipation due to constituent of fiber-reinforced composites should, also, be reflected. This is due to the fact that the damping of fiber-reinforced composites is 10 –100 times higher than that of metallic components. Very limited studies have been conducted to consider the contribution of damping from both fiber-reinforced composites and embedded damping layers in a damped composite component [24].

Composite materials exhibit relatively higher damping with an anisotropic property, depending on the constitution of materials. This features another advantage of composite materials over conventional engineering materials so as to reduce the amplitude of vibrations at the resonance or near-resonance. In general, the damping mechanism in fiber-reinforced composites is a complex phenomenon, which is not well understood. While fiber-matrix interface, thermoplastic and viscoplastic damping, as well as defects such as interfacial bond failure, cracks, or broken fibers contribute to damping to some extent [2], studies show that viscoelastic nature of matrix has predominant effect on material damping characteristics of composite materials [1,25]. Also, fiber volume fraction, fiber aspect ratio, constituent materials, ply angle, stacking sequence, and reinforcement geometrical properties greatly influence structural damping which can be tailored to maximize structural damping factors [26-29]. Additionally, the geometry and constraints of a structure have a significant effect on the structural damping. Hwang and Gibson [30] studied the variation of the loss factor with the fiber angle for several laminates, considering the effect of width-to-thickness ratio ( $w/t$ ) as a structural variable. Of particular interest in their work were the effect of ply angle rather than the width-to-thickness ratio, which yields an insignificant variation in the loss factor for a given angle (see Figure 1.2). Therefore, for a fiber-reinforced



composite system, damping capacity is highly tailored to micromechanical, laminate, and structural parameters.

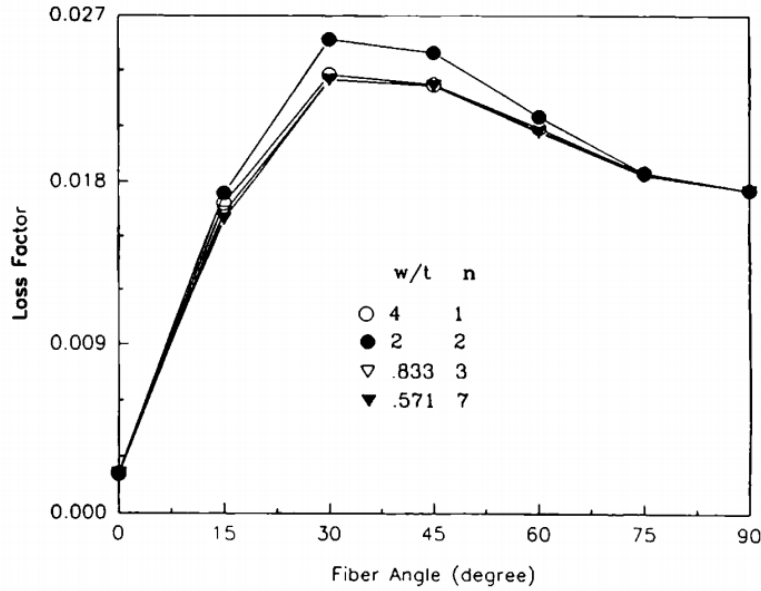


Figure 1.2. Variation of structural loss factor with fiber orientation for symmetric angle-ply laminates  $[n(\pm\theta)]_s$  with different thicknesses/number of layers [30].

### 1.2.2.1 Temperature, frequency, and stress dependency

Considering metallic and nonmetallic materials, the damping characteristic is a function of temperature, frequency, and stress or strain amplitude. It has been observed that the material damping solely features frequency- and temperature-dependency for polymer-matrix composites, except at stresses approaching the fatigue limit or strains exceeding the linear threshold [23,31,32]. As a result, a wide range of frequency and temperature has been considered in experimental examinations to study damping as a low stress amplitude is ensured. For the purpose of damping characterization, a closer examination is specifically needed at higher-angle unidirectional beams, where a higher degree of sensitivity to the level of stress is observed. Therefore, it has been recommended to retain the same stress level for all samples used for identification [32]. In this respect, the two generally used material damping notations, the loss factor,  $\eta$ , and the specific damping capacity (SDC),  $\psi$ , can be expressed as:

$$\psi = f_{\psi}(T, \omega) \quad \text{or} \quad \eta = f_{\eta}(T, \omega) \quad (1-1)$$

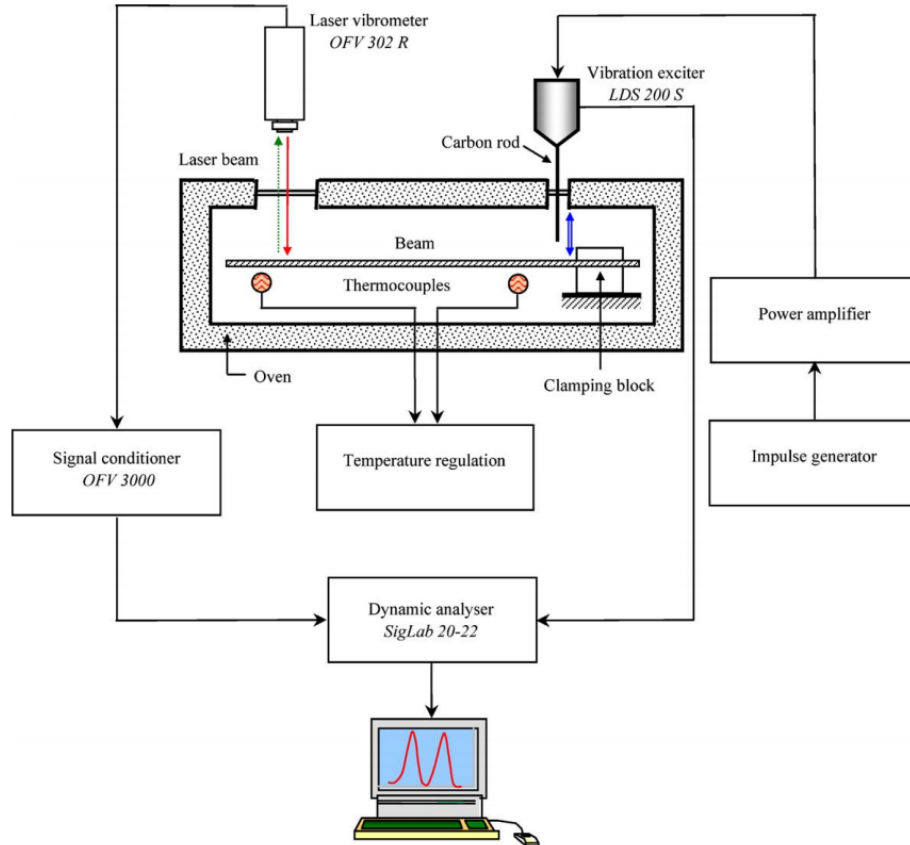


Figure 1.3. Schematic view of the experimental setup for evaluation of damping property against temperature [33].

The thermal effect is, however, dominant within the range of glass transition temperature, when the matrix softens, leading to higher viscosity and loss factors, to the detriment of stiffness. Therefore, the effect of temperature may be ignored under normal conditions of application. From an application point of view, the inherent damping in any material coordinate can be considered as a constant in a specific working range of frequency [1].

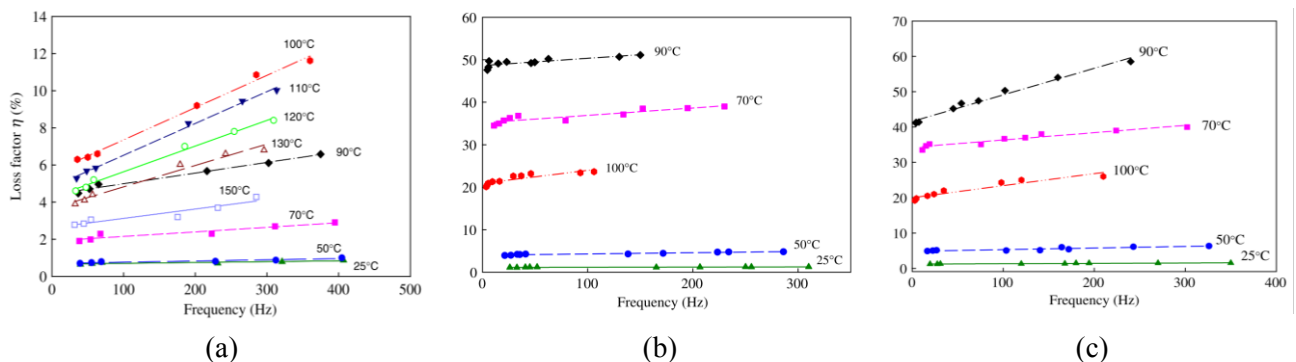


Figure 1.4. Experimental measurements for damping as a function of frequency for various temperatures for glass fiber composite beams, with (a) 0°, (b) 45°, (c) 90° ply angle [33].

To examine the effect of the temperature and frequency simultaneously, Sefrani and Berthelot [33] experimentally evaluated the damping property of a glass-fiber composite in the form of rectangular cross-section beams by modal vibration response measurements (see Figure 1.3). Three types of clamped beam with fiber orientations of  $0^\circ$ ,  $45^\circ$ , and  $90^\circ$  were considered. It was noticed that the maximum damping occurs at  $100^\circ\text{C}$  for  $0^\circ$  specimen and at  $90^\circ\text{C}$  for  $45^\circ$  and  $90^\circ$  samples (see Figure 1.4). It was also observed that the damping remains low and constant within the frequency range under consideration (below 400 Hz), where the temperature varies from  $25^\circ\text{C}$  to  $50^\circ\text{C}$  for all the fiber orientations examined.

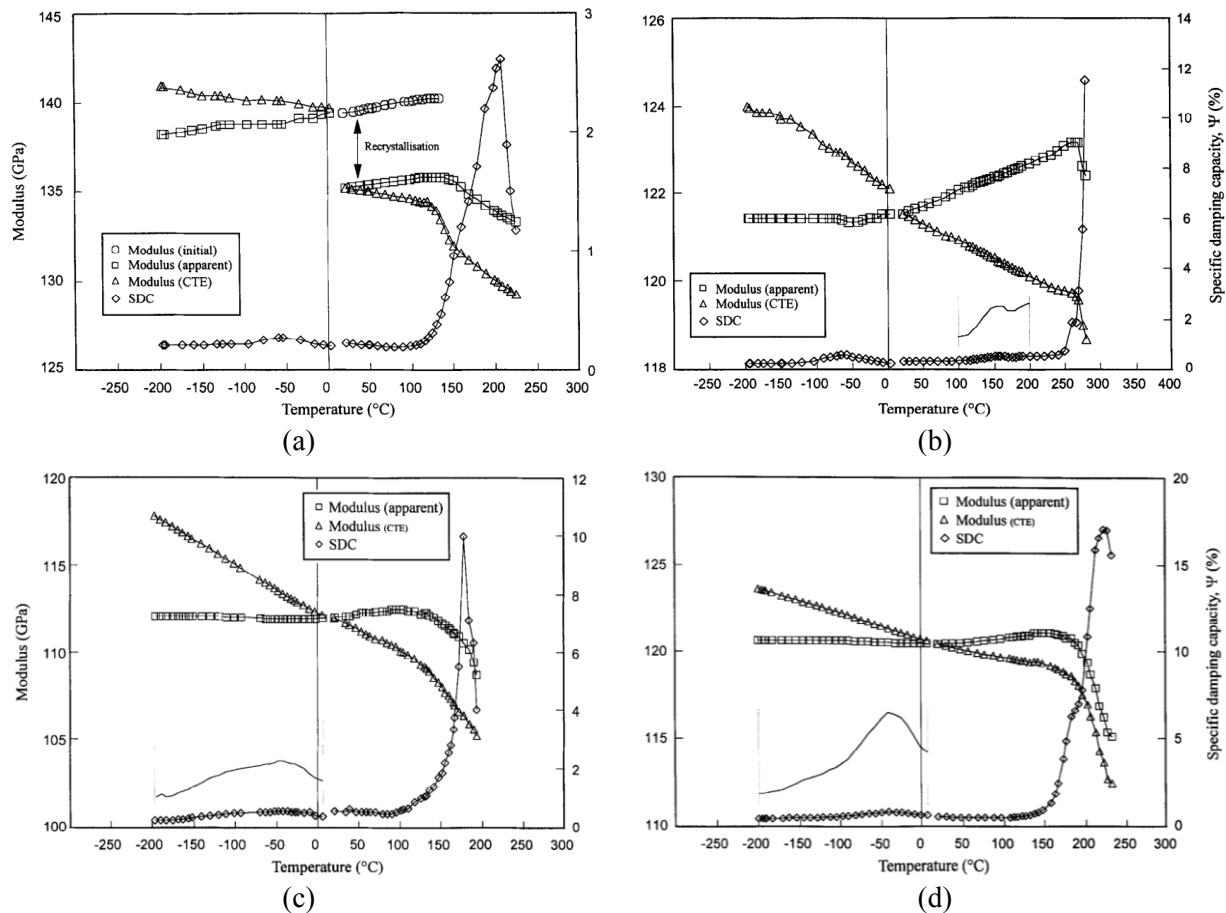


Figure 1.5. Variation of SDC ( $\diamond$ ) with temperature for  $0^\circ$  composites; thermoplastics (a) PEEK/AS4, (b) HTA/AS4, and thermosets (c) 913C/TS40, (d) 914C/XAS [34].

Maheri et al. [34] also studied the dynamic mechanical properties of two thermoplastic and two epoxy-based thermoset fiber-reinforced composite materials with respect to the temperature ranging from room temperature to  $200^\circ\text{C}$ . It was observed that all four composite systems exhibit low damping at lower side of the temperature range, while all materials are highly damped at

elevated temperatures around the glass transition point. A fully-automated commercial cryostat was used in order to control the temperature and moisture in the heating-up process. Figure 1.5 represents the variation of the damping parameter (SDC) for the materials tested in their study.

### 1.2.3 Damping analysis and modeling

To describe the behavior of material damping of composites, different damping models and approaches have been proposed [1,2]. Damping in composite materials can be studied using micromechanical and macromechanical models. Table 1.1 compares the required input data and the output of these two models for the damping study of composite systems. These models are then integrated with mathematical formulations such as lamination theories to evaluate dynamic response of composite structures. The micromechanical model mainly involves damping determination at the constituent level, i.e. fiber, matrix, and interphase in view of its condition effect, while the macromechanical model is mostly focused on effects of lamination arrangement, boundary conditions, and lamina dissipation properties on the structural damping.

Table 1.1. Input data and outputs of models for material damping study [31].

Micromechanical Model		Macromechanical Model	
Input	<ul style="list-style-type: none"> <li>• Properties of fibers;</li> <li>• Properties of matrix;</li> <li>• Properties of interface region;</li> <li>• Fiber volume fraction;</li> <li>• Geometries and arrangement of fibers; etc.</li> </ul>	Input	<ul style="list-style-type: none"> <li>• Properties of lamina;</li> <li>• Geometries;</li> <li>• Lamination arrangement;</li> <li>• Boundary conditions; etc.</li> </ul>
Output	Damping properties of the lamina	Output	Damping characteristics of the structure

#### 1.2.3.1 Macromechanical approach

With respect to the macromechanical analysis, two general damping models, namely the viscoelastic damping (VED) and the modal strain energy (MSE) have been developed for the analytical prediction [2,31]. These approaches require the knowledge of damping parameters in principal material directions for each lamina. Both models basically lead to the same modal damping identification in the context of linear vibration theory if the system is slightly damped [31,35].

### 1.2.3.1.1 Viscoelastic damping method

Using the VED model, the dissipative response of a system is predicted from either numerical or analytical analysis in which the dissipative parameters are defined through the concept of the complex-valued moduli, established by Hashin [36] and then adopted by other researchers such as Sun et al. [37], Crane and Gillespie [38], and Yim [39]. In accordance with Hashin's concept or the elastic-viscoelastic correspondence principle, the complex expressions of the engineering constants can be represented as:

$$\begin{aligned}
 E_{LL}^* &= E_{LL}(1 + i \eta_{LL}) & E_{TT}^* &= E_{TT}(1 + i \eta_{TT}) \\
 G_{LT}^* &= G_{LT}(1 + i \eta_{G_{LT}}) & G_{T\hat{T}}^* &= G_{TT}(1 + i \eta_{G_{T\hat{T}}}), & i &= \sqrt{-1} \\
 G_{L\hat{T}}^* &= G_{L\hat{T}}(1 + i \eta_{G_{L\hat{T}}}) & \nu_{LT}^* &= \nu_{LT}(1 + i \eta_{\nu_{LT}})
 \end{aligned} \tag{1-2}$$

where subscript  $L$  represents the principal material axes of a ply aligned with fibers, and  $T, \hat{T}$  are two directions transverse to fibers and through the thickness, respectively, as shown in Figure 1.6.  $\eta_{LL}$  and  $\eta_{TT}$  are material loss factors along the longitudinal or fiber direction, and the transverse direction which is perpendicular to the fiber orientation, respectively.  $\eta_{G_{LT}}$ ,  $\eta_{G_{T\hat{T}}}$ , and  $\eta_{G_{L\hat{T}}}$  represent, respectively, the shear loss factors in planes  $L_T$ ,  $T_{\hat{T}}$ , and  $L_{\hat{T}}$ . Considering a thin lamina of a transversely isotropic viscoelastic material,  $\eta_{G_{L\hat{T}}}$  and  $\eta_{G_{T\hat{T}}}$  are considered to be equal. The loss factor of the major Poisson's ratio,  $\eta_{\nu_{LT}}$ , is generally considered to be negligible in the damping analysis under insignificant thermal and chain expansions [28,38,40].

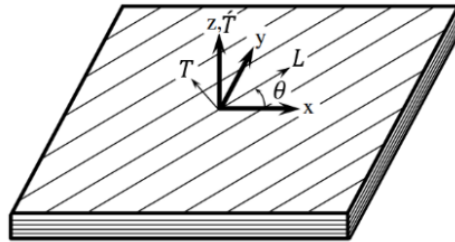


Figure 1.6. Illustration of on-axis and off-axis coordinate systems.

The modal loss factor of a structure as a measure of structural damping is typically predicted by the ratio of the imaginary part to the real part of the squared complex eigenfrequencies obtained from the numerical modeling as [31,41]:

$$\eta_s = \frac{Im(\omega^{*2})}{Re(\omega^{*2})} \tag{1-3}$$

### 1.2.3.1.2 Modal strain energy method

One of the frequently used approaches to analyze the damped vibration response of composites is referred to as the strain energy method. The concept of this method was firstly introduced in a work by Ungar and Kerwin [42]. The basis of the strain energy method is represented by the ratio of the sum of dissipative strain energy elements due to corresponding stress components to the maximum strain energy stored in a material [30]. One approach towards quantifying the dissipative energy and total strain energy of a system is through experimental measurements under cyclic loading to obtain the hysteretic loop during a complete stress cycle as shown in Figure 1.7. For a general nonlinear material the shape of the hysteresis loop is a nonlinear function of temperature, frequency and stress amplitude.

Using expressions for the energy dissipation and the maximum strain energy introduced into a system undergoing one complete cycle of a steady-state oscillatory condition [41,43], one can readily find the relationship between the specific damping capacity (SDC) and loss factor,  $\eta$ . The total dissipated energy in one cycle is equal to the area inside the elliptical hysteresis loop shown in Figure 1.7. Given the stress  $\sigma(t) = \sigma_0 \sin(\omega t + \delta)$  and strain  $\varepsilon(t) = \varepsilon_0 \sin(\omega t)$ , the energy dissipated in one cycle is expressed as [43]

$$\Delta U = \int_0^T \sigma(t) \frac{d\varepsilon(t)}{dt} dt = \int_0^T (\sigma_0 \sin(\omega t + \delta)) (\omega \varepsilon_0 \cos(\omega t)) dt = \sigma_0 \varepsilon_0 \pi \sin(\delta) \quad (1-4)$$

where  $\delta$  is the phase lag between the applied stress and the induced strain due to the viscosity of a material. As represented by the cross-hatched triangle in Figure 1.7, the maximum strain energy can also be obtained as

$$U = \frac{1}{2} \left( \sigma_0 \sin\left(\frac{\pi}{2} + \delta\right) \right) \left( \varepsilon_0 \sin\left(\frac{\pi}{2}\right) \right) = \frac{1}{2} \sigma_0 \varepsilon_0 \cos(\delta) \quad (1-5)$$

Then, if  $\sigma_0$  is the only stress component applied, the ratio of the dissipated energy  $\Delta U$  to the maximum strain energy is expressed as

$$\frac{\Delta U}{U} = \frac{\sigma_0 \varepsilon_0 \pi \sin(\delta)}{\frac{1}{2} \sigma_0 \varepsilon_0 \cos(\delta)} = 2\pi \tan \delta \quad (1-6)$$

where  $\Delta U/U$  is known as the SDC factor, which is frequently utilized to quantify energy dissipation based on the definition of the strain energy method. As a measure of damping,  $\tan \delta$  also represents the loss factor.

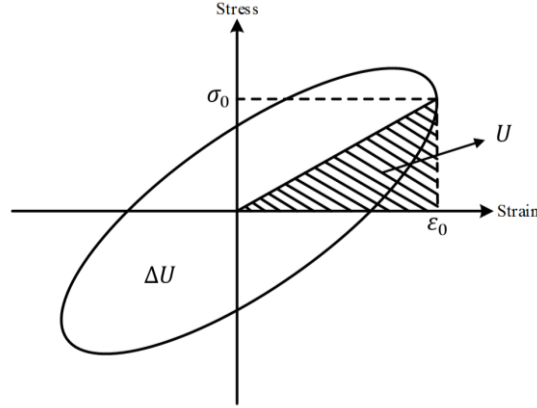


Figure 1.7. Elliptical hysteresis loop for one cycle.

According to the superposition principle of the energy method, the total energy loss in a structure under an arbitrary stress state can be assumed to be equal to the sum of energy loss components due to stresses along each direction. The SDC of a component is, accordingly, defined as [44]

$$\psi_s = \frac{\Delta U_s}{U_s} = \frac{\frac{1}{2} \int_V \psi_{ij} \sigma_{ij} \varepsilon_{ij} dV}{\frac{1}{2} \int_V \sigma_{ij} \varepsilon_{ij} dV} \quad i, j = L, T, \hat{T} \quad (1-7)$$

where  $\psi_s$  is the structure's SDC and  $\psi_{ij}$  denote the damping parameters ( $\psi_{LL}$ , along the fiber,  $\psi_{TT}$ , perpendicular to the fiber, and  $\psi_{LT}$ , in-plane shear, as well as transverse shears  $\psi_{T\hat{T}}$  and  $\psi_{L\hat{T}}$ ). The total dissipated energy and the maximum strain energy of a structure are, respectively, represented by  $\Delta U_s$  and  $U_s$ . In the case of the plane stress state of the transversely isotropic body, it is sufficient to attribute the damping energy to the reduced in-plane dissipation components, that is  $\psi_{LL}$ ,  $\psi_{TT}$ , and  $\psi_{LT}$ , according to the Adams-Bacon damping criterion [44,45].

Provided that the damping is low, the two aforementioned definitions of damping are, thus, interrelated as [46]

$$\psi_s = 2\pi\eta_s \quad (1-8)$$

As a measure of damping of a vibrating system, other dimensionless quantities can also be employed, which are interconnected to the loss factor as [47]

$$\eta_s = 2\xi = \frac{1}{Q} = \frac{\Delta}{\pi} = \frac{E''}{E'} = \tan(\delta) \quad (1-9)$$

where  $\xi$ ,  $Q$ ,  $\Delta$ ,  $E''$ ,  $E'$ , and  $\delta$  designate the damping ratio, quality factor, logarithmic decrement, loss modulus, storage modulus, and phase lag, respectively.

### 1.2.3.2 Micromechanical approach

The goal of micromechanical models is to predict damping properties of fiber-reinforced composite components, using dissipation characteristics of constituent materials and their interactions. For damping study, micromechanical models have been developed as extensions to corresponding methods/models for prediction of elastic moduli or engineering constants through the application of either strain energy or correspondence principle technique. Material damping characteristics of fiber-reinforced composites are basically affected by various parameters associated with constituents. The micromechanical damping analysis of unidirectional or aligned short fiber-reinforced composites are also divided into two categories: two-dimensional and three-dimensional models [2]. In the latter case, the fiber is considered in a form such as elliptic cylinders (see Figure 1.8) rather than circular cylinders (see Figure 1.9) which is generally treated in the former case. Using the approach proposed by Zhao and Weng [48], the effect of the microgeometry i.e. the shape of the fiber cross-section, was studied in Ref. [49]. As presented in Figure 1.8a, the shape (cross-section) of fiber was defined as aspect ratio  $\alpha$ , which is referred as the ratio of thickness to its width ( $t/w$ ).

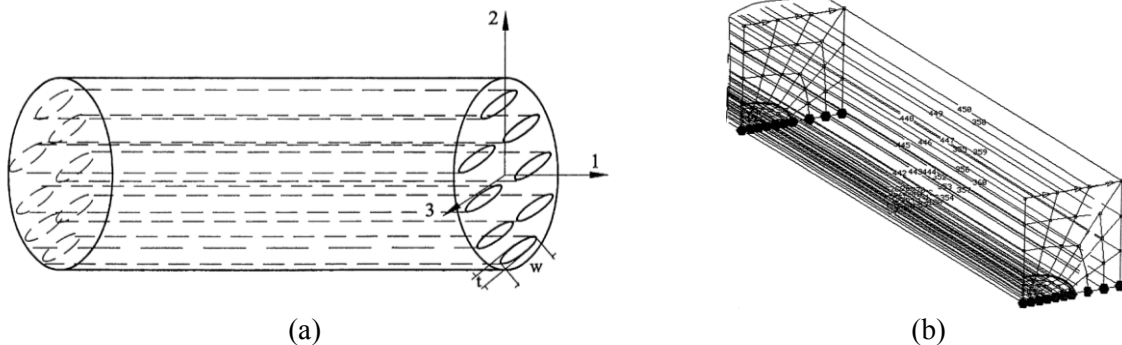


Figure 1.8. Illustration of a two-phase 3D micromechanical model with elliptical fibers, (a) schematic view, (b) FE model [49].



Moreover, each individual type of micromechanical model is classified into the two-phase and three-phase analysis. Two-phase studies mainly involve the determination of contribution of two components i.e. fiber and matrix. When the fiber-matrix interface accounts for the analysis, the modeling is referred as the three-phase study. The state, size (interphase volume fraction), and viscoelastic properties of interfacial region are the factors mostly observed. The bonding state (degree of adhesion) of the fiber-matrix interface can be presumed as weak, ideal (perfect), or strong. The ideal bonding is referred as an interface transferring loads without any contribution to the damping mechanism.

Numerical investigations from micromechanical methods generally underestimate the damping of composite structures, compared with those obtained experimentally. This major problem is attributable to unknown elastic and damping properties of the interphase. Accordingly, interpolations and presumptions are required to address the effect of this distinct third phase between the fiber and the bulk matrix. The discrepancy in results for the damping level is, thus, quite dependent on assumptions for each factor.

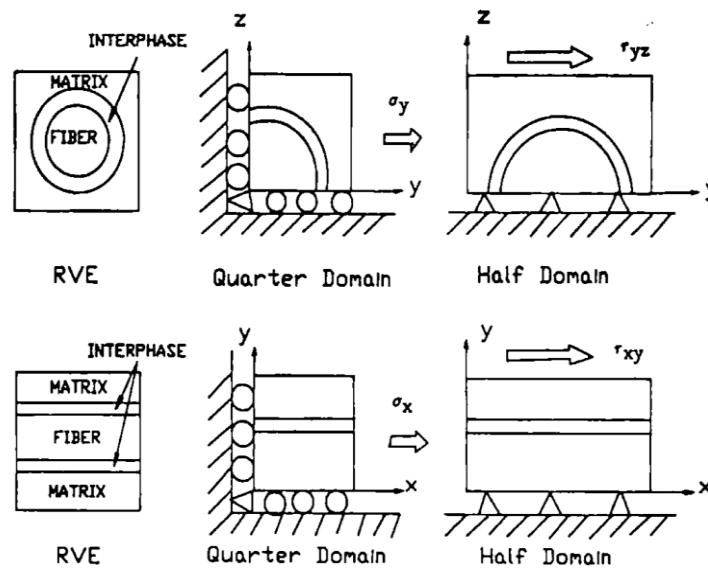


Figure 1.9. Illustration of the representative volume element (RVE) for a three-phase 2D micromechanical model [50].

The input data for properties of fiber-matrix interface or even defects and flaws, which mainly accounts for the damping, is not available in the literature. Moreover, qualitative information about the condition of the interface has been scarcely investigated in the light of experiments. In Refs.

[51,52], the DMA testing was employed as a reliable method to qualify the interfacial region of carbon and glass fiber composites with different fiber volume fractions. It was observed that the greater the degree of bonding, the inferior the interfacial damping. The DMA test was performed in flexural mode of deformation as it provides more accurate results in terms of interfacial properties, compared with the torsional mode.

The type of fiber, material of matrix [53], fiber length [27], shape of fiber cross-section [49], fiber volume fraction (see Figure 1.10) [54], the gap size between the ends of adjacent short fibers [55], and etc. have been treated as other variables in the micromechanical modeling and studies. Suarez et al. [27] perceived that the damping is improved by reducing the length of fiber, while the optimum fiber length is not practically attainable. Further, manipulation of the fiber orientation was recommended as a better approach for the control and enhancement of damping in composites.

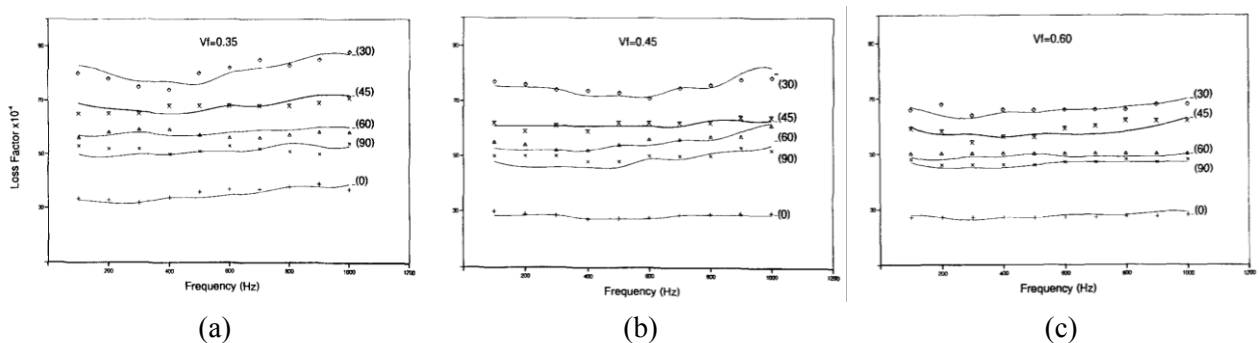


Figure 1.10. Measurements (+,  $\Delta$ ,  $\diamond$ ,  $\times$ ,  $\bar{x}$ ) and predictions (—) for damping as functions of frequency for glass/epoxy beams with the fiber volume fraction of (a) 35%, (b) 45%, (c) 60% [54].

Compared to many micromechanical damping theories restricted to some aspects, Sarvanos and Chamis [56] proposed the unified micromechanical damping methodology for the prediction of damping performance in unidirectional fiber-reinforced polymer composites. In addition to the damping contribution from the fiber, matrix, and interface, the damping due to the friction of broken fibers as well as the hygrothermal effect have been synthesized in their modeling. They also considered all six damping coefficients associated with all six stress components due to the off-axis loading.

#### 1.2.4 Experimental methods- identification of damping properties

As for estimating the elastic characteristics, damping of fiber-strengthened composites has been tackled either for characterization or validation of theories. All damping analytical models

have been mainly developed based on the experimental parametric investigations and measurement of damping quantities, which were established in the early studies reported in Ref. [23,57,58]. A chronological review of damping characterization test methods have demonstrated that the level of agreement between damping measures and predictions were unsatisfactory due to imperfect measurement and instrumentation in the earlier time. As reported in Refs. [22,59], there were no strong correlation between damping predictions from the modeling and corresponding results from experiments on laminated plates using the inverse lamination theory, whereby elastic constants were determined with sufficient accuracy. Crane and Gillespie [60] also underlined failure to validate theoretical results by experimental analyses, which were related to non-perfect clamping or supporting conditions and the mass effect of traditional or standard accelerometers and cables contributing in the total damping. As a result, refinement of experimental test procedures, proposition of new test rigs, and application of new exciting and sensing devices have thus received much more attention [61].

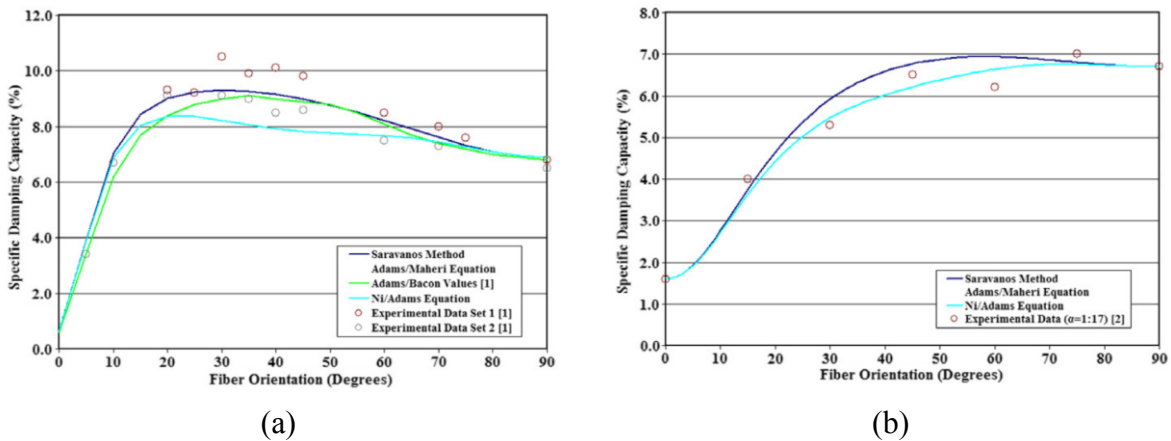


Figure 1.11. Variation of damping parameter (SDC) with fiber orientation for (a) carbon/epoxy, and (b) glass/epoxy laminate from various methods [62].

In respect of validation of results from the developed models, the study by Billups and Cavalli [62] shows the variation of the damping parameter (SDC) with respect to the fiber orientation of unidirectional beams for carbon/epoxy and glass/epoxy composites. As shown in Figure 1.11, it is observed that numerical predictions from various damping models agree reasonably well with measurements from carbon fiber beams  $[\theta]_{10}$  and glass fiber beams  $[\theta]_8$  excited at the fundamental flexural mode of vibration. Maheri and Adams [61] also found a good agreement between theoretical and experimental values for plate components, using the elastic and damping data obtained from unidirectional beams subjected to the first mode of flexural vibration in the air

and at room temperature. They compared the experimental and predicted damping results for four different materials.

In the view of experimental studies on damping in composite materials, considerable work has further been contributed to the characterization of constitutive damping parameters. There are two main methods that are used in practice to determine the damping characteristics. The methods of the first group deal with the direct measurement of the energy loss of a material under stable cyclic deformation. The measurement of the area inside the elliptical hysteresis loop, once the material is under steady-steady state cyclic deformation, provides the material energy loss directly. Whereas, measurement of other parameters such as the phase lag, frequency, and amplitude once the sample undergoes steady-state harmonic or transient motions have also been utilized to evaluate damping indirectly, considered as the second group [63,64].

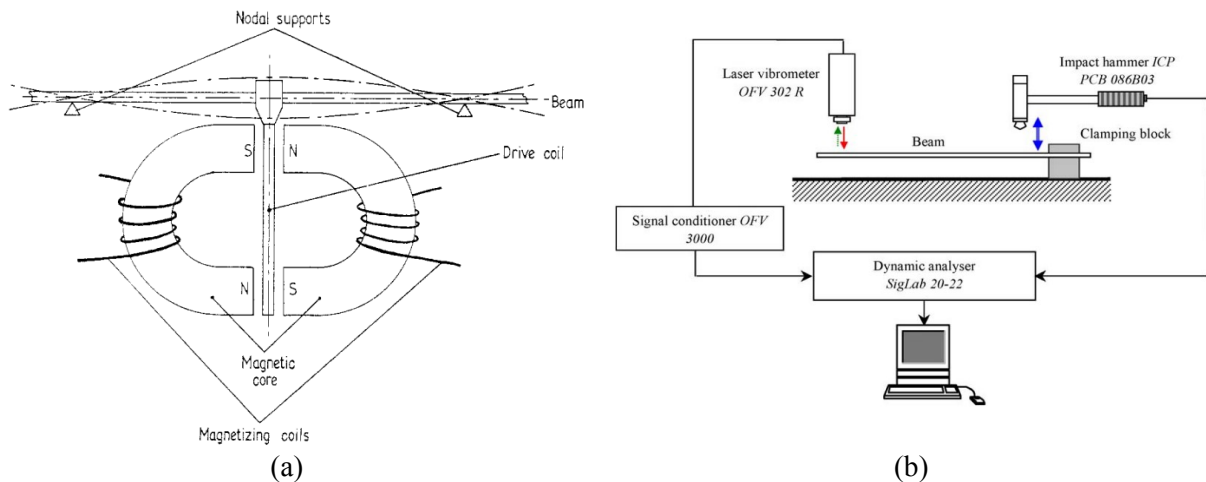


Figure 1.12. Schematic view of experimental equipment for damping characterization using (a) the coil/electromagnet drive [58], (b) the impulse excitation [65].

Concerning the indirect methods, the reduced number of independent damping parameters can be identified using DMA testing [40,66-68]. The free decay method [69] and the technique of resonance curve (frequency response function) [64,70,71] integrated with lamination theories have also gained wide acceptance as the indirect schemes. These empirical investigations have mostly dealt with the determination of damping characteristics along material coordinates by subjecting test specimens to flexural or torsional vibrations with different boundary conditions. As for characterization of these damping coefficients, unidirectional beams are mostly analyzed. The flexural damping of composite beams have been examined by either the forced flexural vibration

excited by a coil/electromagnet drive transducer (see Figure 1.12a) fixed to the midpoint of a free-free beam [57,58] or an impulse excitation (see Figure 1.12b) of a flat cantilever beam [28,72]. However, presence of external factors contributing to damping causes difficulties in distinguishing between the material and structural damping. Therefore, these vibration methods mostly provide damping characteristics in the material direction based on structural damping behavior stemming from the external sources. Consequently, a much-debated question is how to obtain the material damping characteristics on the basis of constituent components.

Berthelot and Sefrani [28] have found a linear trend of modal damping as a function of frequency for different ply angles of clamped unidirectional glass- and Kevlar-fiber beams subjected to an impact excitation. Frequency-dependent characteristic of the damping coefficients was determined by varying the length of beams. Successively, Berthelot [46] deduced damping characteristics along the material directions of a single lamina by fitting the experimental Fourier responses with analytical ones using Ritz method. Kostopoulos and Korontzis [64] also reported the variation of the loss factor along material directions with respect to frequency for a carbon/epoxy composite, using an indirect technique. The beam samples were triggered by an initial velocity excitation, while the response of the system was acquired using a glued dynamic strain gage combined with its amplifier and bridge. In contrast to the results reported in Ref. [28] for glass- and Kevlar-fiber composites, the measurements showed a nonlinear trend, while decreasing within the frequency range of 0 to 250 Hz in all of the directional loss factors (see Figure 1.13).

In a successive work, Berthelot [65] also computationally evaluated the damping characteristics of a simple structure composed of three different materials based on damping properties deduced from vibration tests of beams in terms of modal frequencies and damping factors. The damping response of the composite structure were only obtained using three main damping parameters along the material coordinates at the fundamental level of laminates, i.e. lamina. The results were then assessed experimentally. The agreement between the measurements and predictions confirms the method of characterization to analyze the damped response of a structure from laminates, laminates with interleaved layers, or sandwich materials.

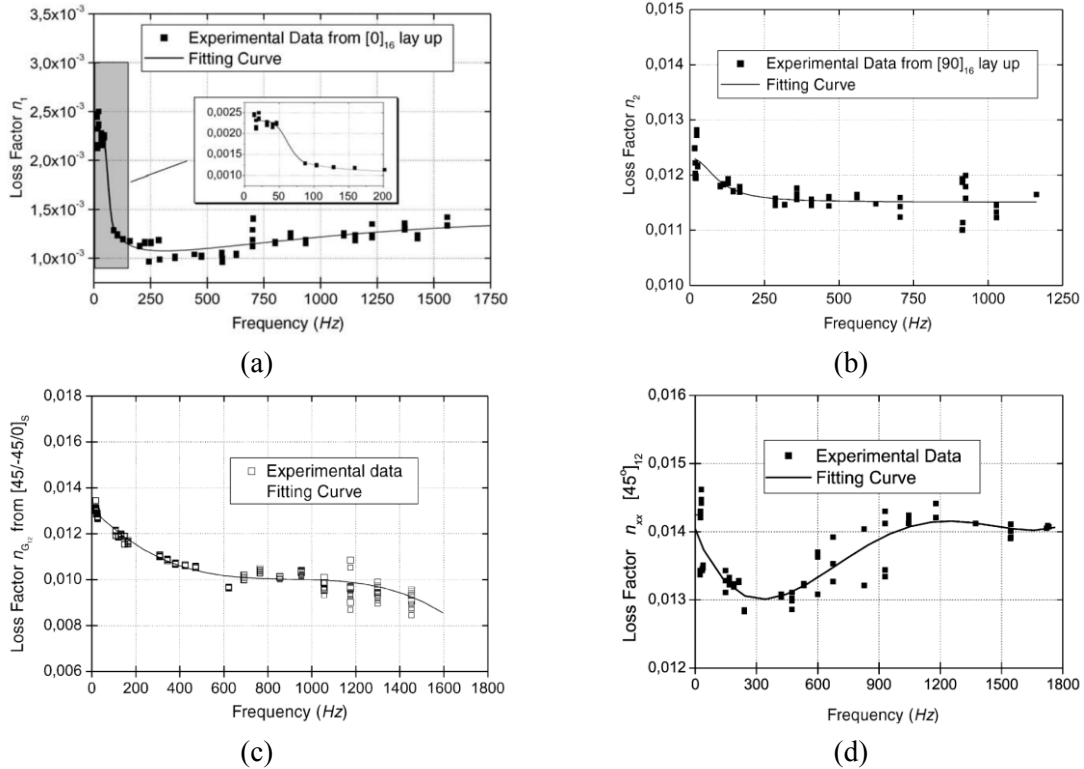


Figure 1.13. Loss factor (a) along fiber direction, (b) normal to fiber direction, (c) of in-plane shear, (d) of a UD laminate, of carbon/epoxy system versus frequency [64].

Note that, in hybrid (experimental-analytical) methods for damping identification, the free vibration of beams have been treated analytically according to either Euler-bernoulli assumptions [64], Timoshenko assumptions [73], or treated as a plate [46]. The configuration of test samples in a form of plates [22] has also examined for the assessment and determination in terms of damping using inverse lamination theories. In this regard, the verification of theoretical results by experimental analyses has been, however, scarce.

### 1.2.5 Vibration coupling effect on damping

An extensive amount of research works has been reported in the literature, dealing with improvement of vibration damping, fatigue endurance, and impact resistance in composite structures, by taking various aspects into account. In addition to passive mechanisms mostly employed for suppressing vibration, particular interest has also been paid to the effect of structural constraints and optimal design parameters on the modal damping. The influence of boundary condition and geometry integrated with the aforementioned effective micromechanical and macromechanical factors on damping has been recently evaluated in a few number of studies on

laminated beams and plates [30,45,74,75]. Among all studied parameters, the arrangement of fiber orientation in a component plays a key role as it can significantly change the damping with or without interleaved layers and/or viscoelastic cores. From a design point of view, the other effective parameter acting on the stiffness distribution and in turn the structural damping is the constraint condition.

The damping performance of a fiber-reinforced composite can be decomposed into the coupling and non-coupling energy dissipation terms which correspond to each of the six resulting stress components [76]. Vibration coupling can be affected by the mode of vibration, which is associated with the defined boundary condition and the lamination sequence (fiber orientation) as the most influential factors along with the fiber orientation. Hwang and Gibson [74] investigated the contribution degree of generated stresses for symmetric and antisymmetric cantilever laminated beams. The results were presented for the first three modes of vibration, including two flexural and one torsional modes. It was found that three major stresses contribute to total damping of beams, which are longitudinal normal stress  $\sigma_x$ , in-plane shear stress  $\tau_{xy}$ , and transverse shear stress  $\tau_{xz}$ . The two key coupling modes, namely bending-twisting and bending-extension, were observed, respectively, for symmetric and antisymmetric laminated beams. It should be noted that a symmetric configuration contributes to elimination of the coupling mode between bending and extension (membrane). It was found that the twisting mode of deformation yields the maximum total damping than the flexural modes due to the higher contribution of shear strain energy in the total damping. However, the coupling components in flexural modes are greater than that in torsional mode of deformation for the symmetric and antisymmetric cases.

Maheri [26] also calculated the damping loss factor of square laminated plates under the mixed boundary conditions composed of only clamped and free edges. Plates with four given lamination sequences were taken into consideration, comparing the modal parameters of the first four modes of vibration. The results obtained in [26] are presented in Figure 1.14.

Zabaras and Pervez [77] investigated the effect of bending-stretching coupling for square laminates only under the simply-supported boundary condition. The variation of SDC with respect to the aspect ratio (thin to thick plates) and the lamination sequence (fiber angle) were also studied, given three materials with dissimilar material anisotropy. Considering a composite material, the

results for the SDC of a single layer, a two-layer antisymmetric angle-ply  $[-\theta^\circ/\theta^\circ]$ , and a three-layer symmetric cross-ply  $[0^\circ/90^\circ/0^\circ]$  plates versus the ply angle are given in Figure 1.15. The results demonstrate that the damping property of a single layer is minimum at a fiber angle about  $45^\circ$ , while the SDC associated with the third mode of vibration attains the highest value at the same ply angle. For laminate  $[-\theta^\circ/\theta^\circ]$ , the fiber angles of  $0^\circ$  and  $90^\circ$  yields the maximum SDC in the first mode. The optimum fiber orientations for the greatest SDC are near  $25^\circ$  and  $65^\circ$  ply angle in the second mode shape, though. In the case of laminate  $[0^\circ/90^\circ/0^\circ]$ , the SDC varies in the same fashion, indicating that the SDC is minimum at  $45^\circ$  for both first and second modes.

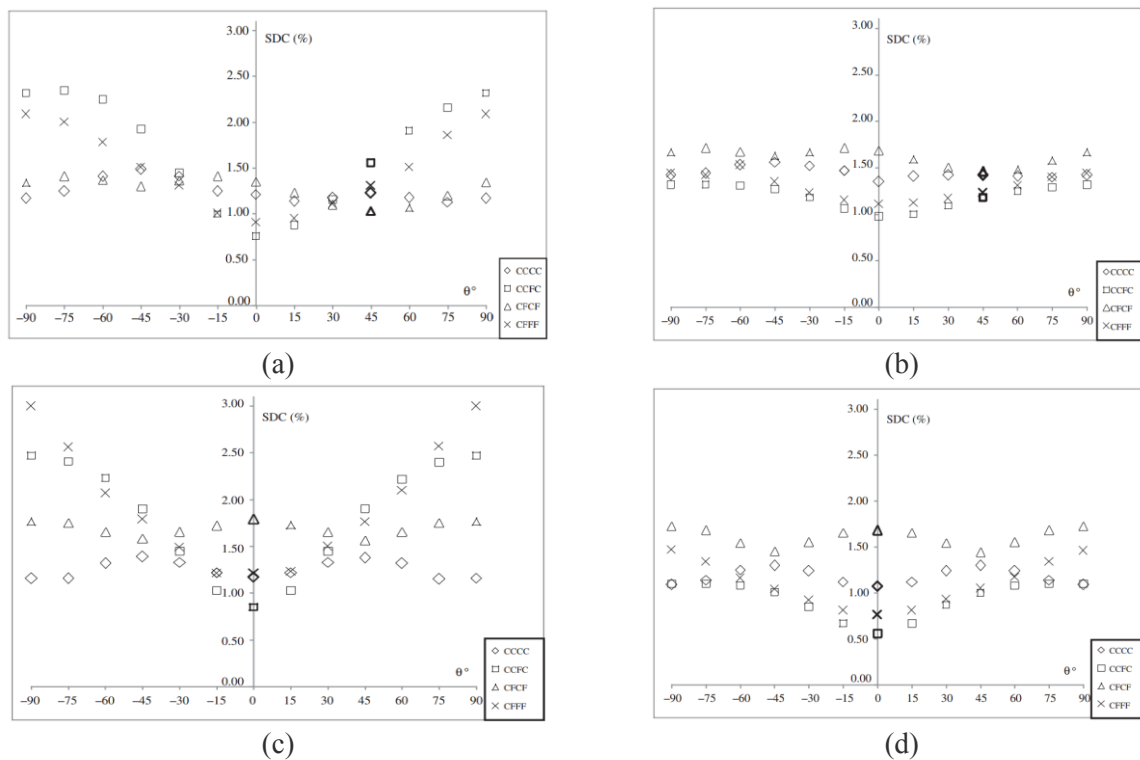


Figure 1.14. Variation of the fundamental SDC (%) for laminate (a)  $\pm 45^\circ$ , (b)  $\pm 45/0^\circ$ , (c) cross-ply, (d) all-zero [26].

Such effects is also examined by Li and Narita [78], where three-layered sandwich square and rectangular plates comprised of a viscoelastic core were considered. In their work, the maximum loss factor associated with the fundamental frequency was found against the fiber orientation of the orthotropic layers. Table 1.2 lists the optimum fiber angle determined for the maximum fundamental loss factor of plates under some general edge conditions chosen from the 18 boundary conditions considered in their research work. In the same work, they also presented the optimal



solution or layup for the maximum loss factor of the fundamental mode for a symmetric 8-layered plate of two different orthotropic materials.

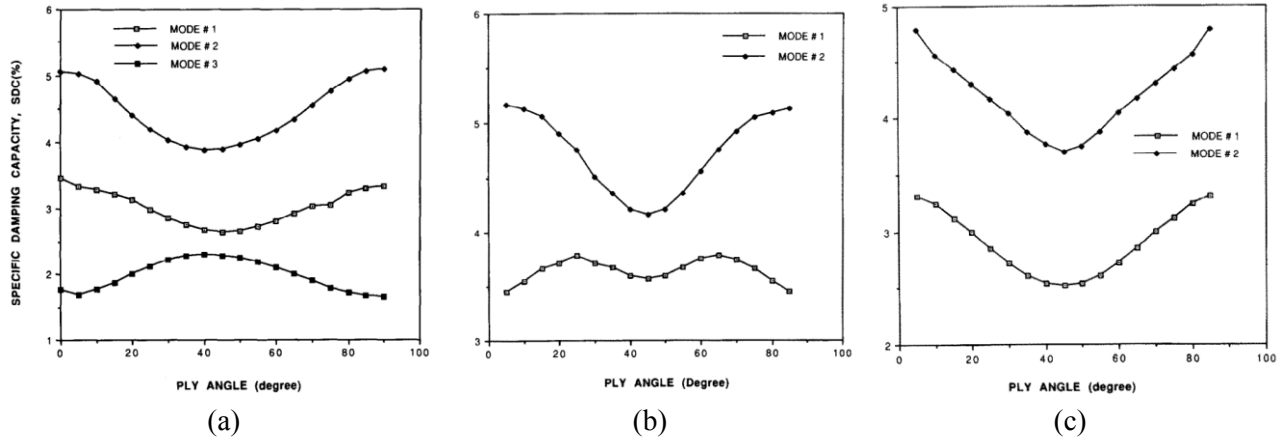


Figure 1.15. Variation of predicted SDC for as a function of ply angle for simply-supported laminates, (a) a single layer, (b) angle-ply  $[-\theta^\circ/\theta^\circ]$ , (c) cross-ply  $[0^\circ/90^\circ/0^\circ]$  [77].

Therefore, the aforementioned analyses done towards the maximum structural damping have demonstrated that it is necessary to take the effect of boundary conditions as well as the layup configuration into account.

Table 1.2. Optimal fundamental loss factor for square and rectangle laminated sandwich plates with viscoelastic core [78].

Square laminates ( $a = b$ )			Rectangular laminates ( $a = 2b$ )		
B.C.	$[\theta]_{opt}$ (°)	$[\eta]_{opt}$ (%)	B.C.	$[\theta]_{opt}$ (°)	$[\eta]_{opt}$ (%)
SSSS	46	15.39	SSSS	38	14.70
SSSF	52	10.50	SSSF	48	18.34
SFCS	-38	14.48	SFCS	-46	19.73
SFCF	34	14.18	SFCF	32	14.33
CSFF	-42	11.63	CSFF	-38	13.32
CFCF	34	14.92	CFCF	-34	16.09
CFSS	44	14.41	CFSS	90	14.89
CCCF	32	14.81	CCCF	32	15.11

B.C.-Boundary condition

### 1.3 Motivation and objective

Composite materials contain a large number of structural components spread through the bulk of a body. It is advisable to consider all the effective elements, i.e. the size, type of material, and volume fraction of reinforcement, medium (matrix), or fiber-matrix interfacial bonding along with inevitable defects. Experimental characterization methods mostly give information on effective

characteristics of composites, considering the influence of all constituents, even those unfavorable. Characterization of the mechanical properties of fiber-reinforced composite materials requires a huge amount of effort due to their non-homogeneity.

Referring to the previous discussions and the presented literature, it has been found that there are a large number of methods to characterize composite materials. Various conventional, refined, and developed experimental procedures for material characterization of composites have been extensively investigated and compared. In regard to damping, a comprehensive review on dissipation mechanisms, mathematical modeling and formulations, as well as experimental characterization methods were also presented, in particular. Furthermore, the complexities and difficulties associated with experimental studies and the sources of errors were addressed. A number of mechanical identification tests and limitations associated with each characterization scheme have arisen the question how to measure a more number of parameters with a fewer number of mechanical tests and less material consumption for the sample preparation, given the purpose of analysis. Considering above, this research work firstly aims to investigate a mechanical testing technique that simultaneously provides elastic constants and damping properties required for a damped vibration analysis.

The present study also aims to characterize a high-modulus carbon-fiber prepreg system. No information on the material under consideration in terms of damping has been reported in the material data sheets by the manufacturer of the prepreg system. Since, the loss factor along with the storage and loss moduli are required in a vibration analysis, it is of great importance to build up an experimental testing, which will permit easy and reliable measurements of the viscoelastic properties of the composite materials simultaneously. Considering above, the dynamic mechanical analysis (DMA) method has been selected for material identification since it allows for more information about various material properties in a single quick test.

Due to lack of accurate guideline for DMA testing, the present work also concerns about the effect of two major factors, which are comprehensively investigated in order to characterize all in-plane moduli and loss factors accurately and reliably. While the shear properties are basically derived from torsional tests, the study is also concerned with illustration and experimental validation of a simple method by which the effective in-plane elastic modulus and damping of a ply can be determined using a beam sample under bending deformation rather than torsional mode.

The characterized properties are then used as input data into a developed finite element code to predict vibration responses of the clamped laminated beams and plates. The vibration properties of the laminated components are evaluated computationally and experimentally so as to evaluate the experimentally measured properties from two different DMA configurations. Finally, the dynamic characteristic of square laminated plates are studied numerically, considering different boundary conditions and lamination sequences. In this respect, a parametric study is formulated to seek optimal fiber orientation of a laminate under a given boundary condition, which results in maximum variations in the natural frequency, loss factor and a normalized objective as a function of resonance frequency and loss factor in free vibrations.

Accordingly, the specific goals of this research study can be summarized as follows:

- (i) To conduct a comprehensive review of reported studies on experimental methods for characterization of viscoelastic properties of fiber-reinforced composites;
- (ii) To examine the DMA technique for accurate identification of viscoelastic properties, considering the clamp configuration and the sample aspect ratio (length-to-thickness);
- (iii) To characterize the unknown damping parameters of a carbon fiber-reinforced prepreg system;
- (iv) To investigate dynamic (vibration) characteristics of laminated beams and plates through modal experiments and FE analyses based on the DMA test results;
- (v) To identify the optimal fiber orientation of a unidirectional beam for the maximum modal loss factor (damping) through experimental modal analyses and FE formulation;
- (vi) To conduct a parametric study by formulation of an objective function for identifying optimal fiber angle in various laminates under different boundary conditions;

## **1.4 Organization of thesis**

This thesis has been compiled on the basis of requirements described in “Thesis Preparation and Thesis Examination Regulation” booklet of the School of graduate Studies at Concordia University. The work includes seven chapters addressing the review, formulations, methods, experiments and results associated with the objective of each chapter.

Chapter 1 features an introduction to the research, and an extensive literature review providing clarification on motivations as well as objectives of the present study. The organization of the thesis is also presented in the same chapter.

Chapter 2 presents the overview on out-of-autoclave materials and remarks associated with their fabrication and application. The method of lamination, curing process as well as sample preparation using the material under consideration are also addressed in this chapter.

Chapter 3 is devoted to comprehensive description on the procedure of dynamic mechanical analysis (DMA) and its principles. The viscoelastic material properties are then characterized using unidirectional beam coupons tested by two clamp setups. The results are then compared in terms of two effective factors under consideration.

Chapter 4 provides an overall summary of lamination theories and solutions. A finite element (FE) formulation based on the first-order shear deformation theory (FSDT) is developed. Then a detailed comparison is made between the developed model and those given in earlier reported studies to validate the accuracy of the FE formulation to obtain modal parameters.

Chapter 5 is dedicated to experimental modal analyses on laminated beam and plates fabricated with identical plies in terms of the material. The experimentally measured resonance frequencies and modal damping factors are then compared with those obtained using the FE model based on the characterized properties using the DMA testing.

Chapter 6 develops a parametric study for realizing optimal fiber angle for maximum modal damping and/or frequency of square laminated plates. The effects of boundary conditions and laminate configurations on vibration characteristic is investigated using the developed FE model.

Chapter 7 finally brings the thesis to the end by providing major contributions of the research work, overall conclusions along with some recommendations for future work.

## CHAPTER 2

### MATERIAL SELECTION AND SAMPLE FABRICATION

#### 2.1 Overview of out-of-autoclave technology

An autoclave-cure process is an integral part of the fabrication of almost all composite material structures. This curing technique was basically developed for resin systems cured at elevated pressure as well as temperature, resulting in a completely uniform final part. Although, the autoclave-cure process is still a reliable and stable procedure in composite manufacturing, the disadvantages in terms of large expenditure on tooling and processing and limitations on the part size have driven the industry to alternate manufacturing processes. To address this issue, various cost-effective alternatives such as resin transfer molding (RTM), and vacuum-assisted resin transfer molding (VARTM), and other liquid molding techniques have been devised to replace the conventional autoclave-cure procedure [79]. The key parameters such as resin infusion and flow pattern, the number and location of vacuum and/or injection ports are regarded as inherent and inevitable concerns involved in these processes. A great deal of work is thus required to perform costly trial-and-error analysis for an optimum quality part. Owing to the capability for fabrication at lower pressure and temperature, the out-of-autoclave (OOA) manufacturing process has demonstrated to be a reasonable manufacturing method as the flaws associated with the aforementioned methods have been generally overcome by the OOA process [80,81].

Among cost saving alternatives to the autoclave processing, the vacuum bagging only (VBO) process has a great appeal. OOA prepregs formulated for VBO processing under atmospheric pressure are basically thermosets because of their low viscosity and capability for low pressure fabrication. Removing the requirement for autoclave pressure has allowed elimination of nitrogen gas, less sizing constraints (larger scale products) and lower operational costs. The two common applied methods to produce VBO prepregs involve either partial impregnation of fibers/fabric or perforated resin films. However, the former has been employed to a large extent rather than the latter. Among three generations of OOA prepregs distributed to date, recent advances have led to a number of third generation commercially available in the market that have desirable mechanical properties and part quality parity with autoclave-cure materials designed for primary aircraft

structures. Figure 2.1 depicts variation of desired parameters of three OOA prepreg generations expected by Boeing.

There still exists some limitations to flexible manufacturing of OOA systems such as automation in lay-up, void reduction, and adhesive compatibility in sandwich panels. Thus, the knowledge of the void volume is always desirable as the void content of a composite material may deteriorate desirable strength and mechanical properties and yield a part with inferior quality. Thus, in addition to the lamination (molding) process, the consolidation and cure cycles must be effectively managed in order to yield a sufficiently void-free laminate. There exists a significant body of knowledge and investigation that shed light on void formation due to ambient factors [82-85]. Owing to recent advances, OOA prepregs intended for VBO processing ensure uniformity of resin distribution with the aim of less resin-rich pockets and dry spots.

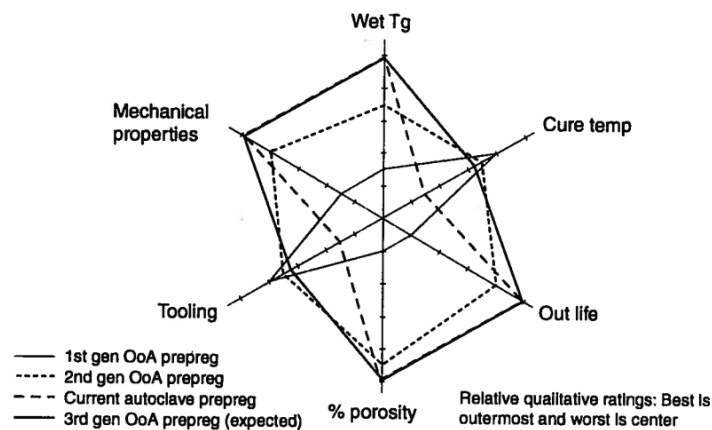


Figure 2.1. OOA prepreg generations targeted by Boeing [81].

Due to the lower level of applied pressure, the OOA process is typically a protracted procedure due to the required time for extraction of entrapped air and moisture, comparing with the autoclave-cure procedure performed under higher pressure. Figure 2.2 represents the consolidation process of pre-impregnated laminates. Further to debulking required after layup (Figure 2.2b), there must be an extension to vacuum time for volatile (i.e., excessive carrier solvent, water, and reaction by-products) management before initiation of curing cycle, depending on the size and complexity of structural parts. Using the edge-breathing or porous dam strategy, it is required to maintain a path for the air to escape. Considering this, porous dams are placed at the edge of the laminate, letting the air or gas to evacuate while restricting resin loss. Edge breathing dams can also be replaced with sealant tape wrapped in a fiberglass cloth.

Edge breathing also restricts resin loss while allowing the air to escape. On the other hand, it is not called an easy job to extract the absorbed moisture by the means of VBO technique, in particular, for epoxy resins highly prone to humidity captivation.

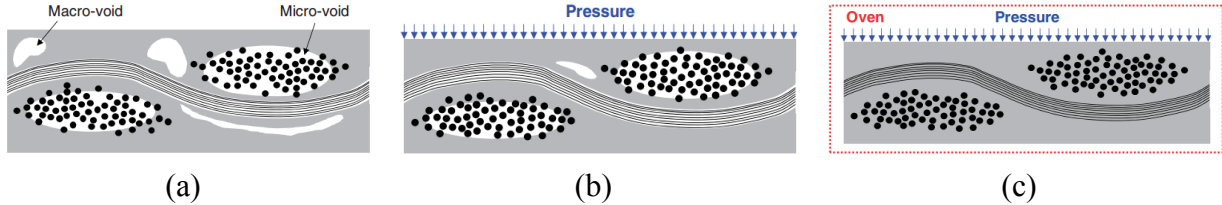


Figure 2.2. Consolidation stages, (a) tape placement with compaction roller, (b) vacuum compaction or debulking under room temperature, (c) Curing with ideally void-free composition [84].

Additionally, OOA partially pre-impregnated composite systems, involving both dry areas and resin-rich regions, are delivered in different initial configurations before consolidation and curing stages. Depending on suppliers, these arrangements have been designed in order to assure uniformly distributed resin with less entrapped air and void. Available architectures for resin distribution in OOA preregs are illustrated in Figure 2.3 [83,84]. Compared with thermoplastic preregs with unlimited shelf life, thermoset composite preregs must be kept frozen since they have limited storage life due to the partly cured resin constituent.

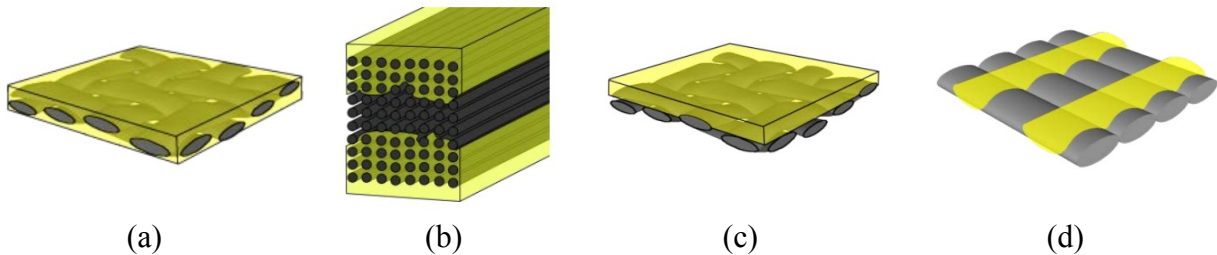


Figure 2.3. Classification of preregs before processing, (a) impregnated with dry tows, (b) UD tape with central dry tows, (c) resin film on fabric bed, (d) resin strips on fabric bed [83].

## 2.2 Material selection

### 2.2.1 CYCOM 5320-1 resin system

Owing to the prospect of the lower curing temperature, and the cost effective fabrication as the most potential benefit of OOA systems, this research is directed towards determination of dynamic mechanical properties of a toughened carbon/epoxy composite designed as a third generation OOA

prepreg system. The material selected for this study is referred as Cycom 5320-1, which is supplied by Cytec Engineered Materials Inc. for aerospace application. The material (an out-of-autoclave cure epoxy/carbon fiber system) is available in a nearly six-inch wide unidirectional prepreg tape. The prepreg system consists of typical fiber areal weight and resin content of 145 g/m<sup>2</sup> and 33%, respectively. This material is tacky and is supplied with a backing paper. Concerning the elastic constants required in this study, Table 2.1 also reports the material properties provided in the open literature by the supplier. However, no information in terms of damping properties have been found.

Table 2.1. Elastic properties from conventional static tests at room temperature.

Test method	Standard	Condition	Test Sample	Elastic Properties (GPa)
Tension Test	ASTM		[0] <sub>8</sub>	E <sub>1</sub> =156
	D3039		[90] <sub>16</sub>	E <sub>2</sub> =9.7
Compression Test	SACMA		[0] <sub>8</sub>	E <sub>1</sub> =143
	SRM01R94		[90] <sub>16</sub>	E <sub>2</sub> =9.9
Shear Test	ASTM	1500-5500 $\mu$ in/in	[+45/-45] <sub>2s</sub>	G <sub>12</sub> =5.2
	D3518	500-3000 $\mu$ in/in		G <sub>12</sub> =5.6

## 2.3 Fabrication process

### 2.3.1 Lamination procedure

The sample laminated plates are fabricated from a unidirectional prepreg tape by hand layup process, using vacuum-bagging, under atmospheric pressure and subsequently cured and post-cured in a convection oven. A schematic drawing illustrating the cross section of the vacuum bagging arrangement of a laminate is shown in Figure 2.4.

Prior to curing, each new ply is compacted on the existing one by applying a compaction force using a compaction roller. This allows physical constraints to relieve, providing passageways to deplete the amount of the entrapped air and possible volatiles. The stack of plies is laid on an Aluminum tool plate, when a thin layer of the release agent dries after 15 minutes. Next, the edge dams are formed using a fiberglass cloth wrapped around the bag sealing compound and then accurately attached to the tool surface along the edges of the laminate stack. A caul plate is also



used to achieve the final laminate net shape. Before the enclosure by a vacuum bag, the entire layup is covered with the fabrics (bleeder and breather) used in the bagging process. The vacuum bag is then sealed around the edges onto the mold plate. The vacuum port is finally placed on the tool plate inside the vacuum bag. Subsequently, the entire assembly is placed in a forced air circulation oven and subjected to a cure cycle as suggested by the prepreg manufacturer. Depending upon the required number of layers, vacuum is also applied after stacking either two or four plies in order to achieve proper debulking and the least level of void content. According to the procedure described in the material data sheet, the composite plates must be held under vacuum for a minimum of 4 hours prior to cure and heat-up as recommended for uniform thickness parts smaller than  $0.6 \text{ m} \times 0.6 \text{ m}$ . The vacuum leak test shows a vacuum loss of 133-400 Pa which is less than the suggested value of 6800 Pa in 5 min.

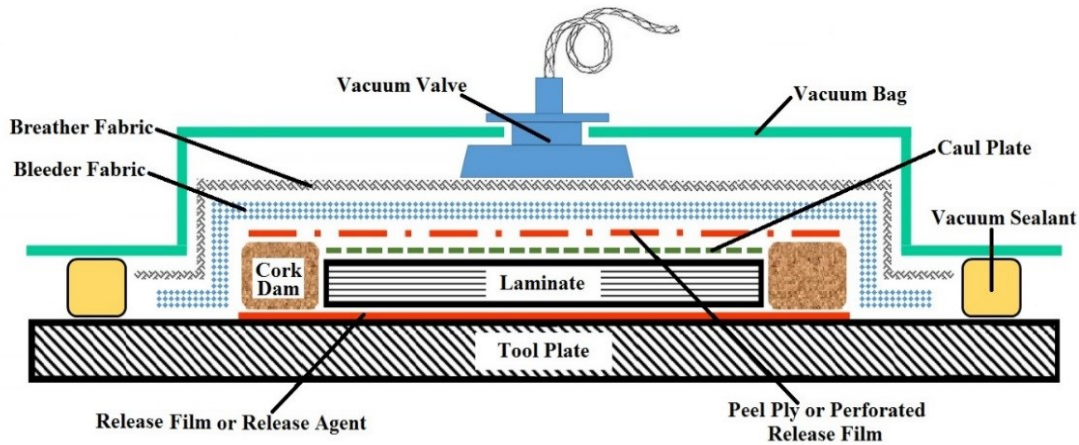


Figure 2.4. Vacuum bag assembly for laminate manufacturing in oven.

Various laminates were fabricated to make coupons for the material characterization and successive experimental verifications. The thickness of each laminate varies between 1.10 mm and 3.25 mm while the nominal thickness per ply of the composite plates remains 0.135 mm and assumed to be the same for all the layers in a laminate component. Ply thickness is calculated by dividing the average measured laminate thickness by the number of plies. It should also be noted that the ply thickness reduces after undergoing the debulking and curing processes, comparing to that of the raw material. The sequence of hand-layup lamination is also depicted in Figure 2.5.

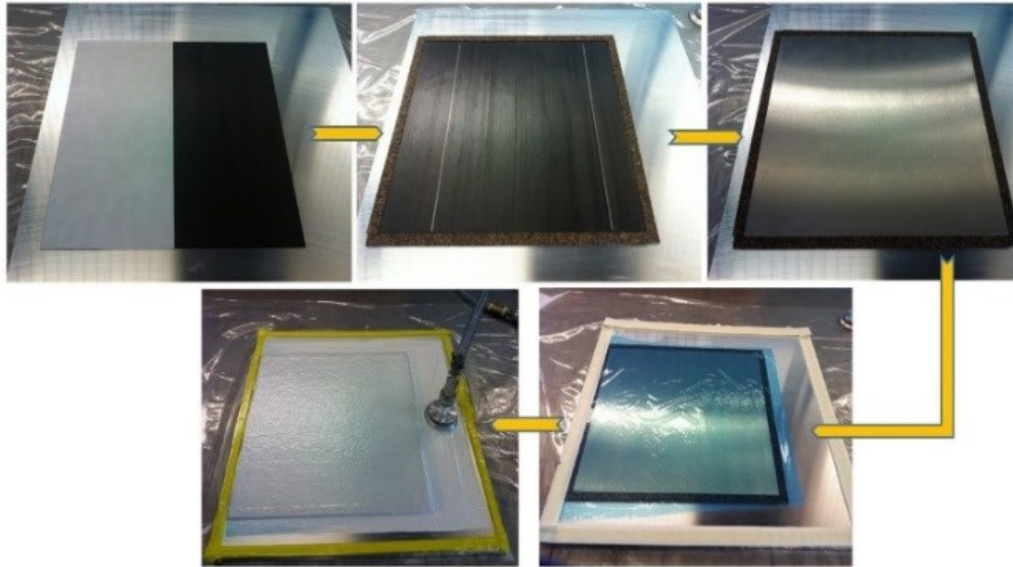


Figure 2.5. Sequence of hand layup process.

### 2.3.2 Curing process

For the given composite system, the thermal profile (temperature and hold duration) through curing steps is flexible, in accordance with the material data sheet. A cure cycle consists of a two-step ramp-and-hold temperature profile. The low temperature ramp-and-hold step represents the curing stage followed by the second (high) temperature ramp-and-hold as the post-cure period. Due to less curing time, between the two alternate curing procedures provided by the supplier, the shorter cure cycle is followed, where the bagged assembly is firstly cured for three hours at  $121 \pm 6^\circ\text{C}$  and then post-cured for two hours at  $177^\circ\text{C}$ , keeping the range of heating ramp between  $0.6^\circ$  and  $2.8^\circ$  per minute, as shown in Figure 2.6. It should also be noted that vacuum pressure is consistently applied through the curing cycle to afford laminate consolidation force. When the curing process is finalized, insignificant resin bleeding or squeeze-out is observed. This can be due to either the vacuum pressure applied consistently or the absence of reaction by-products for epoxy matrix-based composites [86].

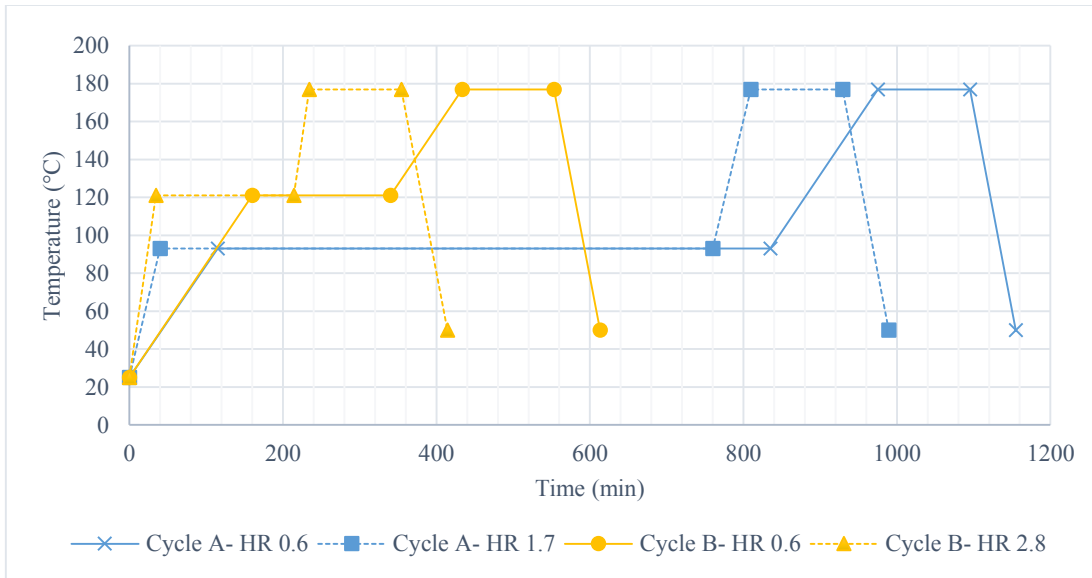


Figure 2.6. Recommended curing cycles by the material supplier.

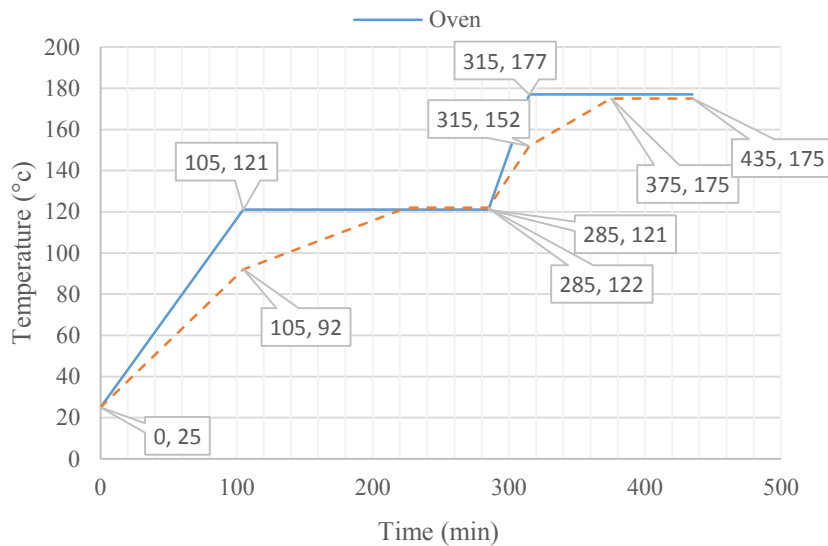


Figure 2.7. Thermocouple measurements of temperature at the tool plate surface (Aluminum base plate) during the cure cycle.

While the cure cycle parameters are attempted to be kept in the manufacturer-recommended range, the conditions of reduced compaction due to bag leaking and temperature difference must be expected. The mismatches associated with the temperature can be due to dissimilar thermal behavior of the tool and part or the non-uniform air circulation inside the oven. Therefore, it is required to control the laminate temperature inside the oven in order to provide the least discrepancy with the recommended thermal profile. The temperature of the part is measured using

a thermocouple directly placed on the part. After running several dummy cycles, a desirable setting point of the oven temperature is obtained on a trial-and-error basis. The oven temperature is then adjusted to compensate for the temperature difference in the system. Figure 2.7 represents the thermal discrepancy that was observed during the initial curing cycle performed.

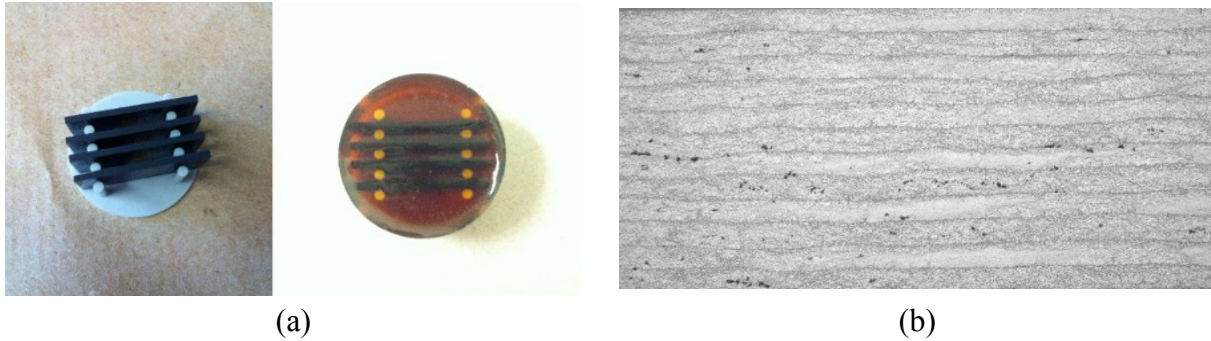


Figure 2.8. Microscopy test, (a) specimens for the microscopic test, (b) digital magnification of fibers aligned perpendicular to image plane.

## 2.4 Quality control

### 2.4.1 Void and fiber fraction analysis

In order to measure the void and fiber volume fractions, the optical photomicroscopy or image analysis is performed using a scanning microscope of type *FeinOptic*<sup>®</sup>. The sheets are sectioned into appropriate sizes to locate samples in the holder, as illustrated in Figure 2.8a. To obtain a representative measurement, sections are cut from the center of cured laminates, where void content is likely to be largest. After curing process, grinding and polishing processes are carried out through the sample thickness. The grinding and polishing processes are crucial since the interpretation of pictures are highly dependent on these processes and the quality of samples. The final values for volume percent of voids and fibers in each laminate is taken as the average from four samples, as shown in Figure 2.8b. The average fiber volume and void content are found to be, respectively, 60-65 % and 1-2 % which are in the same order of those reported in Ref. [87] using acid digestion method, as per ASTM D3171-76.

## 2.5 Summary and conclusions

This chapter mainly focused on an overview of OOA prepreg composite systems, considering the critical remarks on the fabrication processes and properties. In addition, the difference between

an OOA process and an autoclave curing procedure was explained. The mechanical properties of the high-modulus carbon fiber-reinforced composite chosen for the study have been provided, while no information about the damping exists. The manufacturing process of laminates was also fully explained. It was noticed that the curing procedure must be monitored closely due to the temperature discrepancy between the oven and the laminate. Therefore, an optimum thermal profile was found on the basis of trial-and-error in order to attain the laminate temperature profile recommended by the material supplier. Prior to curing, a particular attention was paid to debulking and vacuum bagging to provide less entrapped air and void content. Finally, a scanning microscopic analysis was performed to ensure the quality of samples and to measure the fiber and void volume fractions.

## CHAPTER 3

### DYNAMIC MECHANICAL ANALYSIS (DMA)

#### 3.1 Introduction to DMA

##### 3.1.1 Principles of DMA

The DMA test is considered as a powerful experimental characterization technique performed under oscillating force conditions and analysis of the material's response across a wide temperature and frequency range [88]. DMA tests also give a detailed insight into changes in material curing kinetics and consolidation behavior under imitated practical conditions, such as controlled humidity, temperature, and frequency [89]. Under a harmonic applied force, the specimen exhibits a harmonic deformation or strain lagging behind the load by a phase angle  $\delta$ . The phase difference between the dynamic loading and the dynamic response represents the viscosity of the material or the time required for molecules to rearrange. If the material is purely elastic, the phase difference between the dynamic stress and strain is  $0^\circ$ . On the other hand, a purely viscous material exhibits a dynamic strain lagging of  $90^\circ$ . The behavior of mostly in-service materials reveals a combination of both elastic and viscous behaviors with a phase difference between these two extremes [20,90,91], as shown in Figure 3.1.

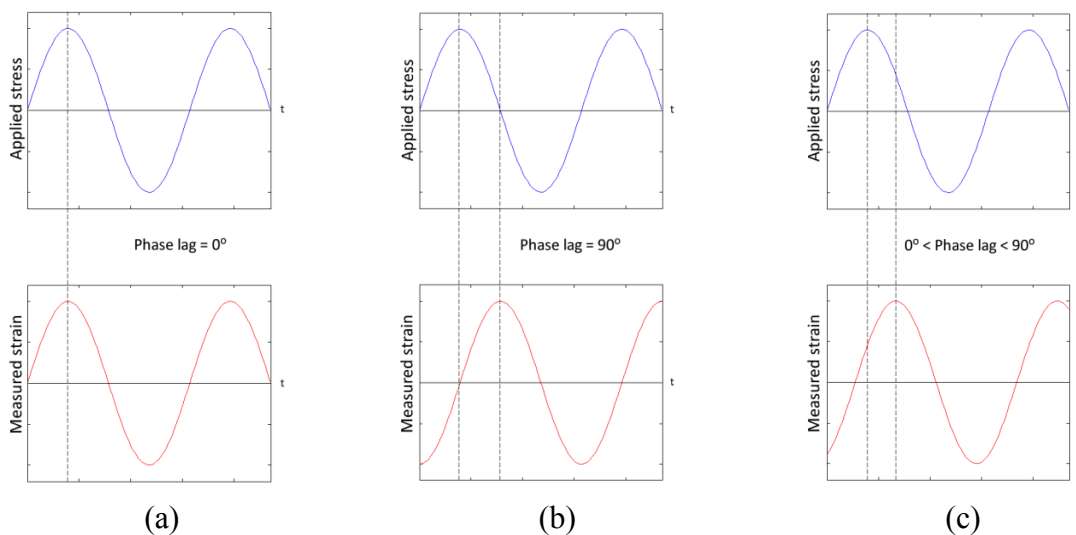


Figure 3.1. Dynamic stress and strain behavior of (a) purely elastic, (b) purely viscos, (c) linear-viscoelastic material [92].

### 3.1.2 Mathematical representation of storage and loss moduli

The applied stress and the strain lagging by the phase angle can be represented as [43]

$$\sigma(t) = \sigma_0 \sin(\omega t + \delta) = \sigma_0 \cos(\delta) \sin(\omega t) + \sigma_0 \sin(\delta) \cos(\omega t) \quad (3-1)$$

$$\varepsilon(t) = \varepsilon_0 \sin(\omega t) \quad (3-2)$$

As noticed from Eq. (3-1), the stress expression can be divided into two components, of which one is in phase with the strain (elastic part) and the other lags 90 degrees behind the strain (viscous part). The resultant of two components is thus  $\delta$  out of phase with the strain.

Using the DMA test, three essential dynamic properties (i.e. the storage modulus, loss modulus, and loss factor) expressing the capability of the material to restore to its initial position can be extracted. For the linear viscoelastic material, the loading input and the response are related by the complex modulus ( $E^*$ ), as [93]

$$\sigma(t) = E^*(\omega)\varepsilon(t) \quad (3-3)$$

The complex modulus is composed of the storage modulus (real component,  $E'$ ), and the loss modulus (imaginary component,  $E''$ ), by

$$E^*(\omega) = E'(\omega) + i E''(\omega) \quad (3-4)$$

The ratio of the loss modulus to the storage modulus is the tangent of the phase angle, called the material loss factor or loss tangent, and represents the material ability to dissipate vibrational energy [88,90].

$$\tan \delta = \frac{E''(\omega)}{E'(\omega)} \quad (3-5)$$

### 3.1.3 Effects of different parameters on DMA results

DMA tests are mostly carried out in many different deformation modes, namely bending, torsion, tension, compression, and shear, using distinct clamping mechanisms. Selection of the clamp type or the test arrangement is dominated by the nature of sample material and geometry. Table 3.1 outlines the test arrangements in terms of the sample geometry and material type, which generally stated in norms and standards [91]. However, there exists other factors such as the magnitude of acting load, sample quality or uniformity, and the degree of orthotropy of material

affecting DMA results. These parameters have been investigated in a few number of research works [19,20].

Table 3.1. Selection of clamp arrangement for DMA testing [91].

Test Arrangement	Material Type	Specimen Geometry
Torsion	High modulus	Long Specimen of rectangular or circular cross section
	Soft or paste-like material	Plate arrangement
Three- or four-point bending	High modulus (fiber reinforced) and low damping material	
Single-cantilever bending	Medium modulus and high thermal expansion	
Dual cantilever bending	Low-to-medium modulus	
Tension		Microtome sections (films, fibers)
Compression	Gels and low modulus	

As reported in the literature, the aforementioned factors in terms of their degree of influence on DMA results are shown in Figure 3.2.

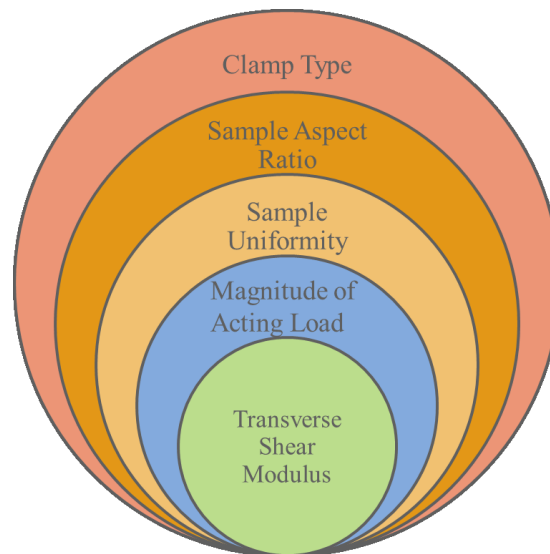


Figure 3.2. Factors playing a role on DMA testing.

### 3.1.4 Disagreements between DMA and static results

Whilst the ASTM standards have been widely employed to exhibit the load-deflection data of fiber-reinforced composite materials, the DMA method is mostly used to investigate the chemical



structure of various polymers (e.g. glass transition and phase transformation temperatures) [90]. As reported in Table 3.2, due to lack of well-defined DMA test procedures for high modulus composites, significant differences exist between the elastic constants obtained from DMA and those extracted from ASTM tests [17,18,94,95]. Substantial discrepancies for similar materials are thus attributed to inadequate understanding of testing conditions and parameters associated with fixtures for the assessment of dynamic properties.

Consequently, the introduced anomalies in values of dynamic elastic modulus of high performance composites have not been regarded as quantitative observations for comparison. Swaminathan et al. [20], however, noticed the anomaly in elastic constants and systematically investigated the factors playing a significant role on accuracy of the DMA results, particularly the longitudinal modulus, using a given clamp type with a nominal span of 20 mm.

Table 3.2. Discrepancies between storage and flexural modulus from DMA and ASTM tests.

Reference No.	Material	Sample size (mm)			Modulus (GPa)	
		Width	Thickness	Span	DMA	ASTM
[94]	Carbon fabric/epoxy 8552	13.0	----	----	10.0 <sup>a</sup>	
[18]	Woven carbon/nanoclay-epoxy	12.0	1.0	10.0	17.99 <sup>a</sup>	37
[17]	Plain weave carbon/nanoclay-epoxy	13.0	1.75	17.5	19.57 <sup>a</sup>	37.11
[95]	Carbon fiber/vinyl ester	5.90	1.0	46.0	63.0 <sup>b</sup>	133.8

<sup>a</sup> Single-cantilevered beam

<sup>b</sup> Three-point bend mode

A number of recent studies addressing accurate measurement of the flexural storage modulus can also be classified in terms of proper choice of test arrangement [90,91] and the effect of load level and span-to-thickness ratio [19,20]. Considering this, the emphasis of the present work is to utilize the DMA in different test configurations to identify the proper test arrangement to yield reliable in-plane elastic and damping properties. To achieve this, the measured material parameters are used into the developed FE model to predict the modal natural frequencies and damping factors. Subsequently, modal vibration tests on various laminated composite structures have been conducted experimentally to validate the simulated modal parameters and thus indirectly the measured material characteristics using the DMA test.

## 3.2 DMA samples

Similar to other mechanical tests, proper specimen preparation and well-conducted test procedures are always emphasized during DMA tests. Sample preparation plays a key role in achieving accurate and reproducible data. Since DMA testing is very sensitive to variations in sample quality and geometry, the laminated plates are cut into specimens using diamond cutter to maintain appropriate plane-parallelism. Uniform thickness is also critical as the plate bending stiffness directly depends on the thickness cubed. Additionally, samples are polished through the thickness to minimize edge roughness and delamination due to machining.

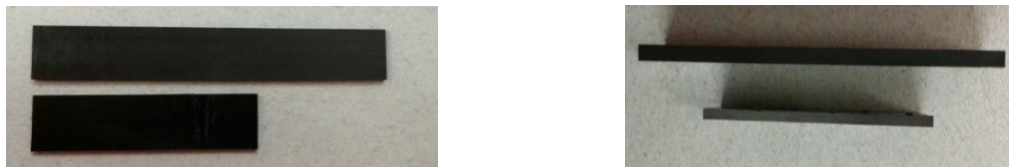


Figure 3.3. DMA specimens for single clamp cantilever and three-point bending setups.

For the set of DMA tests using the three-point bending clamp, the number of plies are 8, 10 and 12. In the case of single-cantilever fixture, the samples are cut from unidirectional laminated plates with 8, 12, and 24 layers. As illustrated in Figure 3.3, the rectangular beam samples with two different dimensions of approximately 35 mm  $\times$  13 mm (length and width) and 60 mm  $\times$  13 mm are used, in the case of single-cantilever and three-point bending setup, respectively. A minimum of three unidirectional specimens for each fiber orientation of 0°, 45° and 90° are used for DMA testing.

## 3.3 Identification of in-plane parameters

### 3.3.1 Determination of in-plane storage moduli

Polymeric fiber reinforced composite structures do not consist of a single lamina in reality. In order to find the engineering constants of a single lamina, more than one lamina bonded together through the thickness are required to bear realistic loads during tests. For any layup sequence, one can find the effective elastic strength or stiffness using a flexural test. The storage moduli of unidirectional laminates in 0° and 90° can thus approximate, respectively, the in-plane elastic mechanical properties in longitudinal and transverse directions.

Furthermore, the off-axis engineering properties of a given orientation can be defined in terms of the extensional moduli of elasticity in the principal material coordinate system. The in-plane shear modulus,  $G_{LT}$ , can thus be evaluated as [27,28]

$$\frac{1}{E_x} = \frac{1}{E_{LL}} \cos^4 \theta + \frac{1}{E_{TT}} \sin^4 \theta + \left( \frac{1}{G_{LT}} - 2 \frac{\nu_{LT}}{E_{LL}} \right) \sin^2 \theta \cos^2 \theta \quad (3-8)$$

where  $E_x$  is the flexural modulus for an off-axis unidirectional laminate. In this study,  $E_x$  is measured using a unidirectional specimen with fibers oriented at an angle of  $45^\circ$  in a DMA bending test, assuming the major Poisson's ratio  $\nu_{LT} = 0.3$ . The moduli  $E_{LL}$  and  $E_{TT}$  also denote the in-plane elastic or storage constants in directions parallel and transverse to the fiber orientation, respectively. The in-plane shear modulus  $G_{LT}$  is then obtained by substituting the values of  $E_{LL}$ ,  $E_{TT}$ , and  $E_x$  from the DMA testing.

### 3.3.2 Determination of in-plane loss factors

Damping properties for composites can be synthesized from on-axis damping value to off-axis damping parameters, and vice-versa, using transformation law. As in the Adams-Bacon approach, the specific damping capacity of an orthotropic laminate in  $x$  direction can be found. According to the assumptions of the classical laminate theory, the total strain energy stored or dissipated in an element of unit volume can be divided into three components associated to the in-plane stresses expressed in the material coordinate system. In the case of the free flexural vibration of a beam along its length, it is assumed that longitudinal normal stress  $\sigma_{xx}$  exists and the rest, i.e.  $\sigma_{yy}$  and  $\tau_{xy}$ , are zero. Thus, the longitudinal normal stress solely accounts for the stress terms in the material axes through the transformation matrix. Considering this and using the strain energy terms as functions of stresses in the material coordinates [28], the specific damping capacity in a given direction is expressed as [28,66]

$$\psi_x = E_x \left\{ \frac{\psi_{LL}}{E_{LL}} \cos^4 \theta + \frac{\psi_{TT}}{E_{TT}} \sin^4 \theta + \left[ \frac{\psi_{LT}}{G_{LT}} - (\psi_{LL} + \psi_{TT}) \frac{\nu_{LT}}{E_{LL}} \right] \sin^2 \theta \cos^2 \theta \right\} \quad (3-9)$$

where  $\psi_{LL}$ ,  $\psi_{TT}$ , and  $\psi_{LT}$  denote the in-plane longitudinal, transverse, and shear specific damping capacities.  $\psi_{LL}$  and  $\psi_{TT}$  are measured, respectively, using test specimens with  $0^\circ$  and  $90^\circ$  configurations, providing the most accurate storage moduli for the material. All of the damping results are recorded at room temperature under linear vibration, leading the damping parameter to

be independent of stress, temperature, and frequency.  $\psi_x$  is also determined by DMA testing on 45° specimen so as to calculate the in-plane shear damping parameter  $\psi_{LT}$ .

### 3.4 Results and discussion

#### 3.4.1 DMA Experiments

Dynamic mechanical measurements of various rectangular samples are carried out using a DMA-Q800 by TA Instruments. The tests are performed in a single-cantilever (with a span of 17.5 mm) and a three-point bending (with a span of 50 mm) fixtures, as illustrated in Figure 3.4

The specimens are loaded in the strain-frequency control mode subject to the controlled isothermal experiment at room temperature with the standard frequency input of 1 Hz. In order to obtain a better result for each test data, tests are repeated three times for each fiber orientation and results are then averaged.

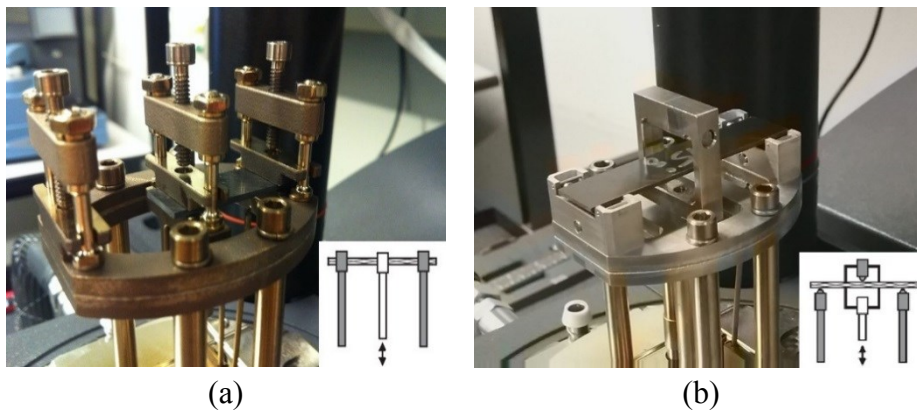


Figure 3.4. DMA test configurations, (a) single-cantilever clamp, (b) three-point bending clamp.

The DMA characterization method is firstly applied to study flexural storage moduli and then damped vibration properties of laminated composites. It should be noted that the procedure focuses only on beam-bend testing method rather than application of two different torsional and bending clamps in order to have consistent boundary conditions in determination of in-plane material properties.

#### 3.4.2 Identification of in-plane storage parameters

##### 3.4.2.1 Single-cantilever arrangement

The specimens under the single-cantilever bending test are examined under a harmonic excitation with frequency of 1 Hz and amplitude of 20  $\mu\text{m}$  applied at the free end. For the study of the aspect ratio, three different thicknesses for the given span are considered. Table 3.3 summarizes the test results for unidirectional carbon/epoxy specimens of 24-ply, 12-ply, and 10-ply using the single-cantilever setup at room temperature. The reported values are averaged over three experiments for each orientation and thickness. Thickness measurements are also taken at four locations and then averaged. Note that the span is the distance between the inside faces of the fixed and movable supports.

Table 3.3. Storage modulus of carbon/epoxy composite using single-cantilever arrangement.

Specimen	Fiber Orientation	Thickness t (mm)	Width w (mm)	Span s (mm)	Aspect ratio (s/t)	Storage modulus (GPa)
24-ply	0°	3.15	14.12	17.60	5.59	27.72
	90°	3.05	14.48	17.65	5.79	6.79
	45°	-----	-----	-----	-----	-----
12-ply	0°	1.60	13.56	17.56	10.97	40.51
	90°	1.64	13.80	17.58	10.72	6.23
	45°	1.63	13.62	17.51	10.74	9.63
10-ply	0°	1.44	12.99	17.59	12.22	46.74
	90°	1.43	12.96	17.49	12.23	5.88
	45°	1.48	12.83	17.59	11.89	11.03

From the data in Table 3.3, it is observed that the higher aspect ratio particularly results in a greater longitudinal storage modulus, while slightly affects other moduli. This demonstrates that the choice of specimen thickness significantly affects the DMA results, as other dimensions are typically kept almost unchanged. Though, the appropriate aspect ratio leading to more accurate parameters cannot be provided easily on account of limitations associated with dimensions and loading performance of DMA analyzers. Given a fiber orientation, the difference in the storage modulus with the thickness can be attributed to the actual stress distribution through the thickness. This is due to the fact that the material can contribute more in a thin specimen than a thick one, which yields a higher value in terms of the storage modulus. Substituting the in-plane storage moduli for 10-ply sample ( $E_x = 11.03$  GPa,  $E_{LL} = 46.74$  GPa and  $E_{TT} = 5.88$  GPa) into Eq. (3-8), the in-plane shear modulus  $G_{LT}$  has been found to be 5.43 GPa.

### 3.4.2.2 Three-point bending arrangement

To investigate the effect of variation in aspect ratio, the coupons of different thickness for a constant span are examined in the case of the three-point bending mode. Note that the range of aspect ratio suggested and studied in the literature and standard guidelines varies from 10 to 40. Although, the aspect ratio for DMA testing recommended by the supplier ranges between 10 and 32, depending upon the material in order to reduce the transverse shear deformation of the beam coupon. This is mainly due to the fact that DMA tests are performed according to the simple beam model, referred to as Euler-Bernoulli theory, which neglects shear deformation and rotational inertia effects in bending mode. The present work is aimed at contributing to the gap between the aforementioned subranges. Thus, the range of 30 to 45 is selected in order to study the effect of aspect ratio.

Results for storage modulus using the three-point bending setup has been provided in Table 3.4. As it can be realized, the storage modulus in longitudinal direction obtained using the three-point bending configuration is much higher than that obtained using the single-cantilever arrangement. Moreover, in contrast to the single-cantilever arrangement, the storage modulus in longitudinal direction decreases as the aspect ratio increases for the case of three-point bending setup.

Table 3.4. Storage modulus of carbon/epoxy composite using three-point bending fixture.

Specimen	Fiber Orientation	Thickness $t$ (mm)	Width $w$ (mm)	Span $s$ (mm)	Aspect ratio $(s/t)$	Storage modulus (GPa)
8-ply	0°	1.15	13.4	50	43.48	133.98
	90°	1.15	13.4	50	43.48	7.82
	45°	1.15	12.97	50	43.48	10.83
10-ply	0°	1.44	12.98	50	34.72	131.02
	90°	1.48	12.89	50	33.78	7.29
	45°	1.45	12.84	50	34.48	12.87
12-ply	0°	1.64	13.01	50	30.49	143.90
	90°	1.64	12.99	50	30.49	9.475
	45°	1.65	12.91	50	30.30	13.962

Examination of Tables 3.3 and 3.4 reveals that there exist substantial differences between storage moduli obtained using single cantilever arrangement and those obtained using three-point bending fixture. For instance, the storage moduli for 10-ply samples with the fiber orientation of

0°, 90°, and 45° obtained by the single-cantilever arrangement are about 35%, 81%, and 86% of the corresponding data obtained using the three-point bending configuration, respectively. Therefore, the greatest difference in properties of elasticity is for samples with the fiber orientation of 0°, followed by specimens with fibers oriented at 90° and 45° in turn. The results clearly show that the types of boundary condition (single-cantilever, three-point bending) have significant effect on the characterized parameters while the effect of aspect ratio is relatively less. It should be noted that DMA testing based on the three-point bending setup provides quite accurate results for elastic storage modulus which reasonably agree with elastic constants reported in the literature using static testing [96]. To better realize this, Table 3.5 compares the results from static and DMA tests. For unidirectional samples, the slight difference between the identified parameters and those obtained as per ASTM standards may be due to the nature of the testing mode, where a flexural loading is applied. It is advisable to perform a comparative analysis, relating the identified parameters to the bending rigidity or modulus as per ASTM D-790, D-6272 or D-7264.

Table 3.5. Comparison of DMA storage moduli with elastic properties from static tests.

Static test					DMA	
Test method	Standard	Test condition	Test sample	Elastic property (GPa)	Storage modulus (GPa) NP*	P*
Tension Test	ASTM D3039		[0] <sub>8</sub>	E <sub>1</sub> =156	140.72	147.1
			[90] <sub>16</sub>	E <sub>2</sub> =9.7	9.428	9.522
Shear Test	ASTM D3518	1500-5500 μin/in	[+45/-45] <sub>2s</sub>	G <sub>12</sub> =5.2	5.442	5.785
		500-3000 μin/in		G <sub>12</sub> =5.6		

NP: Not-Polished

P: Polished

Substituting the storage moduli for the 12-ply specimen from Table 3.4 into Eq. (3-8) yields the in-plane shear modulus of  $G_{LT} = 5.61$  GPa, which is slightly higher (3.5%) than that obtained based on the single-cantilever configuration (5.43 GPa), despite the significant discrepancies in the measured storage moduli.

### 3.4.3 Identification of in-plane damping parameters

As for the evaluation of elastic properties, DMA identification experiments for loss factors are similarly performed at the standard frequency of 1 Hz and room temperature. This means that the

damping dependency on the temperature and frequency is neglected. As a very small strain amplitude is used throughout the DMA measurements, it is assumed that the damping coefficients ( $\psi_{LL}, \psi_{TT}, \psi_{LT}$ ) are also independent of stress. Hence, the variation of stress across the cross section of any unit cube of material is not taken into account. No attempt is made to investigate the micromechanics, yet the overall damping properties of a ply in the material direction, which relates to that of all constituents. This measurement methodology may be useful since manufacturing faults and defects such as incomplete adhesion between plies and voids are likely to happen, which affect the vibration damping.

As shown before, DMA test based on the three-point bending configuration provided results with sufficient accuracy in terms of the elastic (storage) modulus, thus this configuration was chosen to determine damping parameters. The results for in-plane loss factors and also specific damping capacities for unidirectional coupons with fiber angles of  $0^\circ$ ,  $90^\circ$  and  $45^\circ$  are provided in Table 3.6. As expected the sample with unidirectional fiber in longitudinal direction ( $0^\circ$ ) has the lowest loss factor. Whereas damping performance is much higher for  $45^\circ$  coupon.

Table 3.6. Loss factors from DMA testing on 12-ply samples undergoing 3-point bending mode.

Fiber Angle	Loss Factor (%)	SDC parameter (%)
$0^\circ$	$\eta_{LL} = 0.2574$	$\psi_{LL} = 1.6173$
$90^\circ$	$\eta_{TT} = 1.0274$	$\psi_{TT} = 6.4550$
$45^\circ$	$\eta_x = 1.4697$	$\psi_x = 9.2345$

The results from Table 3.6 can then be subsequently substituted into Eq. (3-9) to evaluate the shear loss factor,  $\eta_{LT}$ , and specific damping capacity,  $\psi_{LT}$ , which are found to be 1.76% and 11.058%, respectively. To validate the measured elastic and damping parameters obtained from DMA test, a finite element model including the effect of the transverse shear, is developed based on the DMA test data to evaluate the fundamental damping factors and the natural frequencies associated with the first three vibration modes of unidirectional beam and plate components. The development of the finite element model is described in the following chapter. The FE results are then compared with those obtained using experimental modal test in Chapter 5.

### 3.5 Summary and conclusions

Owing to its distinct advantages of adaptability and controllability, the DMA testing is considered as one of the most powerful and versatile research techniques to investigate the



viscoelastic properties of composite materials and polymers. Due to a number of reports with DMA results for elastic moduli of a high-performance fiber-reinforced material, this chapter was an attempt to bridge this gap by a systematic investigation on the DMA scheme. An experimentally study has been conducted on the DMA method for the identification of the in-plane elastic constants and material damping coefficients of a carbon/epoxy composite system.

The DMA method using two different clamp configurations i.e. single-cantilever and three-point bending has been effectively utilized to measure viscoelastic properties using unidirectional coupons. Under different sample dimensions and quality as well as selection of two DMA fixture setups, determination of the reduced number of viscoelastic parameters was performed using oscillatory bending tests on three individual unidirectional samples with  $0^\circ$  and  $90^\circ$  fiber orientations along with an intermediate angle between the two extremes, i.e.  $0^\circ < \theta < 90^\circ$ . DMA samples are in the form of beams with two distinct length and three length-to-thickness (aspect) ratios. The results clearly demonstrated that the clamp type followed by the aspect ratio significantly affect the accuracy of elastic measures. The experimentally measures from the three-point bending fixture are considerably higher than those from the single-cantilever clamp. Moreover, it has been demonstrated that the storage moduli from DMA testing under three-point bending are in good agreement with those based on static tests. In addition to a proper DMA clamp configuration, an appropriate aspect ratio of 30 yielded more precise results, in the case of high-modulus composites tested in the bending mode.

The damping properties have only been evaluated and quantified using the three-point bending configuration, where the closest correlation has been achieved in terms of the storage moduli. In order to assess the capability of the DMA test for predicting damping properties, in particular, the measured properties will be utilized in a developed FE model to estimate the modal frequencies, which depend on elastic properties, as well as damping factors.

## CHAPTER 4

### FINITE ELEMENT FORMULATION AND MODELING

#### 4.1 Introduction

In the analysis of structural problems, besides experiments, the response characteristics can be obtained mathematically using exact (analytical) or approximate techniques based on existing plate theories. Either numerical or analytical approach is utilized according to the nature of the problem, the degree of accuracy required, and the complexity of a structure due to geometric and lamination parameters, loading and support conditions, as well as complex effects [97]. To predict the mechanical behavior of multilayered laminated composite and sandwich plates and shells for bending, buckling, vibration, failure, and fatigue assessment, analyses of composite plates are generally conducted based on either the two- or three-dimensional plate theories. Using three-dimensional approaches, each layer is modeled as a 3-D element, while 2-D approaches treat a problem of a laminated system as an equivalent single layer through the thickness direction. 3-D solutions are inherently difficult to obtain for a general or practical layered structure. 2-D theories are the reduced form of the traditional 3-D elasticity theory by making suitable assumptions for the displacement distribution or the stress state in the thickness coordinate [98].

The classical lamination plate theory (CLPT) and its refinements, namely the classical first-order shear deformation theory (FSDT) and advanced higher-order shear deformable theories (HSDT), are known as the equivalent single layer (ESL) theories. The other class of variable formulation for composite structures are referred as the layer-wise (LW) theories [99]. Compared with ESL theories, the LW or layer-by-layer descriptions were proposed with aim at overcoming the restriction of the available ESL type models. LW theories satisfy the required continuity conditions at layer interfaces toward a better understanding and representation of the structural behavior due to localized and interlaminar effects, which are of great importance and interest in the framework of analysis of thick multilayered structures [100]. The application of layer-wise theories lead to costly computations for accurate results, on account of numerous unknowns directly dependent on the number of layers. While ESL approaches yield inaccurate results across interfaces, they sufficiently provide satisfactory overall responses in terms of transverse deflection,

natural frequencies, and force or moment resultants at low computational cost. Another alternative formulation avoiding deficiencies pertaining to the ESL and LW models is known as zig-zag models, where interface equilibrium and compatibility conditions are introduced with a less number of unknown variables [101]. The application of zig-zag models for the analysis of laminated composite structures can be done in the framework of the required variational statement, namely the displacement, stress, or mixed theorem, for the formulation and derivation of governing equations [102]. In the case of the displacement-based theories, the zig-zag models can be integrated into the conventional CLPT, FSDT, and HSDT theories. Whereas, both the displacement and stress fields are considered in enhanced mixed models or theories that have been established based on the Reissner's mixed variational theorem (RMVT) appeared in 1980s [103]. The displacement and/or stress fields in the thickness and in-plane directions can be separately described using functions with different orders of expansion or continuity.

The degree of continuity of a variable through the laminate thickness, i.e. displacement and/or stress, has inspired many researchers to intensify further effort on the development of a large variety of 2-D theories in order to provide approximate results with relatively higher magnitude of agreement with exact elasticity solutions. Various shape functions expressed with linear, parabolic [104], trigonometric [105], hyperbolic [106], and exponential [107] representations for transverse displacement or stress variables have also been proposed and adopted in the literature. The refinement and expansion of variable fields have led to introducing additional unknowns. Among them, a number of higher-order or advanced theories require numerous terms that may not have physical meaning

The free or forced vibration analyses of components made by composite materials are considerably complicated than isotropic counterparts, because various parameters must be taken into account due to the nature of non-homogeneity. In the open literature, among all developed and applied theories, two displacement-based ESL models, i.e. CLPT and FSDT, have been widely used. In both CLPT and FSDT [108], the inextensibility and/or normality restrictions are applied to transverse straight lines before and after deformation. While both transverse shear and transverse normal effects are neglected in CLPT, a constant transverse shear strain is assumed in FSDT. Therefore, FSDT is more quite acceptable for the study of relatively thick laminates to predict the dynamic properties. Compared with other shear deformation theories respecting free

boundary conditions on the top and bottom surfaces, FSDT requires arbitrary shear correction factors, though.

With respect to the approaches applied on the basis of the lamination theories, a large amount of attempt have been devoted to develop approximate (numerical) techniques to encompass all of the conditions that cannot be satisfied by the exact or analytical solutions. This is due to the fact that analytical solutions are generally limited to relatively simple geometries and loading situations. For the purpose of dynamic modelling, three approximate methods are usually adopted: the Rayleigh's method, the Rayleigh-Ritz (RR) technique, and the finite element (FE) analysis. The application and accuracy of the first two techniques completely depends on the choice of admissible functions representing the variable field in the conformity with the prescribed boundary conditions. Thanks to their applicability and suitability for analysis of a practical component with any complex geometry and loading situations, either commercial or in-house FE codes are considered as a viable approach to analyze dynamic and vibration characteristics of laminated composite structures [11].

A further discussion and various comparative studies on plate theories and models available for the stress and vibration analysis of layered structures have been well assessed in the exhaustive review articles [97,101,109-113].

## **4.2 FE Formulations**

In this research study, an in-house FE program is developed in the MATLAB<sup>®</sup> environment to analyze the free vibration behavior of multilayered components. A displacement-based lamination theory is formulated to calculate the linear elastic behavior and damping properties of structures from the properties of an individual ply. Among the various plate theories developed for modeling of laminated composite structures, the first-order shear deformation theory (FSDT) is employed in the present study. Compared with other theories, the advantage of the FSDT is the balance between computational efficiency and accurate global response of thin and moderately thick multilayered composites [114,115].

#### 4.2.1 Displacement, strain and stress fields

A finite element (FE) model for beam and plate structures is developed based on the FSDT to predict natural frequencies. The FE model is formulated using a four-node rectangular element with five degrees of freedom (DOFs) per node including spatial translations and rotations of the transverse normal about  $x$ - and  $y$ -axis. It should be mentioned that a selective numerical integration technique is also applied so as to avoid shear locking associated with the FSDT model. The method used for the numerical integration is successively explained in detail. Figure 4.1a depicts an equivalent single-layer rectangular element representing a multilayered element formed by layers of unidirectional long fibers embedded in a matrix material.

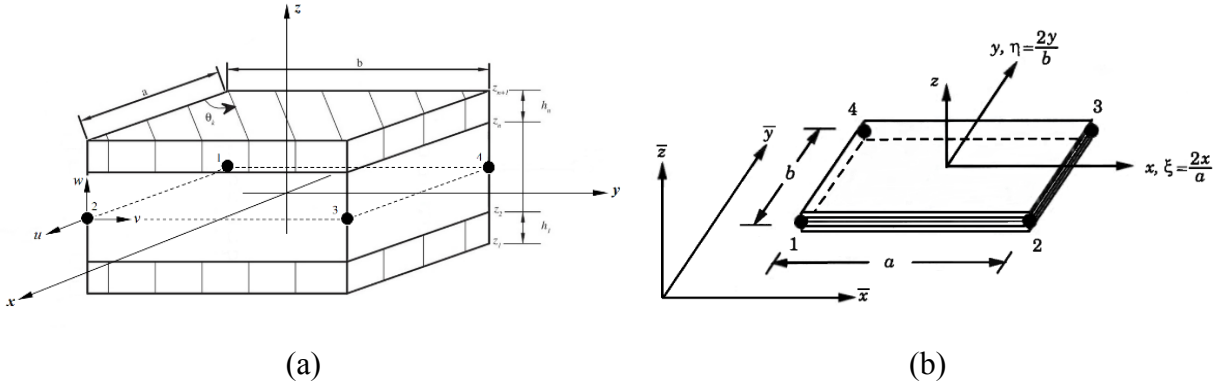


Figure 4.1. Illustration of (a) the laminated composite element, (b) the coordinate systems.

The longitudinal and transverse displacement fields at a point  $(x, y, z)$  in an element can be approximated as functions of the displacements of the corresponding node on the reference plane ( $z = 0$ ). The displacements at point  $(x, y, 0)$  are also defined by interpolation of shape functions and the associated variables in the nodal displacement vector of an element,  $q^e(t) = \{q_1(t) \ q_2(t) \ q_3(t) \ q_4(t)\}^T$ , where  $q_i(t) = \{u_i, v_i, w_i, \theta_{x i}, \theta_{y i}\}^T$  and  $i = 1, 2, 3, 4$  [98]. The evaluation of the displacement fields within an element can thus be described as:

$$\begin{aligned}
 u_e(x, y, z, t) &= u_0^e(x, y, t) + z \theta_{x0}^e(x, y, t) = \sum_{i=1}^4 N_i(x, y) u_i + z \sum_{i=1}^4 N_i(x, y) \theta_{x i} \\
 v_e(x, y, z, t) &= v_0^e(x, y, t) + z \theta_{y0}^e(x, y, t) = \sum_{i=1}^4 N_i(x, y) v_i + z \sum_{i=1}^4 N_i(x, y) \theta_{y i} \quad (4-1) \\
 w_e(x, y, z, t) &= w_0^e(x, y, t) = \sum_{i=1}^4 N_i(x, y) w_i
 \end{aligned}$$

where  $\theta_{x i}$  and  $\theta_{y i}$ , respectively, represent rotations about  $y$ - and  $x$ -axes.  $N_i(x, y)$  also denote the linear Lagrangian interpolation functions of the element for all variables used in the displacement field. The shape functions are required to provide continuity of displacements along common sides between adjacent elements after deformation as expressed in a linear fashion. Bilinear shape function  $N_i$  is, thus, equal to a unit value at node  $i$ , while the rest three functions are zero at the same node [116], as presented in Figure 4.2.

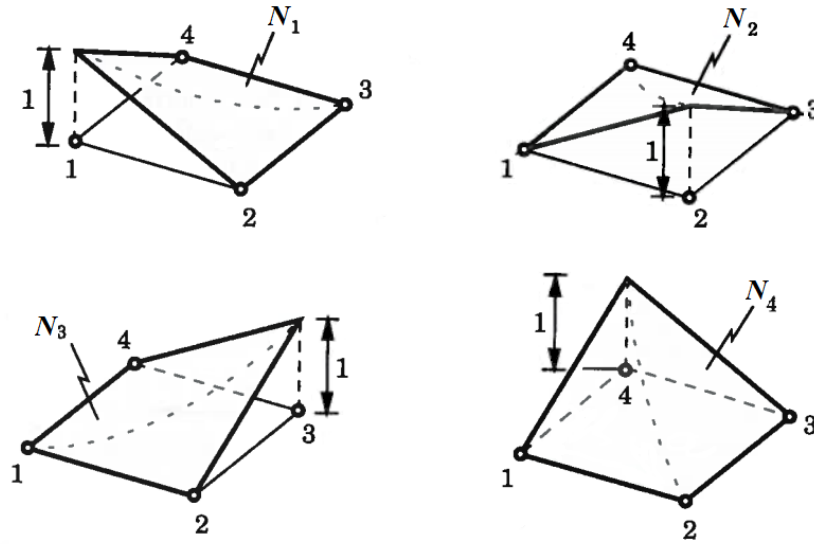


Figure 4.2. Linear rectangular element and shape functions in non-dimensional coordinate [98].

For the sake of simplicity of evaluation and numerical stability, the integrals can be easily expressed in terms of non-dimensional or normalized coordinates by means of transformation from  $(x, y, z)$  coordinates to  $(\xi, \eta, \zeta)$  coordinate system. Therefore, the displacement field in Eq. (4-1) may be rewritten in the following form:

$$\begin{aligned}
 u_e(x, y, z, t) &= \sum_{i=1}^4 N_i(x(\xi, \eta), y(\xi, \eta))u_i + z \sum_{i=1}^4 N_i(x(\xi, \eta), y(\xi, \eta))\theta_{x i} \\
 v_e(x, y, z, t) &= \sum_{i=1}^4 N_i(x(\xi, \eta), y(\xi, \eta))v_i + z \sum_{i=1}^4 N_i(x(\xi, \eta), y(\xi, \eta))\theta_{y i} \\
 w_e(x, y, z, t) &= \sum_{i=1}^4 N_i(x(\xi, \eta), y(\xi, \eta))w_i
 \end{aligned} \tag{4-2}$$

In the normalized coordinate system, functions  $N_i(x, y)$  can be defined by taking product of linear displacement functions in the coordinate  $(\xi, \eta)$  of node point  $i$  in the form

$$N_i = \frac{1}{4} (1 + \xi_i \xi)(1 + \eta_i \eta) \quad \text{and} \quad \eta_i, \xi_i = \pm 1 \quad (4-3)$$

where  $\xi_i$  and  $\eta_i$  represent the position of the side joining nodes 1 to 4 according to the non-dimensional coordinate system, as depicted in Figure 4.1b. The coordinates  $\xi$  and  $\eta$  also denote the positions of any point within the element, i.e.  $-1 \leq (\xi, \eta) \leq +1$ . It should be noted that the coordinate transformation in two dimensions is completely accomplished using the Jacobian operator as

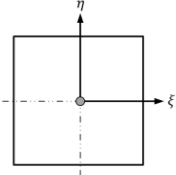
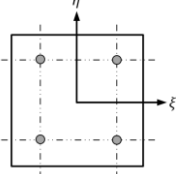
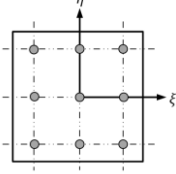
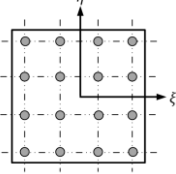
$$\iint dx dy = \iint \det[J] d\xi d\eta \quad \text{or} \quad \begin{Bmatrix} \frac{\partial O}{\partial x} \\ \frac{\partial O}{\partial y} \end{Bmatrix} = [J]^{-1} \begin{Bmatrix} \frac{\partial O}{\partial \xi} \\ \frac{\partial O}{\partial \eta} \end{Bmatrix} \quad (4-4)$$

where  $[J]$  denotes the Jacobian matrix of the geometrical mapping which is developed by the chain rule of partial differentiation. The integration is done by changing the integration lower and upper limits to -1 and +1 in  $x$  and  $y$  dimensions over a typical element. The Jacobian is, thus, given by

$$\begin{aligned} [J] &= \begin{bmatrix} \frac{\partial x}{\partial \xi} & \frac{\partial y}{\partial \xi} \\ \frac{\partial x}{\partial \eta} & \frac{\partial y}{\partial \eta} \end{bmatrix} = \begin{bmatrix} \sum_{i=1}^4 x_i \frac{\partial N_i}{\partial \xi} & \sum_{i=1}^4 y_i \frac{\partial N_i}{\partial \xi} \\ \sum_{i=1}^4 x_i \frac{\partial N_i}{\partial \eta} & \sum_{i=1}^4 y_i \frac{\partial N_i}{\partial \eta} \end{bmatrix} \\ &= \begin{bmatrix} \frac{\partial N_1}{\partial \xi} & \frac{\partial N_2}{\partial \xi} & \frac{\partial N_3}{\partial \xi} & \frac{\partial N_4}{\partial \xi} \\ \frac{\partial N_1}{\partial \eta} & \frac{\partial N_2}{\partial \eta} & \frac{\partial N_3}{\partial \eta} & \frac{\partial N_4}{\partial \eta} \end{bmatrix} \begin{bmatrix} x_1 & y_1 \\ x_2 & y_2 \\ x_3 & y_3 \\ x_4 & y_4 \end{bmatrix} \end{aligned} \quad (4-5)$$

where  $x_i$  and  $y_i$  are the spatial coordinates of defined nodes in the global coordinate system. In order to avoid tedious calculations due to the spatial transformation, a most widely used numerical integration method, known as the Gauss quadrature, is applied to evaluate the integral expressions. The numerical integration is performed on the basis of appropriate selection of the Gauss point number, considering the order of the interpolation shape function. The location of Gauss points and the conforming weights are provided in Table 4.1.

Table 4.1. Gauss quadrature points, locations, and weights [98].

No. of points	Points	weights	Location in element
1	0.0000000000	2.0000000000	
2	$\pm 0.5773502692$	1.0000000000	
3	0.0000000000 $\pm 0.7745966692$	0.8888888889 0.5555555555	
4	$\pm 0.3399810435$ $\pm 0.8611363116$	0.6521451548 0.3478548451	

Then, the integration of a function  $G$  in terms of spatial variables in the normalized coordinate system  $(\xi, \eta)$  can be approximated as

$$\int_{-1}^{+1} \int_{-1}^{+1} G(\xi, \eta) |J| d\xi d\eta = \int_{-1}^{+1} \left[ \sum_{p=1}^P G(\xi_p, \eta) |J| W_p \right] d\eta \quad (4-6)$$

$$\approx \sum_{q=1}^Q G(\xi_p, \eta_q) |J| W_p W_q$$

where  $W_p$  and  $W_q$  are the weights of Gauss points located at  $(\xi_p, \eta_q)$  in  $\xi$  and  $\eta$  directions. Selection of integration points and the corresponding weights depends on the type of element as well as the integration type, namely exact, reduced, or selective.

Using the displacement function, the strain-displacement relations can then be written as

$$\varepsilon^e(x, y, t) = [B](x, y)q^e(t) \quad (4-7)$$

where  $\varepsilon^e(x, y, t) = \{\varepsilon_p^e, \varepsilon_f^e, \varepsilon_s^e\}$ , with  $\varepsilon_p^e$  and  $\varepsilon_f^e$  denoting the extensional and flexural components of in-plane strains and  $\varepsilon_s^e$  representing the transverse shear strain.  $[B]$  represents the



matrix of the derivatives of element shape functions. Matrix  $B$  is composed of submatrices  $[B_p]$ ,  $[B_f]$ , and  $[B_s]$  that constitute the differential operators for extensional, flexural, and shear components, respectively [117]. The strain-displacement matrix  $[B_p]$  is then given by

$$[B_p] = \begin{bmatrix} \frac{\partial N_1}{\partial x} & 0 & 0 & 0 & 0 & \dots & \frac{\partial N_4}{\partial x} & 0 & 0 & 0 & 0 \\ 0 & \frac{\partial N_1}{\partial y} & 0 & 0 & 0 & \dots & 0 & \frac{\partial N_4}{\partial y} & 0 & 0 & 0 \\ \frac{\partial N_1}{\partial y} & \frac{\partial N_1}{\partial x} & 0 & 0 & 0 & \dots & \frac{\partial N_4}{\partial y} & \frac{\partial N_4}{\partial x} & 0 & 0 & 0 \end{bmatrix} \quad (4-8a)$$

The strain-displacement matrix  $[B_f]$  is also provided by

$$[B_f] = \begin{bmatrix} 0 & 0 & 0 & \frac{\partial N_1}{\partial x} & 0 & \dots & 0 & 0 & 0 & \frac{\partial N_4}{\partial x} & 0 \\ 0 & 0 & 0 & 0 & \frac{\partial N_1}{\partial y} & \dots & 0 & 0 & 0 & 0 & \frac{\partial N_4}{\partial y} \\ 0 & 0 & 0 & \frac{\partial N_1}{\partial y} & \frac{\partial N_1}{\partial x} & \dots & 0 & 0 & 0 & \frac{\partial N_4}{\partial y} & \frac{\partial N_4}{\partial x} \end{bmatrix} \quad (4-8b)$$

The strain-displacement matrix  $[B_s]$  is given as

$$[B_s] = \begin{bmatrix} 0 & 0 & \frac{\partial N_1}{\partial x} & N_1 & 0 & \dots & 0 & 0 & \frac{\partial N_4}{\partial x} & N_4 & 0 \\ 0 & 0 & \frac{\partial N_1}{\partial y} & 0 & N_1 & \dots & 0 & 0 & \frac{\partial N_4}{\partial y} & 0 & N_4 \end{bmatrix} \quad (4-8c)$$

Note that the aforementioned strain-displacement matrices can also be expressed in terms of the normalized coordinates to facilitate the integration process for mass and stiffness matrices as expressed in the succeeding section.

#### 4.2.2 FE model of laminated plates

Using strain-displacement relations in conjunction with the constitutive stress-strain equations for an orthotropic material in the  $k$ th lamina and integrating through the thickness yield the expressions for element mass and stiffness matrices as follows;

$$M^e = \sum_e \int_{A_e} [N]^T ([M_1] + [M_2])[N] dx dy \quad (4-9a)$$

$$K^e = \sum_e \int_{A_e} \left( [B_p]^T [\mathcal{A}] [B_p] + [B_p]^T [\mathfrak{B}] [B_f] + [B_f]^T [\mathfrak{B}] [B_p] + [B_f]^T [\mathcal{D}] [B_f] + [B_s]^T [\mathcal{R}] [B_s] \right) dx dy \quad (4-9b)$$

where  $[M_1]$  and  $[M_2]$  denote the inertia matrices and  $[N]$  is the matrix of all interpolation functions. Inertia matrices are described as:

$$[M_1] = \begin{bmatrix} I_1 & 0 & 0 & 0 & 0 \\ 0 & I_1 & 0 & 0 & 0 \\ 0 & 0 & I_1 & 0 & 0 \\ 0 & 0 & 0 & I_3 & 0 \\ 0 & 0 & 0 & 0 & I_3 \end{bmatrix} \quad \text{and} \quad [M_2] = \begin{bmatrix} 0 & 0 & 0 & I_2 & 0 \\ 0 & 0 & 0 & 0 & I_2 \\ 0 & 0 & 0 & 0 & 0 \\ I_2 & 0 & 0 & 0 & 0 \\ 0 & I_2 & 0 & 0 & 0 \end{bmatrix} \quad (4-10)$$

where  $I_1$ ,  $I_2$ , and  $I_3$  are the normal, coupled normal-rotary, and rotary inertia coefficients, respectively, which are defined as [31]:

$$(I_1, I_2, I_3) = \int_{-h/2}^{h/2} \rho (1, z, z^2) dz = \sum_{k=1}^N \rho^{(k)} \int_{z_m}^{z_{m+1}} (1, z, z^2) dz \quad (4-11)$$

where  $\rho^{(k)}$  represents the density of the  $k$ th layer

In Eq. (4-9b), matrices  $[\mathcal{A}]$ ,  $[\mathfrak{B}]$ ,  $[\mathcal{D}]$ , and  $[\mathcal{R}]$  are, respectively, the extensional, coupling, bending, and shear rigidity components of the stiffness matrix of a laminated element, which are used to relate the stresses or resultants to strains [77] as:

In-plane force resultants:

$$\begin{Bmatrix} N_x \\ N_y \\ N_{xy} \end{Bmatrix} = \begin{bmatrix} \mathcal{A}_{11} & \mathcal{A}_{12} & \mathcal{A}_{16} \\ \mathcal{A}_{12} & \mathcal{A}_{22} & \mathcal{A}_{26} \\ \mathcal{A}_{16} & \mathcal{A}_{26} & \mathcal{A}_{66} \end{bmatrix} \begin{Bmatrix} \varepsilon_x^0 \\ \varepsilon_y^0 \\ \gamma_{xy}^0 \end{Bmatrix} + \begin{bmatrix} \mathfrak{B}_{11} & \mathfrak{B}_{12} & \mathfrak{B}_{16} \\ \mathfrak{B}_{12} & \mathfrak{B}_{22} & \mathfrak{B}_{26} \\ \mathfrak{B}_{16} & \mathfrak{B}_{26} & \mathfrak{B}_{66} \end{bmatrix} \begin{Bmatrix} \kappa_x \\ \kappa_y \\ \kappa_{xy} \end{Bmatrix} \quad (4-12a)$$

In-plane moment resultants:

$$\begin{Bmatrix} M_x \\ M_y \\ M_{xy} \end{Bmatrix} = \begin{bmatrix} \mathfrak{B}_{11} & \mathfrak{B}_{12} & \mathfrak{B}_{16} \\ \mathfrak{B}_{12} & \mathfrak{B}_{22} & \mathfrak{B}_{26} \\ \mathfrak{B}_{16} & \mathfrak{B}_{26} & \mathfrak{B}_{66} \end{bmatrix} \begin{Bmatrix} \varepsilon_x^0 \\ \varepsilon_y^0 \\ \gamma_{xy}^0 \end{Bmatrix} + \begin{bmatrix} \mathcal{D}_{11} & \mathcal{D}_{12} & \mathcal{D}_{16} \\ \mathcal{D}_{12} & \mathcal{D}_{22} & \mathcal{D}_{26} \\ \mathcal{D}_{16} & \mathcal{D}_{26} & \mathcal{D}_{66} \end{bmatrix} \begin{Bmatrix} \kappa_x \\ \kappa_y \\ \kappa_{xy} \end{Bmatrix} \quad (4-12b)$$

Transverse force resultants:

$$\begin{Bmatrix} V_y \\ V_x \end{Bmatrix} = \begin{bmatrix} \mathcal{R}_{44} & \mathcal{R}_{45} \\ \mathcal{R}_{45} & \mathcal{R}_{55} \end{bmatrix} \begin{Bmatrix} \gamma_{yz}^0 \\ \gamma_{xy}^0 \end{Bmatrix} \quad (4-12c)$$

The equations relating the force and moment resultants to strains can also be written in concise notation as

$$\begin{Bmatrix} \mathcal{N} \\ \mathcal{M} \end{Bmatrix} = \begin{bmatrix} [\mathcal{A}] & [\mathfrak{B}] \\ [\mathfrak{B}] & [\mathcal{D}] \end{bmatrix} \begin{Bmatrix} \varepsilon_p^e \\ \varepsilon_f^e \end{Bmatrix} \quad \text{and} \quad \{\mathcal{V}\} = [\mathcal{R}]\{\varepsilon_s^e\} \quad (4-13)$$

It is noted that the stiffness submatrices  $[\mathcal{A}]$ ,  $[\mathfrak{B}]$ ,  $[\mathcal{D}]$ , and  $[\mathcal{R}]$ , which are evaluated using the piecewise integration through the thickness of the laminated element, are defined as

$$\begin{aligned} ([\mathcal{A}_{ij}], [\mathfrak{B}_{ij}], [\mathcal{D}_{ij}]) &= \sum_{k=1}^N \int_{z_k}^{z_{k+1}} [\bar{Q}_{ij}]^k (1, z, z^2) dz \quad \text{and} \quad i, j = 1, 2, 6 \\ [\mathcal{R}_{ij}] &= K_i K_j \sum_{k=1}^N \int_{z_k}^{z_{k+1}} [\bar{Q}_{ij}]^k dz \quad \text{and} \quad i, j = 4, 5 \end{aligned} \quad (4-14)$$

where  $K_i$  and  $K_j$  are shear correction factors, typically taken at 5/6 for the rectangular cross section.  $z_k$  and  $z_{k+1}$  also represent the ordinates of the lower and upper surfaces of the  $k$ th layer and  $N$  is the number of layers. The transformed elastic or stiffness coefficients of the  $k$ th layer with respect to  $x$ -axis in the global coordinate  $\bar{Q}^k(\theta_k)$  are related to the components of elastic matrix in the material coordinates  $Q^k(\theta_k)$  by

$$\bar{Q}^k(\theta_k) = T(\theta_k) Q^k(\theta_k) T^T(\theta_k) \quad (4-15)$$

where  $T(\theta_k)$  is the corresponding rotation matrix, and  $\theta$  is the angle of fibers. For a layer with an arbitrary fiber angle, the transformed reduced stiffness components are also given in an expanded form as

$$\begin{cases} \bar{Q}_{11} = Q_{11}m^4 + 2(Q_{12} + 2Q_{66})n^2m^2 + Q_{22}n^4 \\ \bar{Q}_{12} = (Q_{11} + Q_{22} - 4Q_{66})n^2m^2 + Q_{12}(n^4 + m^4) \\ \bar{Q}_{16} = (Q_{11} - Q_{12} - 2Q_{66})nm^3 + (Q_{12} - Q_{22} + 2Q_{66})n^3m \\ \bar{Q}_{22} = Q_{11}n^4 + 2(Q_{12} + 2Q_{66})n^2m^2 + Q_{22}m^4 \\ \bar{Q}_{26} = (Q_{11} - Q_{12} - 2Q_{66})n^3m + (Q_{12} - Q_{22} + 2Q_{66})nm^3 \\ \bar{Q}_{66} = (Q_{11} + Q_{22} - 2Q_{12} - 2Q_{66})n^2m^2 + Q_{66}(n^4 + m^4) \\ \bar{Q}_{44} = Q_{44}m^2 + Q_{55}n^2 \\ \bar{Q}_{45} = (Q_{55} - Q_{44})nm \\ \bar{Q}_{55} = Q_{55}m^2 + Q_{44}n^2 \end{cases} \quad (4-16)$$

where  $n$  and  $m$  denote  $\sin(\theta)$  and  $\cos(\theta)$ , respectively.  $Q_{ij}$  are the reduced stiffness components in the material (on-axis) coordinate of each single layer in a laminated structure, which are functions of engineering parameters as

$$\begin{aligned} Q_{11} &= \frac{E_L}{1 - (\vartheta_{LT})^2(E_T/E_L)} & Q_{44} &= G_{TT} \\ Q_{12} &= \frac{\vartheta_{LT}E_T}{1 - (\vartheta_{LT})^2(E_T/E_L)} & Q_{55} &= G_{LT} \\ Q_{22} &= \frac{E_T}{1 - (\vartheta_{LT})^2(E_T/E_L)} & Q_{66} &= G_{LT} \end{aligned} \quad (4-17)$$

Next, the governing equations of motion are derived, using the kinetic,  $K$ , and total potential energy,  $\Pi$ , expressions, according to the Hamilton's principle based on the virtual displacements. Substituting the prescribed descriptions for the strains, stresses, and resultants into the Lagrangian expression ( $L = K - \Pi$ ) leads to the standard eigenvalue problem for the vibration analysis of a multilayered element in FE form. For a free vibration problem, the energy terms representing the work done by external body or surface forces vanishes. Thus, the equations of motion in the matrix form can be described as

$$[M^e]\ddot{q}(t) + [K^e]q(t) = 0 \quad (4-18)$$

According to standard finite element assemblage procedures, from the elementary matrices accounting for the node connectivity, the system mass and stiffness matrices are constructed. The global governing equations for free vibrations can then be expressed in terms of the system mass  $[M]$ , the system stiffness  $[K]$ , and the vector of global DOFs  $\{d(t)\}$ , as

$$[M]\ddot{d}(t) + [K]d(t) = 0 \quad (4-19)$$

which can then be used to extract the natural frequencies and the associated mode shapes as

$$([K] - \omega^2[M])\{D\} = \{0\} \quad (4-20)$$

where  $\omega$  is the natural frequency, and  $\{D\}$  is the corresponding nodal mode shape amplitude or the eigenvector of the system undergoing free vibration. The FE formulation is successively validated by comparing the results with those reported in the literature in terms of the frequency and damping. It is worth mentioning that in the present work, the complex expressions of the engineering constants (Eq. (1-2)) are employed to represent the dynamic properties of composite

structures based on the VED model. By introducing the complex-valued properties into the developed FE code as input data, the aforementioned equations and matrices are inverted to the form of complex quantities, which leads to the complex expressions for  $[Q_{ij}^*]$ ,  $[\overline{Q_{ij}}^*]$ ,  $[\mathcal{A}^*]$ ,  $[\mathcal{B}^*]$ ,  $[\mathcal{D}^*]$ ,  $[\mathcal{R}^*]$ , and  $[K^*]$ . The asterisk is intended to indicate that the reduced material stiffness, rigidity, and structure stiffness matrices are in a complex form. Afterwards, solution of the complex-valued eigenvalue problem (Eq. 4-20) yields complex eigen frequencies,  $\omega^*$ , and in turn one can extract the modal loss factor of a structure according to Eq. (1-3).

### 4.3 Validation of the FE model

In this section some comparative results on the free vibration of different laminated plates are provided in order to validate the developed FE code. In the current investigation, both undamped and damped vibration analysis have been conducted. This is attempted by means of appropriate comparisons of numerical results with corresponding experimental measurements or predictions based on some lamination theories in conjunction with analytical or approximate methods such as Rayleigh-Ritz (RR) and FE. For this purpose, the in-house FE code is validated against the existing results, considering a wide range of parameters such as ply angle, lamination sequence, boundary conditions, length-to-thickness ratio, and orthotropy degree. Regarding the damping study mentioned earlier, either the VED or SDC model has been adopted by researchers to estimate the structural damping of different multilayered composite plates from known constituent material data, using various laminated plate theories and approaches. The modal damping parameter from the current numerical model based on the FSDT formulation is also compared to ensure the precision and capability of the method. The comparisons in terms of the frequency and modal damping have been provided in two separate successive sections. In the following sample problems, it should also be noted that all layers accounting for a laminate are considered to be of equal thickness.

#### 4.3.1 Verification of natural frequencies

As the first numerical example, the free vibration of symmetrical cantilevered rectangular laminated plates is investigated since practical components such as fan blades and aerodynamic surfaces are in the form of cantilevered structures. Narita and Leissa [118] presented the first five numerical frequency parameters and mode shapes using the Ritz method based on a displacement-

based formulation expressed in algebraic polynomials. In Table 4.3, the predictions from the present model are compared with the reported values for 8-ply cantilever square plates fabricated by a graphite/epoxy (Hercules) system with the degree of material orthotropy of 11.60. The properties of the material under investigation is given in Table 4.2. It should be noted that the thickness,  $h$ , of the laminate is 13.65 mm. The circular natural frequency and the length of plate sides are presented by  $\omega$  and  $a$ . The results show a good agreement with those reported by Narita and Leissa [118]. The non-dimensional frequencies predicted by the present FE code are also in a close correlation with another numerical (FE) and experimental study conducted by Crawley [119], where an FE analysis was performed using a moderately thick quadrilateral shallow shell element composed of 8 nodes with 5 degrees of freedom each. The fair correlation between the results observed from the experiment and those from theory is possibly due to the inevitable flexibility in the clamping section and the difference between the effective dynamic-flexural moduli and in-plane elastic characteristics obtained by static tests.

Table 4.2. Material properties for plates studied in Refs. [118,119].

Material	Elastic mechanical properties						
	$E_L$ (GPa)	$E_T$ (GPa)	$G_{LT}$ (GPa)	$E_{LT}$ (GPa)	$\nu_{LT}$	$E_L/E_T$	$\rho$ (kg/m <sup>3</sup> )
Graphite/epoxy (Hercules)	128	11	4.48	1.53	0.25	11.60	1.50

Table 4.3. Frequency parameter ( $\Omega$ ) of 8-ply clamped square plates.

$$\Omega = \omega a^2 (\rho / (E_T h^2))^{0.5}$$

Mode	1	2	3	4	5
<b>Hercules [0<sub>2</sub>,±30°]<sub>s</sub></b>					
Present	3.363	4.648	9.791	21.130	21.315
Ref [118] -Ritz	3.409	4.725	9.874	20.78	23.32
Ref [119] -FEM	3.379	4.468	9.827	21.44	22.05
Ref [119] -Experiment	3.021	4.670	9.395	18.69	19.39
<b>Hercules [45°, -45°, -45°, 45°]<sub>s</sub></b>					
Present	1.77	6.329	10.299	16.914	20.744
Ref [118] -Ritz	1.813	6.553	10.48	17.29	21.49
Ref [119] -FEM	1.792	6.443	10.38	17.11	21.26
Ref [119] -Experiment	1.692	6.089	10.20	15.07	19.17

To further establish the validity of the developed code, the results from the currently used FE code are validated against those reported by Khdeir and Reddy [120]. As an example, the free vibration of a four-layered antisymmetric angle-ply laminated composite plate under different boundary conditions is addressed. Two opposite edges are invariably assumed to be simply

supported (S) and the rest can be clamped (C), simply-supported, or free (F) edge conditions, independent of the other. A typical composite having an orthotropy degree of 40 is taken into consideration. Khdeir and Reddy [120] studied the problem using the Levy type solution in conjunction with the state space concept based on the second-order shear deformation theory. The elastic moduli taken from Ref. [120] are presented in Table 4.4. The variation of frequencies for the plate versus the aspect ratio is also examined in this study. As can be seen in Table 4.5, the aspect (side-to-thickness) ratio is varied from 5 to 100. As expected, the gradual increase in the aspect ratio results in higher frequencies, while for the aspect ratios of 50 and 100, the frequencies remain almost unchanged.

Table 4.4. Material properties for plates studied in Ref. [120].

	Elastic mechanical properties						
	$E_L$ (GPa)	$E_T$ (Gpa)	$G_{LT}$ (Gpa)	$G_{L\bar{T}}$ (Gpa)	$G_{T\bar{T}}$ (Gpa)	$\nu_{LT}$	$\rho$ (kg/m <sup>3</sup> )
Material I	40	1	0.6	0.6	0.5	0.25	1

Table 4.5. Dimensionless fundamental frequency parameter ( $\Omega$ ) of four-layered anti-symmetric angle-ply laminated square plate [45/-45/45/-45], material I.

$$\Omega = \omega a^2 (\rho / (E_T h^2))^{0.5}$$

Aspect ratio	a/h=5	a/h=10	a/h=20	a/h=50	a/h=100
<b>B.C.: SSSS</b>					
Present	12.610	18.535	22.050	23.470	23.700
Ref. [120] -SSDT-Levy	12.928	18.665	21.954	23.252	23.458
Ref. [121] -FSDT-Levy		18.46			
Ref. [122] -FSDT-Navier		18.46			
Ref. [123] -FSDT-FEM		18.609			
Ref. [124] -CLPT-Levy		23.53			
<b>B.C.: SSCC</b>					
Present	13.044	20.644	26.910	30.460	31.156
Ref. [120] -SSDT-Levy	13.457	20.887	26.770	29.979	30.598
Ref. [121] -FSDT-Levy		20.48			
Ref. [124] -CLPT-Levy		30.83			
<b>B.C.: SSSC</b>					
Present	12.780	18.960	22.730	24.280	24.530
Ref. [120] -SSDT-Levy	13.189	19.706	24.141	26.229	26.599
Ref. [121] -FSDT-Levy		19.41			
Ref. [124] -CLPT-Levy		26.73			
<b>B.C.: SSSF</b>					
Present	7.796	10.129	11.330	11.910	12.060
Ref. [120] -SSDT-Levy	7.873	10.121	11.261	11.808	11.954
Ref. [121] -FSDT-Levy		10.05			
Ref. [124] -CLPT-Levy		12.08			

B.C.: Boundary condition

SSDT: Second-order shear deformation theory

For a thick laminate with the aspect ratio of 10, comparing the results in the Table 4.5 reveals that all the shear deformation theories with analytical or numerical solutions [120-123], including the present formulation, have a close agreement. Using the Levy solution within the CLPT assumptions [124], however, results in inaccurate predictions in terms of the frequency parameter.

#### 4.3.2 Verification of modal damping parameters

To assess the accuracy of the theoretical predictions, besides the natural frequency, the modal damping property of plate components fabricated by two fiber-reinforced composites with different degree of orthotropy is investigated. The most commonly examined composites in the literature, namely glass fiber-reinforced polymer (GFRP) and carbon fiber-reinforced polymers (CFRP), are taken into account for the comparative study. Note that the purpose of this part is only aimed at evaluation of damping estimations of the present FE program regardless of the evaluation of assumptions adopted and measurements employed for input data.

Lin et al. [125] investigated the SDC for six modes of vibration for symmetric laminated plates with all edges free, using the FE model assuming the effect of the transverse shear deformation in each ply (layerwise). The element had 40 degrees of freedom for 8 nodes. The values from the experiment were also presented in their work, where the free boundary condition was provided by supporting a specimen on a soft foam rubber. Two plates used in their study were fabricated of glass fibers in DX-210 epoxy resin system. Although the same material was used, due to different values of fiber volume fraction, it was necessary to adjust the dynamic material properties of each plate sample. Thus, moduli and damping parameters given in Tables 4.6 and 4.7 were adjusted using basic data given for a fiber volume fraction of 50% by applying the correction method proposed in Ref. [29]. The respective data regarding the dimension, ply angle, fiber volume fraction  $v_f$ , and density  $\rho$  are also reported in Table 4.8. Considering the shear effect through the thickness, the dissipated energy of an element was separated into five components. The input damping data were also obtained by testing  $0^\circ$  and  $90^\circ$  beam and rod specimens in two different deformation modes, i.e. flexure and longitudinal shear.

Table 4.6. Elastic material properties for GFRP studied in Ref. [125].

Material	$E_L$ (GPa)	$E_T$ (GPa)	$G_{LT}$ (GPa)	$G_{L\hat{T}}$ (GPa)	$G_{T\hat{T}}$ (GPa)	$\nu_{LT}$
Plate 761	42.62	12.5	5.71	5.71	2.855	0.30
Plate 734	34.49	9.40	4.49	4.49	2.245	0.30



Table 4.7. Layer damping properties ( $\psi, \eta$  (%)) for plates studied in Ref. [31,125].

Plate ID	$\psi_L$	$\psi_T$	$\psi_{LT}$	$\psi_{L\dot{t}}$	$\psi_{T\dot{t}}$	$\eta_L$	$\eta_T$	$\eta_{LT}$	$\eta_{L\dot{t}}$	$\eta_{T\dot{t}}$
Plate 761	0.87	5.05	6.91	6.91	6.91	0.1385	0.8037	1.1000	1.1000	1.1000
Plate 734	0.87	4.75	6.13	6.13	6.13	0.1385	0.7560	0.9756	0.9756	0.9756

Table 4.8. Data for glass/epoxy plates 761 and 734.

Plate ID	Material	$v_f$	$\rho(\text{kg/m}^3)$	Dimension (mm×mm)	h (mm)	Lamination
Plate 761	GFRP	0.57	1971	182.75×182.75	1.64	$[0^\circ]_8$
Plate 734		0.45	1813.9	227.0×270.0	2.05	$[0^\circ, 90^\circ]_{2s}$

Tables 4.9 and 4.10, respectively, give the results for frequencies and the SDC associated with the first six modes of deformation. The frequencies associated with the lower six modes of deformation from the present FE code agree closely with those reported in Ref. [125].

Table 4.9. Comparison of damped natural frequencies (Hz) for free plates in Ref. [125].

Mode	1	2	3	4	5	6
<b>Plate 761</b>						
Present	88.12	128.94	221.503	241	296.3	376.10
Ref [125] -FEM	88.08	130.74	222.19	246.1	297.78	374.36
Ref [125] -Experiment	78.1	131.2	211.5	246	287.1	326.6
<b>Plate 734</b>						
Present	66.41	127.63	161.82	186.28	208.64	344.435
Ref [125] -FEM	66.42	131.62	164.46	189.79	208.87	347.16
Ref [125] -Experiment	62.2	131.4	159.2	180.5	200.1	326.7

Regarding the damping parameter, the results are also evaluated against those of Hu and Dokainish [31]. In their study, a FE scheme based on both damping models, i.e. the VED and the SDC, was developed in order to obtain associated system damping parameters. By adopting the FSDT, the discretization of FE analysis was done using a nine-node plate element with five degrees of freedom per node, replacing the eight plies of the layered plate.

All the results from the present developed FE model show good agreement between predictions and measurements in terms of damping from the earlier reported results. The discrepancies between the theoretical and experimental results are also expected due to manufacturing imperfections such as displaced fibers and thickness unevenness [125].

Table 4.10. Comparison of modal damping ( $\psi$  (%))=  $2\pi\eta$ ) for free square plates [31,125].

Mode	1	2	3	4	5	6
<b>Plate 761</b>						
Present	6.75	5.02	6.14	1.02	3.05	5.10
Ref [125] -FEM	5.99	4.44	5.40	0.93	2.80	4.34
Ref [125] -Experiment	6.00	4.80	5.80	1.30	2.80	4.00
Ref [31] -VED model	6.75	5.03	6.14	1.01	3.04	5.09
Ref [31] -SDC model	6.73	5.19	6.11	0.93	3.15	4.95
<b>Plate 734</b>						
Present	5.94	2.22	1.50	4.22	3.23	4.42
Ref [125] -FEM	7.16	2.47	1.62	4.87	3.73	5.09
Ref [125] -Experiment	6.70	2.80	1.90	4.90	3.20	5.80
Ref [31] -VED model	5.93	2.22	1.49	4.21	3.22	4.38
Ref [31] -SDC model	5.91	2.39	1.31	4.17	3.20	4.26

Alam and Asnani [126] conducted damping analysis for four types of fiber material and three different length-to-width ratios, while the ratio of the length to the thickness was kept the same for all cases in their study. The elastic characteristics for GFRP and CFRP composites are tabulated in Table 4.11. The material damping parameters were taken arbitrarily and presumed to be constant, irrespective of frequency, strain, or temperature, for all the fiber-reinforced composite materials, despite the fact that each material has its own damping property. It was also assumed that the material damping property in the fiber direction only originates from fibers which is sufficiently small to be neglected compared with that of the matrix. Thus, the damping along fiber direction was taken as zero, as provided in Table 4.12. The damping analysis was performed based on the correspondence principle of linear viscoelasticity or VED, using a double series trigonometric solution (Navier) for a four-layer crisscross simply-supported laminate by considering the transverse shear deformations of each single layer separately (layerwise). The defined simply-supported boundary condition is illustrated in Figure 4.3.

Table 4.11. Elastic and geometric properties of composite materials taken from Ref. [126].

Material	$E_L$ (GPa)	$E_T$ (GPa)	$G_{LT}$ (GPa)	$G_{L\bar{T}}$ (GPa)	$G_{T\bar{T}}$ (GPa)	$\nu_{LT}$	$\rho$ (kg/m <sup>3</sup> )	a × b (mm×mm)	h (mm)
CFRP	211	5.30	2.60	2.60	1.30	0.25	1524	1500×375	10
GFRP	55	18.3	9.10	9.10	4.55	0.25	1993	1500×375	10

The other damped vibration analysis was also studied, comparing the results with the corresponding findings obtained by Hu and Dokainish [31], where a FE scheme in conjunction with the FSDT formulation was applied, using the input data taken from Ref. [126]. The same

four-layer antisymmetric angle-ply lamination configuration  $[\theta, -\theta, \theta, -\theta]$  was also taken into account in this study.

Table 4.12. Damping properties ( $\psi, \eta$  (%)) for materials in Ref. [126].

Material	$\psi_L$	$\psi_T$	$\psi_{LT}$	$\psi_{L\dot{t}}$	$\psi_{T\dot{t}}$	$\eta_L$	$\eta_T$	$\eta_{LT}$	$\eta_{L\dot{t}}$	$\eta_{T\dot{t}}$
CFRP	0	50	50	50	50	0	7.96	7.96	7.96	7.96
GFRP										

Table 4.13 lists the values of the fundamental SDC with respect to the fiber orientation varying in a step of  $15^\circ$  for the first flexural mode of rectangular plates with the length-to-width ratio of 4. The discrepancies in the results are due to the formulation schemes, solutions employed, and damping models. Note that while the plate element in the present work has less degrees of freedom compared with those in the earlier studies, the simulated results in the current study are in excellent agreement with those reported in Ref. [31] with respect to the VED model.

Table 4.13. Comparison of fundamental modal damping ( $\psi$  (%)) for four-layered simply-supported rectangular crisscross  $[\theta, -\theta, \theta, -\theta]$  plates in Refs. [31,126].

Angle $\theta$	$0^\circ$	$15^\circ$	$30^\circ$	$45^\circ$	$60^\circ$	$75^\circ$	$90^\circ$
<b>CFRP</b>							
Present	44.25	25.89	10.58	4.97	3.47	5.03	2.95
Ref [31] -VED model	44.18	25.65	10.33	4.86	3.33	4.93	2.87
Ref [31] -SDC model	42.92	24.61	9.665	4.49	3.17	4.81	2.86
Ref [126] -Navier	42.90	23.10	8.15	3.43	2.20	2.12	2.20
<b>GFRP</b>							
Present	50.47	47.32	37.89	25.22	14.11	6.80	3.92
Ref [31] -VED model	50.68	47.46	37.89	25.09	13.87	6.48	3.66
Ref [31] -SDC model	48.16	44.40	34.13	21.58	11.30	4.77	2.20
Ref [126] -Navier	48.20	44.20	33.40	20.30	9.95	4.03	2.16

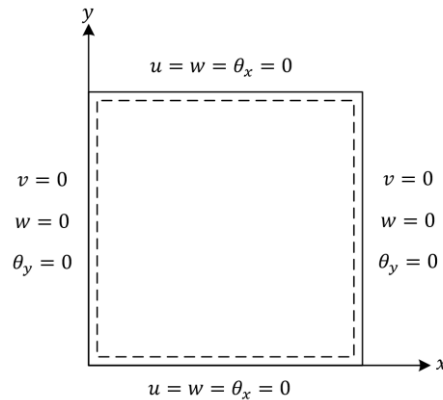


Figure 4.3. SSSS boundary condition of plates taken from Ref. [126].

The results based on the SDC model [31] are closer to those presented in Alam and Asnani's analysis [126], while the same damped element was adopted as Ref. [126]. This can be due to the fact that the selected material damping in their study is high. In the case of low damped materials, these two models reach close predictions, as examined for plates 761 and 734.

#### **4.4 Summary and conclusions**

This chapter mainly summarizes different lamination theories as well as analytical and mathematical modeling and formulations based on different assumptions, inclusive of the associated difficulties and limitations. The formulation for solution of an eigenvalue problem based on the FSDT concept was also thoroughly explained. An FSDT-based FE code was then developed using a 4-node plate element. Additionally, the free vibration response of various laminated components under numerous boundary conditions were obtained through the developed FE code, using the material characteristics provided in the literature. To evaluate the damping of a structure, the properties are introduced in a complex form composed of elastic and damping properties as the real and imaginary parts of the complex quantities, respectively, using the VED model. The vibration parameters were subsequently compared with those from the earlier studies on the basis of different modeling and formulations from simple to advanced. The results in terms of the modal damping factor and resonance frequencies demonstrated a good agreement between predictions from the present model and corresponding ones from existing experiments and theories. This, therefore, confirms the accuracy and capability of the formulated FE code to predict modal parameters in terms of damping factors and resonance frequencies.

## CHAPTER 5

### EXPERIMENTAL MODAL ANALYSIS AND VALIDATION

#### 5.1 Introduction

The modal testing is conducted for the validation of elastic constants and loss factors obtained from the DMA testing. The impulse technique is adopted to perform modal experiments to identify eigenfrequencies and eigenmodes of structures under consideration. The measurements are made in the study of the free vibrations of cantilever beams and plates laminated from the material characterized using the DMA method. Vibration testing and modal analysis are performed to accentuate validation of the properties extracted from the DMA tests, comparing the natural frequencies and modal damping factors obtained from FEM analysis to those from empirical modal tests. As depicted in Figure 5.1, beam and plate structures for conducting the modal analysis are prepared in the same fashion as panels fabricated for the DMA testing.

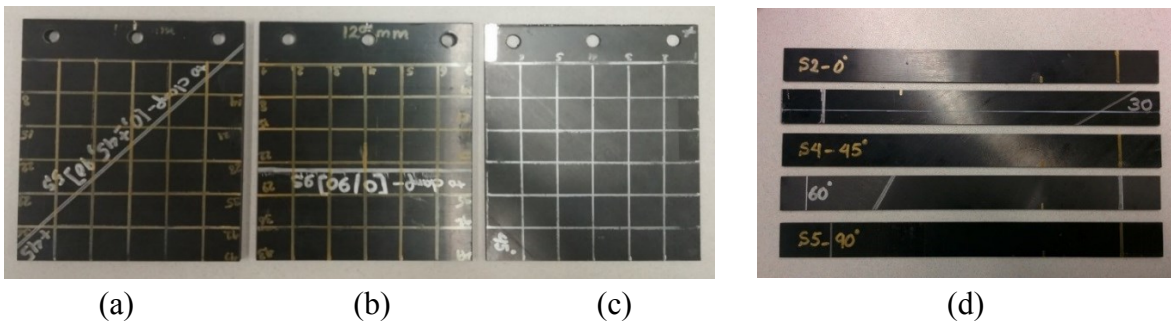


Figure 5.1. Samples for modal analysis, (a) Plate  $[0/\pm 45/90]_{5s}$ , (b) Plate  $[0/90]_{9s}$ , (c) Plate  $[45]_{12}$ , (d) UD beams.

#### 5.2 Experimental setup and samples

Five unidirectional beams with ply angle of  $0^\circ$ ,  $30^\circ$ ,  $45^\circ$ ,  $60^\circ$ , and  $90^\circ$  are investigated in this study. The plate specimens under investigation are made with different numbers of ply and stacking sequences. For the sake of simplicity, all thin and moderately thick plates used in this search are mid-plane symmetric so as to eliminate the coupling between the bending and stretching deformations. The geometry, stacking sequence, and number of plies are reported in Table 5.1. It should be noted that at the clamped end, 25 mm is left for the grip. The density ( $1520 \text{ kgm}^{-3}$ ) of the material is also found from the direct measurement of the volume and the weight.

Table 5.1. Properties of beam and plate samples for modal analysis.

Modal Sample	layup	Number of Layers	Geometry (mm)		
			Thickness	Length	Width
Beam	0, 30, 45, 60, 90	12	1.63	200	20
Plate A	[45] <sub>12</sub>	12	1.64	125	120
Plate B	[0/±45/90] <sub>5s</sub>	40	5.46	130	120
Plate C	[0/90] <sub>9s</sub>	36	4.93	130	120

The frequency response characteristics are obtained using the impulse excitation of the firmly clamped structures in the frequency range of 0 to 2000 Hz. The experimental set-up and its sketch are shown in Figure 5.2. An impulse hammer with a built-in transducer, model PCB-086C03, is used to induce the excitation for the flexural vibration, as shown in Figure 5.2. The transverse response is detected using a miniature accelerometer (PCB Piezotronic, model: 356A03), weighing 1.5 grams including the mass of connecting wire, which is positioned at 45 mm from the clamping block. For the purpose of modal damping measurement, the response gauge must be placed on samples with special attention to its location. The accelerometer is attached near the nodal line of the mode under observation in order to minimize the effect of extraneous mass loading and additional damping due to the accelerometer inertia. It is also of crucial importance to keep it sufficiently away from the clamping block as the prestressed area of clamping can significantly disturb the damping measurement. Likewise, damping measurement can be adversely affected under inappropriate clamping conditions. In the present work, cantilever support conditions are secured using a torque wrench for applying uniform clamping condition at the fixed end for the purpose of excellence repeatability of tests, in particular damping measurement. The magnitude of clamping force must be kept in a certain range so that no damage is produced in the material and no damping misreading arises.

The acquisition of excitation and response signals are performed by ME'scopeVES analyzer. Frequency-response-functions (FRF) are extracted subsequently using Fourier transform of the structure response to an impulse input by means of the analyzer associated with a computer. The responses show peaks corresponding to the flexural natural frequencies of the system. It should be noted that the accelerometer mass has also been taken into account for the numerical predictions of the thin plate and beams. For moderately thick plates B and C, the accelerometer mass has insignificant effect on the results computed.

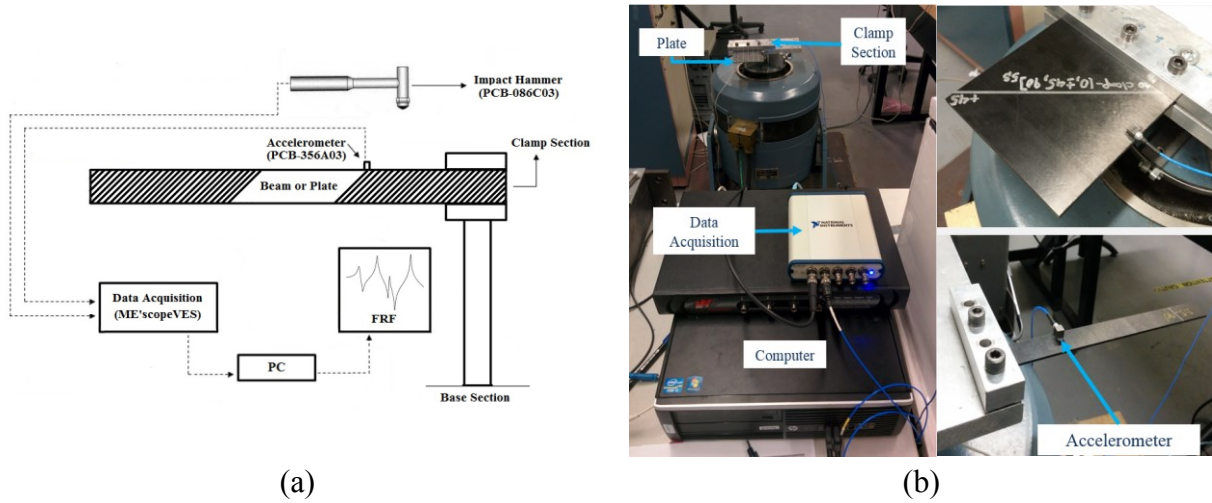


Figure 5.2. (a) Schematic view, and (b) real image of the experimental setup.

The modal damping ratios are experimentally evaluated by the half-power bandwidth method for unidirectional beam components supported horizontally in a clamping block. From the frequency response, the damping factor associated with a vibration mode is determined as half of the bandwidth of the half-power points, which are 3 dB less than the resonant frequency in terms of the magnitude of response. The modal loss factor,  $\eta_i$ , which is theoretically the ratio of the imaginary part of the complex eigenvalue to the real part, is equal to twice the modal damping ratio,  $\zeta_i$ , given by

$$\eta_i = 2\zeta_i = \frac{(f_2 - f_1)_i}{f_n} \quad (5-1)$$

where  $f_1$  and  $f_2$  are the frequencies at half-power points and  $f_n$  denotes the resonance frequency for the  $i$ th mode. The numerically determined modal loss factors are then compared to the measured modal damping factors for the purpose of validation of damping parameters identified by DMA and introduced into the FE code.

Flexural damping of beams is studied in a number of studies [53,58,127], where it was noticed that the aerodynamic damping (air pressure) contributes to the damping measurements, depending upon the vibration amplitude. In the early works of Adams and Bacon [58], they found that the higher the amplitude of vibration is, the greater the air damping is for lightly damped specimens. It was indicated that air damping emerges due to the air viscosity and inertia in the course of energy transfer from the vibration system to the surrounding air at the beam tip. Crane and Gillespie [53],

however, observed that the damping results have no significant dependency on air damping in case of low amplitude vibration of a composite beam.

It should also be noted that the amount of force generating deformation needed for stiff and reinforced materials tested in bending mode is relatively low due to limitations associated with dynamic analyzers. Accordingly, the DMA damping measurements are performed based on the concept of the linearity of imposed forces and deformations at room temperature. It is thus required to maintain the consistency between the DMA testing and the modal analysis conditions. Hence, the maximum modal vibration amplitude is kept very low in the present study while all the damping measurements are executed in the air. As a result, the air damping is expected to be negligible enough in order to nullify its effect on the total measured damping.

### **5.3 Modal experiments**

#### *5.3.1 Validation of elastic properties*

Here the developed FE model has been utilized to evaluate the natural frequencies associated with the first three vibration modes using the elastic parameters obtained from DMA tests described in Chapter 3. The finite element results are then compared with those obtained using modal experimental test. The finite element model has a mesh grid of  $4 \times 40$  for the beams and  $20 \times 20$  for the plates to achieve appropriate accuracy. The test articles are clamped at one side and free from other sides (CFFF boundary condition). The notation  $m \times n$  mesh denotes  $m$  subdivisions in  $x$  direction and  $n$  subdivisions along the  $y$ -axis with the same type of elements. Tables 5.2 provides the numerically and experimentally determined frequencies for the first three bending modes of unidirectional beams with five different fiber angles.

The results from Table 5.2 clearly show that the finite element model for beams using elastic parameters obtained from three-point bending tests on 12-ply specimens as input data generates results for natural frequencies which agree very well with those obtained experimentally. The single-cantilever configuration, however, does not yield accurate results, using DMA data for 10-ply specimens. This confirms the validity of results for elastic storage moduli obtained using the DMA three-point test configuration, considering the proper aspect ratio of about 30.



Table 5.2. First three experimental and numerical flexural natural frequencies (Hz) for unidirectional beams.

Fiber Orientation	Modal Experiment			Finite Element					
				Using DMA test data for 10-ply and single-cantilever clamp configuration			Using DMA test data for 12-ply and 3-point bending clamp configuration		
	$f_1$	$f_2$	$f_3$	$f_1$	$f_2$	$f_3$	$f_1$	$f_2$	$f_3$
0°	62.98	371.1	915.9	36.22	216.5	554.4	63.50	372.80	906.28
30°	27.61	168.0	441.3	23.21	140.3	354.5	27.24	166.16	429.74
45°	20.33	124.3	324.6	17.94	108.4	277.3	20.58	124.96	322.36
60°	17.54	106.2	280.2	14.88	89.8	230.3	17.68	106.68	274.23
90°	15.79	94.95	246.9	12.84	77.12	198.4	16.29	97.85	250.83

Figures 5.3-5.5 illustrate the schematics of first two bending mode shapes of the unidirectional beams with fiber orientation of 0°, 45°, and 90°. The graphs have been plotted using the FE code developed. It should be noted that beam components are numerically treated and modeled as plates, where the width of beams is taken into account. All the beams are clamped at the left edge in the width direction. It should also be mentioned that the mode shapes attributable to relatively low deformation of planar or torsional modes cannot be captured experimentally for the beam components. Therefore, as reported in Table 5.2, the first three bending frequencies correspond to the lower flexural deformations among all mode shapes captured computationally.

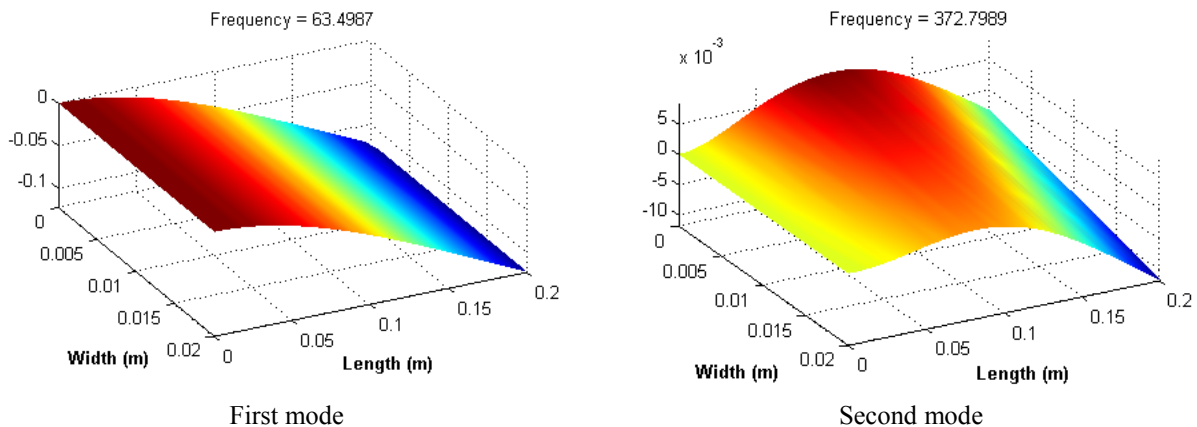
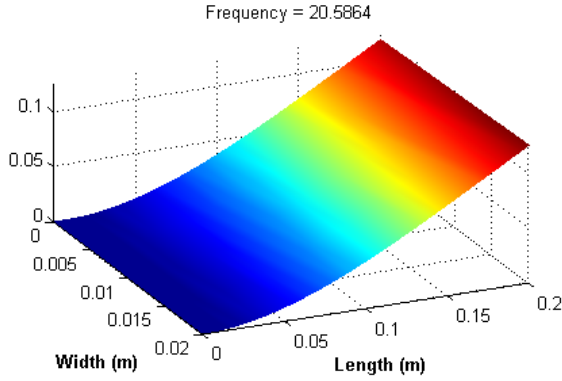
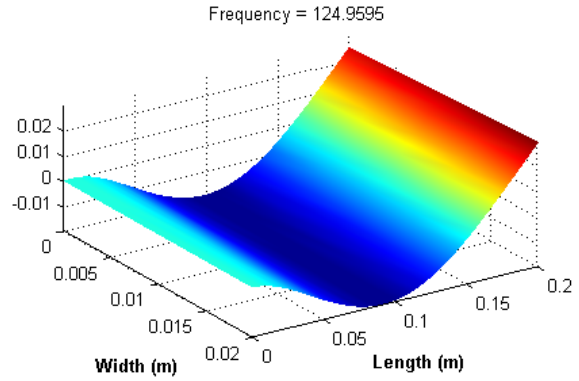


Figure 5.3. Bending modes of cantilever unidirectional beam with fiber angle of 0° corresponding to the lower two natural frequencies.

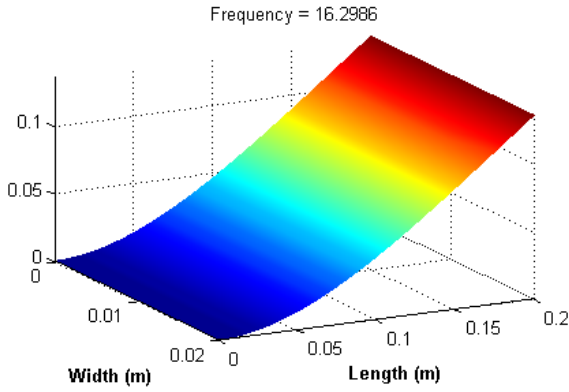


First mode

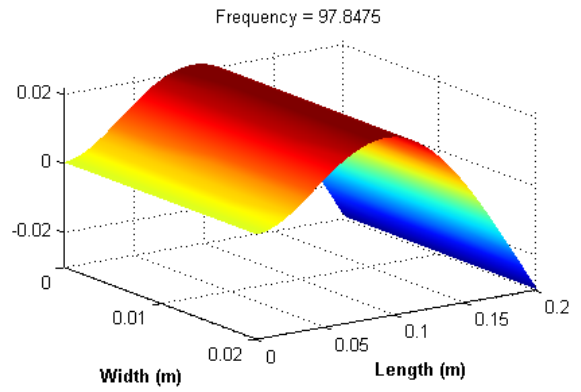


Second mode

Figure 5.4. Bending modes of cantilever unidirectional beam with fiber angle of 45° corresponding to the lower two natural frequencies.



First mode



Second mode

Figure 5.5. Bending modes of cantilever unidirectional beam with fiber angle of 90° corresponding to the lower two natural frequencies.

The validity of material properties is further demonstrated by comparing the first three natural frequencies obtained numerically and experimentally for both thin plate (A) and moderately thick plates (B and C), as specified in Table 5.1. The results for the plates with different layups are summarized in Table 5.3, comparing the numerical frequencies with the experimental counterparts. Assuming isotropy in the  $T\hat{T}$  plane of material coordinates and approximating  $\nu_{T\hat{T}} = 0.45$ ,  $G_{T\hat{T}}$  for thick plates B and C can be determined by the relation

$$G_{T\hat{T}} = \frac{E_{TT}}{2(1 + \nu_{T\hat{T}})} \quad (5-2)$$

Again as expected, very good agreement between measured and predicted frequency values is found in terms of elastic properties established from DMA analyses using the three-point bending

clamp. The comparative results show less than 3% error for beams and about 5% error for plates. On the contrary, the adjusted constants based on the findings from DMA tests under the single-cantilever clamp configuration yield significant deviations in flexural frequencies. The results suggest that the presented characterization method can effectively define the in-plane storage moduli of elasticity utilizing the three-point bending arrangement.

Table 5.3. Experimental and numerical natural frequencies (Hz) for laminated plates.

Plate layout	Modal Experiment			Finite Element					
				Using DMA test data for 10-ply and single-cantilever clamp configuration			Using DMA test data for 12-ply and 3-point bending clamp configuration		
	$f_1$	$f_2$	$f_3$	$f_1$	$f_2$	$f_3$	$f_1$	$f_2$	$f_3$
[45] <sub>12</sub>	65.3	197.0	402.0	51.1	141.2	333.6	65.7	199.3	410.1
[0/±45/90] <sub>5s</sub>	309.2	798.3	1835.0	190.6	519.6	1174.8	303.0	796.6	1831.7
[0/90] <sub>9s</sub>	309.4	505.5	1974.4	192.8	411.9	1196.0	325.9	506.1	1985.8

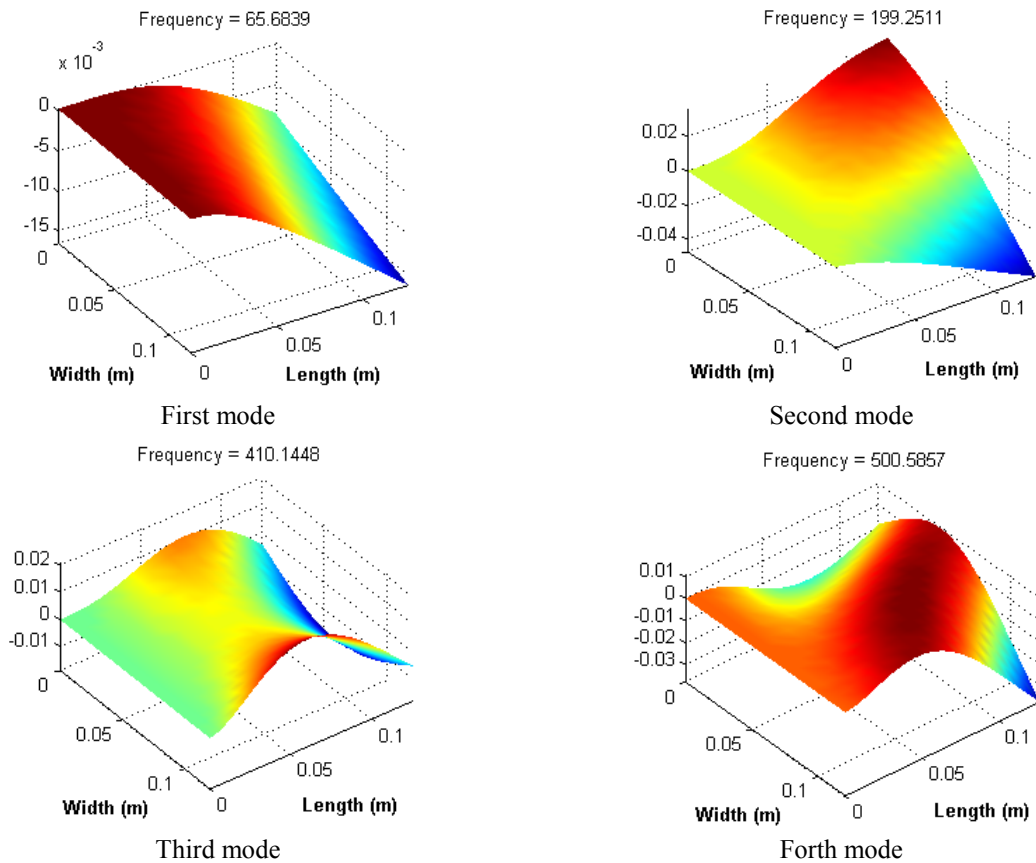
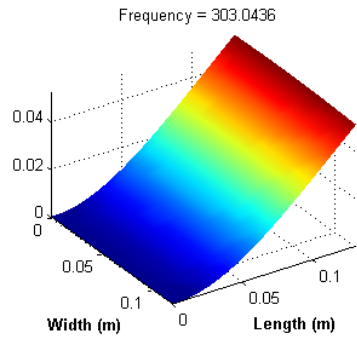
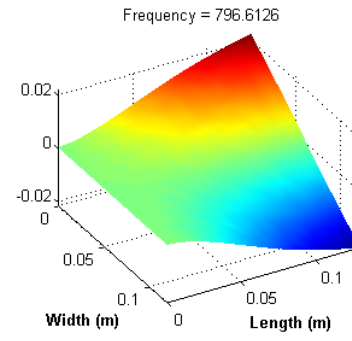


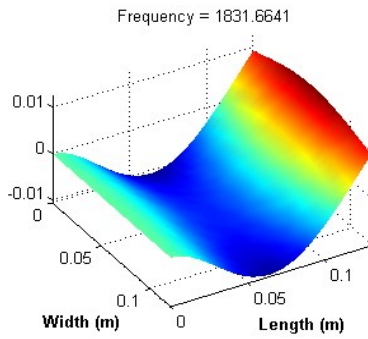
Figure 5.6. First four mode shapes of plate A ([45]<sub>12</sub>).



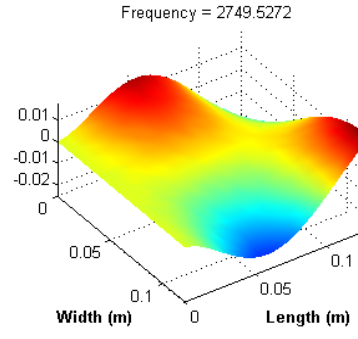
First mode



Second mode

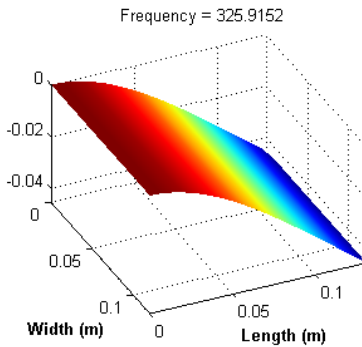


Third mode

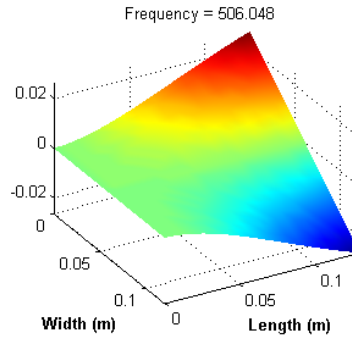


Forth mode

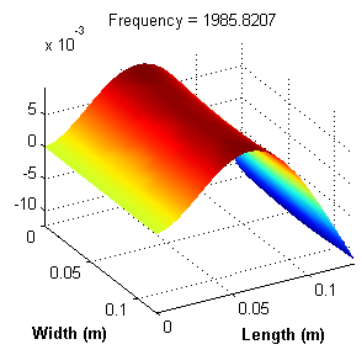
Figure 5.7. First four mode shapes of plate B ( $[0/\pm 45/90]_{5s}$ ).



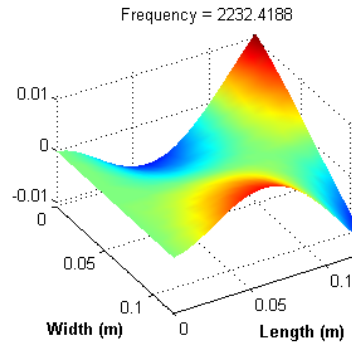
First mode



Second mode



Third mode



Forth mode

Figure 5.8. First four mode shapes of plate C ( $[0/90]_{9s}$ ).

Using the developed numerical model, the deformation modes of plates A, B, and C considered for the experimental modal testing are illustrated in Figures 5.6-5.8. It is observed that plates B and C show bending deformation in the first and third mode shapes. While the second and fourth modes demonstrate torsional deformations. Compared with the beam components solely revealing flexural modes, the first three frequencies correspond to the bending, torsion, or the mixed mode of deformation which could be captured experimentally for the plates.

### 5.3.2 Validation of loss factors

This section aims at investigation of damped vibrations of the given polymer-based composite material. The developed FE model has been used to evaluate the modal damping factor, using the loss coefficients in the material directions of a layer obtained by the DMA test. The material loss factors ( $\eta_{LL}, \eta_{TT}, \eta_{LT}$ ) and the elastic moduli ( $E_{LL}, E_{TT}, G_{LT}, G_{L\hat{T}}, G_{T\hat{T}}$ ) are incorporated through modifying the moduli of elasticity in the form of complex quantities. The simulation results for modal loss factors are then compared with the experimental results for the flexural vibrations of unidirectional beams of 20 mm  $\times$  200 mm under an impact excitation. It should be noted that beam structures are numerically treated as plates, where the width of beams are taken into account. However, the damping characteristics are identified based on the beam theories through the DMA method. Thus, the length-to-width ratio of 10 is considered as a good compromise. This is due to the fact that this ratio reaches a better compatibility to implement an analysis of a beam experimentally by reducing the edge effect in terms of damping study [46].

The FE results for loss factor associated with the fundamental mode of vibration of unidirectional beams with a given fiber orientation increment of 15° are provided in Table 5.4. It is noted that FE analysis provides the modal loss factor using Eq. (1-3) and then damping factor can be found using Eq. (5-1). The results show that the modal loss factor or damping is maximum at a fiber orientation of about 30° in the case of an increment of 15°. It should be noticed that, due to lack of coupling effects for cantilever laminated beams, the resulting damping is generated because of the extensional stress and/or through the thickness shear stress components. As expected, the beam with  $[0_6]_s$  lamination has a better flexural stiffness, so the capacity of the matrix to deform and dissipate energy is reduced in flexural mode of vibration. The damping factor is strongly depends on the mode shapes.

Next, the modal damping are evaluated experimentally to be compared with simulation results. For experiments, the unidirectional beams in cantilever configuration are excited using an impact hammer. In order to observe the correlation of the damping results from the experiment and the FE model, the beams with preferential fiber orientations of 0°, 30°, 45°, 60° and 90° are just examined. The frequency response function (FRF) is then utilized to extract the modal damping factor associated with the first bending mode using the half-power bandwidth method. In order to assure the reliability of test results, the modal tests are conducted in two series including five runs individually and then averaged. The experimental results for the fundamental modal damping factor for unidirectional beam components with different fiber angles are provided in Table 5.5. It should be noted that damping factors for higher modes are very difficult to capture experimentally and thus could not be obtained with reasonable accuracy due to the experimental limitations.

Table 5.4. Fundamental modal damping parameter for unidirectional beams using FE model.

Orientation	Frequency (Hz)	Loss Factor $\eta$ (%)	Damping Factor $\zeta$ (%)
0°	63.891	0.2510	0.1255
15°	43.698	1.0789	0.5395
30°	27.790	1.4518	0.7259
45°	20.808	1.4312	0.7156
60°	17.622	1.2678	0.6339
75°	16.269	1.0859	0.5429
90°	15.923	1.0004	0.5002

Table 5.5. Fundamental modal damping factor  $\zeta$  (%) for unidirectional beams of 20 mm × 200 mm obtained experimentally.

Fiber Orientation	0°		30°		45°		60°		90°	
	1 <sup>st</sup>	2 <sup>nd</sup>	1 <sup>st</sup>	2 <sup>nd</sup>	1 <sup>st</sup>	2 <sup>nd</sup>	1 <sup>st</sup>	2 <sup>nd</sup>	1 <sup>st</sup>	2 <sup>nd</sup>
Test Series										
1 <sup>st</sup> run	0.117	0.148	0.731	0.739	0.730	0.690	0.653	0.633	0.554	0.600
2 <sup>nd</sup> run	0.131	0.135	0.753	0.700	0.700	0.704	0.699	0.623	0.593	0.546
3 <sup>rd</sup> run	0.133	0.136	0.791	0.721	0.720	0.730	0.615	0.634	0.656	0.584
4 <sup>th</sup> run	0.124	0.134	0.707	0.683	0.712	0.732	0.667	0.636	0.652	0.563
5 <sup>th</sup> run	0.131	0.144	0.715	0.696	0.702	0.737	0.649	0.612	0.550	0.521
Average	0.127	0.139	0.739	0.707	0.712	0.718	0.656	0.627	0.601	0.562

Examination of results reveals that fundamental modal damping factor obtained using FE model based on DMA data for 12-ply samples tested by three-point bending clamp generally agrees very well with those obtained experimentally irrespective of fiber angles. This can be

further demonstrated in Figure 5.9 where the upper bound (UB) and lower bound (LB) on averaged experimental data for test series 1 and 2 together with numerical results are shown. As it can be realized the numerical results for modal damping factor,  $\zeta$ , falls into the range between lower and upper experimental bounds except for fiber angle  $90^\circ$  which is slightly less than the experimental lower bound value. For the unidirectional beams examined, the damping factor obtained using the FE model are also compared with the averaged measurements in Table 5.6.

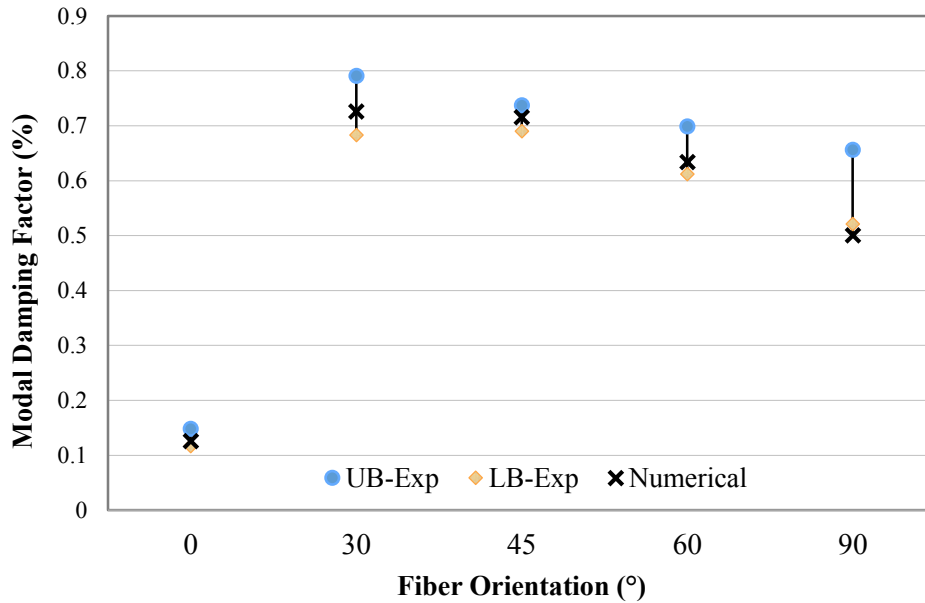


Figure 5.9. Comparison between numerical results (×) and experimental scatter for fundamental modal damping factor.

This again confirms the validity of damping parameters evaluated using the DMA three-point bending test configuration. Thus DMA testing on samples with the appropriate length-to-thickness ratio, utilizing the three-point bending clamp setup can provide accurate result for viscoelastic properties of high modulus anisotropic materials.

Table 5.6. Fundamental modal damping parameter (%) for unidirectional beams of 20 mm × 200 mm obtained experimentally.

Fiber Orientation	0°		30°		45°		60°		90°	
	FE	EXP	FE	EXP	FE	EXP	FE	EXP	FE	EXP
Frequency (Hz)	63.89	62.98	27.79	27.61	20.81	20.33	17.62	17.54	15.92	15.79
Loss factor	0.251	-----	1.452	-----	1.431	-----	1.268	-----	1.001	-----
Damping factor	0.126	0.133	0.726	0.723	0.716	0.715	0.634	0.642	0.500	0.582

FE- Finite element  
EXP- Experiment

## 5.4 Parametric study on the fiber angle

As can be seen in Table 5.6, the fiber angle greatly affects not only the frequency but also the modal loss factor or damping. It was found that the maximum damping occurs around fiber angle of  $30^\circ$ . This is further clarified in Figure 5.10 which shows the variation of the first bending frequency and damping factor as a function of the fiber orientation with a finer increment of  $5^\circ$ . According to the plot, the optimal result for maximum damping factor is found to be at fiber orientation of  $35^\circ$  for the unidirectional beams. The more accurate optimum result may be, therefore, observed if the ply angle increment is decreased. As the angle approaches  $35^\circ$ , the highest predicted loss factor results at the expense of the natural frequency or the bending strength. Comparing with the fiber orientation of  $0^\circ$ , a decrease of 61.26 % in the natural frequency leads to the maximum loss factor. Therefore, from an engineering point of view, there must be a trade-off between natural frequency and modal damping parameter in composite laminates as damping exhibits behavior as opposed to the stiffness performance. In the case of unidirectional beams, Figure 5.11 also presents the variation of the modal loss factor with respect to the fundamental frequency obtained computationally.

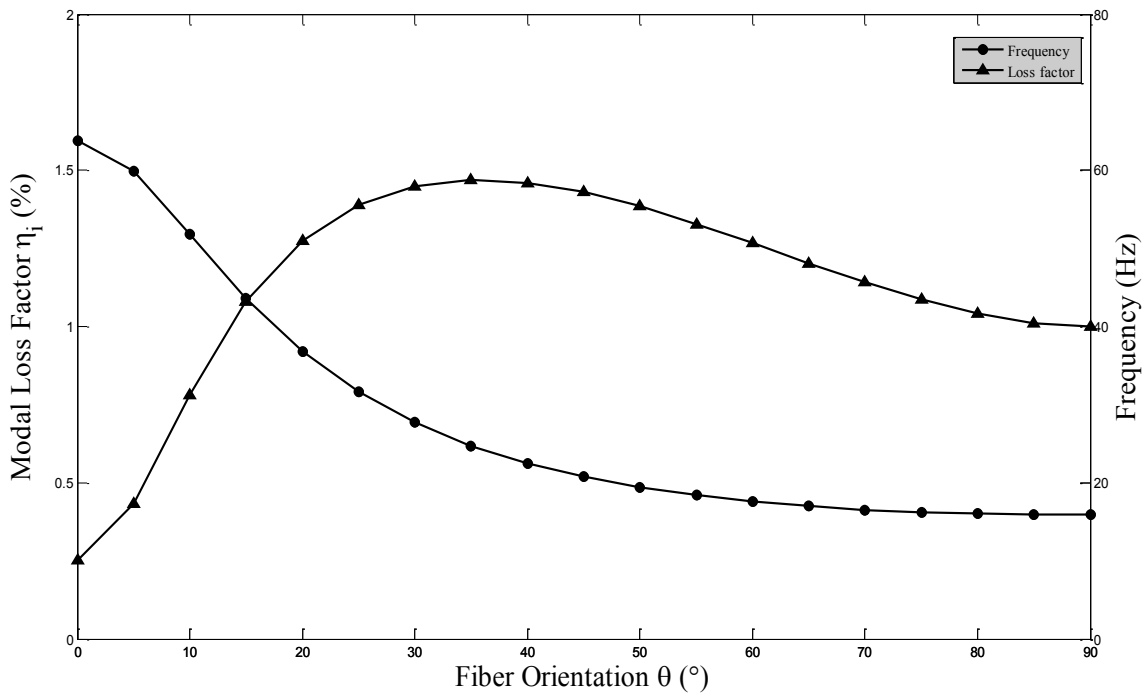


Figure 5.10. Variation of numerical fundamental loss factor and natural frequency with ply angle.



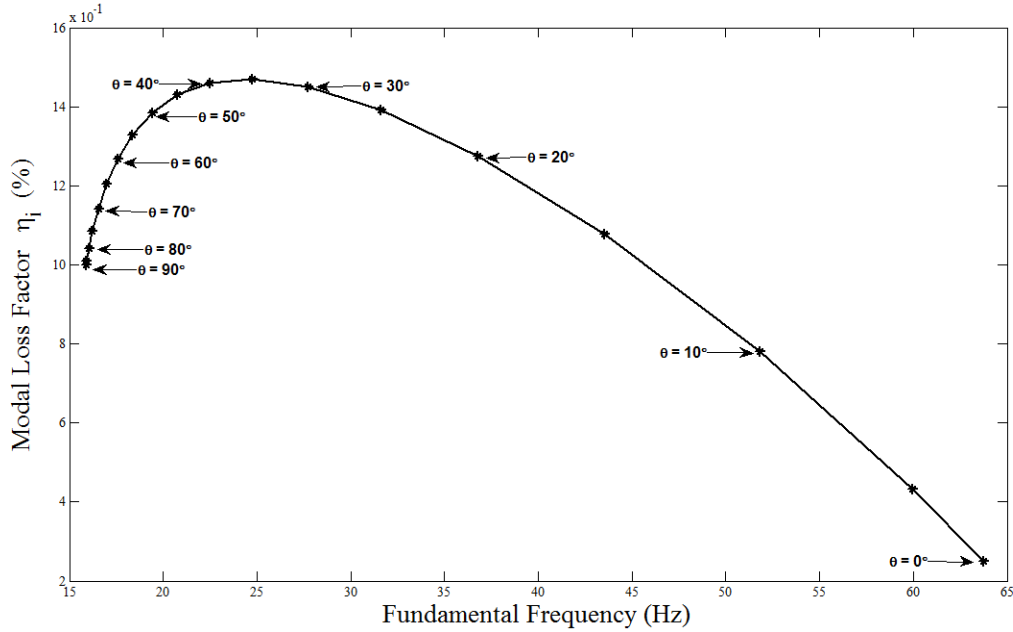


Figure 5.11. Variation of numerical fundamental loss factor with natural frequency of unidirectional beams with different fiber angles.

## 5.5 Summary and conclusions

In this chapter, an experimental modal test was conducted to identify modal parameters to validate the accuracy of the FE simulation results and thus indirectly evaluate the measured elastic and damping properties obtained by the DMA testing. The modal frequencies and damping factors of unidirectional beams of various ply angles as well as plates with different layups made from identical plies were investigated. The determined viscoelastic properties of the transversely isotropic material were also used in the FE model in order to predict the modal frequencies and damping factors of components. For modal experiments, the beams and plates in cantilever configuration are excited using an impact hammer. A reasonably good agreement between the measured natural frequencies and those from the FE model based on the DMA test data resulted in validation of the elastic constants obtained from the three-point bending test on the 12-ply DMA specimens.

The experimental evaluation of material damping was only performed on the unidirectional laminated cantilever beams in response to an impact excitation. In order to observe the correlation of the damping results from the experiment and the FE model, the beams with preferential fiber orientations of 0°, 30°, 45°, 60° and 90° were only examined. After validation of the elastic properties from three-point bending test on 12-ply samples, the corresponding damping parameters

as the input data into the FE code were extracted from the same experiment. The frequency response function (FRF) were then utilized to extract the modal damping factor associated with the first bending mode using the half-power bandwidth method. A good correlation between predicted and measured damping factors of the unidirectional beams was observed. Then, an optimum fiber angle for the maximum modal damping associated with the first mode of vibration was found numerically. The optimum result for the maximum damping was also found to be around  $35^\circ$  for a unidirectional beam.

Further, the experimental modal analysis indirectly demonstrated that the DMA method is capable of identifying the material properties, i.e. elastic and damping characteristics, of a high modulus anisotropic material with sufficient accuracy, using a proper DMA clamping and sample aspect ratio.

## CHAPTER 6

# PARAMETRIC STUDY AND OPTIMUM DESIGN OF LAMINATED PLATES UNDER MIXED BOUNDARY CONDITIONS

### 6.1 Introduction

A considerable amount of parametric studies and optimal design methodologies are available in the open literature in order to meet requirements for high performance and light weight. In this regard, studies on constant or variable stiffness/strength [128], and damping improvement [129], for the best use and understanding of potentials associated with both static and dynamic performance of composite components have been widely carried out by manipulation at the constituent and laminate level. In the course of optimum design or optimization process of composite components and structures, the static and free/forced dynamic responses of composite components are highly tailorable to and controllable by either micromechanical or macromechanical characteristics, i.e. fiber and/or matrix materials [126], the fiber/matrix volume fraction [49], stacking sequence, ply angle/thickness [130], the reinforcement aspect ratio ( $l/d$ ) [131], shape of the fiber cross-section [49], and state of fiber/matrix interface (fiber coating) [132]. Besides the influence of fundamental elements, other issue that needs to be addressed in the design space entails the effect of the structural characteristics such as the structural geometry [133], boundary condition [26], and loading/damage mode [56]. For a more realistic analysis yielding close correlation with experimentally measured values, it is worthwhile to encompass all aspects in effect. On the theoretical side, it is, although, tedious and complicated to involve all effective parameters in each single work.

With regard to designing composites where vibration control is essential, useful combination of damping, strength and stiffness plays a crucial role by providing the best configuration or treatment aligned with demanded requirements for further improvement in the dynamic performance and fatigue endurance. The frequency response of a composite structure has been widely investigated to study the effect of material properties and structural conditions near resonances in an undamped vibration analysis. However, damping and stiffness are inversely interdependent. Thus, the optimal damped vibration design must be carried out based on trade-offs

between damping, strength and stiffness. Considering this, the damping performance and frequency response of laminated composite components must be treated together so that the superior performance and optimal vibration design arise. Among all the constituent factors, it has been also shown that the ply angle has been highly effective and can be manipulated to fulfill design objectives and requirements.

In this chapter, the developed FE model has been utilized in order to conduct parametric study to investigate the effect of fiber angle on the fundamental natural frequency and loss factor, and their weighted combinations for different boundary conditions, lamination sequences and thicknesses. The optimal fiber angles, at which the objective is maximized, will then be identified for each configuration.

## **6.2 Assumptions and design parameters**

In general, lower vibration modes, especially the fundamental mode, significantly contribute to the overall structural response. Therefore, by maximizing the damping, or shifting the frequency associated with the fundamental mode, the vibration may be significantly suppressed. This study, therefore, put the main emphasis on predicting the modal properties associated with the fundamental mode of deformation as it usually has a great impact on structural parts and components.

The developed FE model discussed in Chapter 4 in combination with the damping and elastic parameters obtained by the DMA testing (Chapter 3) has been used to predict the variation of the fundamental modal loss factor and frequency with the fiber orientation for laminates under the combination of clamped and free boundary conditions. In order to eliminate the effect of geometry, i.e. the length-to-width ratio, and rigidity coupling terms, only square symmetric layups (120mm × 120mm) are taken into consideration. Whereas, the effect of geometry is only studied for unidirectional laminates under CFFF boundary condition. The results are then compared with those from a unidirectional beam studied in the earlier chapter. The nature of the layup is also investigated for three different symmetric lamination sequences, namely unidirectional, cross-ply, and angle-ply. The effect of laminate thickness on the loss factor and frequency is then assessed, given 6-, 12-, and 24-ply laminated plates.

The physical meaning of fiber orientation is defined with respect to the first uppermost layer as the reference ply. It is inferred that the fiber angle of plies is kept alternately at  $90^\circ$  and  $-2\theta$  with respect to that of the reference layer in the direction toward the mid-surface, in the case of cross- and angle-ply laminates, respectively. The ply angle is defined with respect to the  $x$ -axis of the plate coordinate system, where the principal axes  $x$  and  $y$  are along the horizontal and transverse directions with the origin at the low-left intersection point. Referring to the clamped and free edges as C and F, the boundary conditions under investigation are also shown in Figure 6.1.

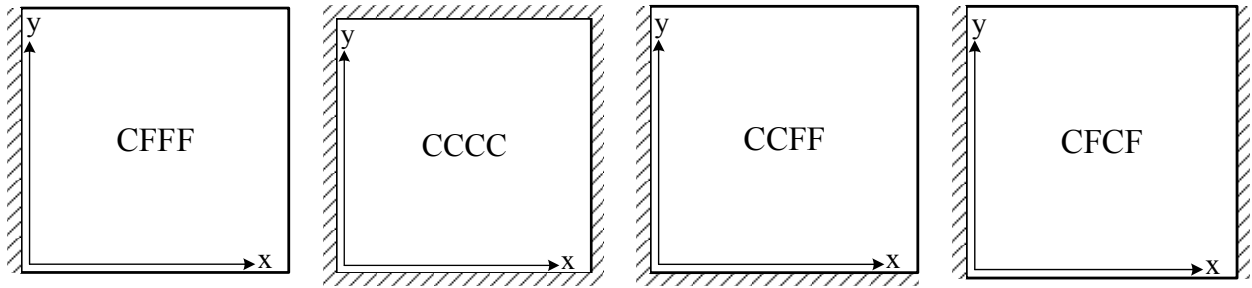


Figure 6.1. Combination of clamped and free boundary conditions studied for modal parameters.

Under each single boundary condition, the degree of influence of the fiber orientation on the modal damping and frequency is studied. The fiber orientation is established as the discrete variable, varying from  $-90^\circ$  to  $90^\circ$  with an interval of  $5^\circ$ . The plate modal parameters presented here are theoretical predictions obtained by applying the damping and elastic characteristics taken from the DMA testing. Further, an optimum fiber orientation is investigated in order to achieve the maximum value of an objective function  $F_{obj}$  defined as

$$F_{obj} = w_1 * \left( \frac{\eta_i}{\eta_{max}} \right) + w_2 * \left( \frac{f_i}{f_{max}} \right) \quad (6-1)$$

where  $\eta_{max}$  and  $f_{max}$  represent the maximum value of the laminate loss factor and frequency found for each lamination configuration under any of the boundary conditions.  $\eta_i$  and  $f_i$  are also the modal loss factor and frequency corresponding to each fiber orientation.  $w_1$  and  $w_2$  are weighting factors. The parametric objective function is thus composed of two weighted normalized modal parameters i.e. the non-dimensional damping and resonance frequency.

Three different combinations of weighting factors of the two objectives are considered in this parametric study. In the first case,  $w_1$  and  $w_2$  are, respectively, set to 1 and 0 to obtain the optimum

fiber angle that yields the maximum fundamental damping. As the second problem,  $w_1$  and  $w_2$  are chosen 0 and 1 in turn to only assess the maximum modal frequency corresponding to the first mode of deformation. Designing for each objective function individually (considering only one objective function) may result in a considerable improvement in that respect, but at the expense of a probably substantial decrease in the other objective function. Therefore, considering the same importance for each individual normalized modal parameter as single objectives, both  $w_1$  and  $w_2$  are thus assumed to be identical ( $w_1 = w_2 = 0.5$ ) in the third case of study. The normalization is done as it plays an important role in the consistency of the optimal solution to a bi- or multi-objective problem composing of several competing objective functions with different order to satisfy simultaneously.

## 6.3 Results and discussions

This section presents the predictions obtained for variation of the defined objective functions in previous section with respect to the fiber orientation. The results are presented in three sections addressing the effect of the boundary condition, lamination sequence and the thickness.

### 6.3.1 Effect of boundary condition

#### 6.3.1.1 Optimal fiber orientation for maximum damping

The variation of the first objective function ( $w_1 = 1, w_2 = 0$ ) is plotted in Figure 6.2 for 12-ply lamination configurations for three sequences (unidirectional, angle-ply and cross-ply) and four boundary conditions (CFFF, CCCC, CCFF, CFCF). As accepted, except for CCFF, the graphs are symmetric with respect to a vertical line passing through  $0^\circ$  fiber angle for all other constraint configurations due to their symmetric nature with respect to the center line along the  $x$  axis.

It is seen from Figure 6.2 that the trend of modal loss factor is changed with the fiber orientation, given different boundary conditions of laminated plates. Moreover, the optimum fiber angle resulting in the maximum fundamental loss factor is affected by the imposed boundary condition. The observation of Figure 6.2 also demonstrates that the fundamental loss factor significantly varies for all laminates under weak constraints, i.e. CFFF and CFCF cases, when the angle is changed from  $0^\circ$  to  $90^\circ$ . It is to say that the difference between the maximum and minimum loss factors (two extremes) is considerably notable under these boundary conditions. For CFCF

and CFFF constraints, the loss factor varies from 50% to 60% for cross-ply laminates, while it varies in a large range of 80% for unidirectional and angle-ply laminates. On the contrary, the loss factor varies in a range of 10% to 35% (range between two minimum and maximum loss factor), considering the strict constraint, i.e. CCCC boundary condition. Therefore, the improvement of damping performance or more flexibility in damping design can be achieved under weak constraints by manipulation of the fiber angle, compared with the strictest one.

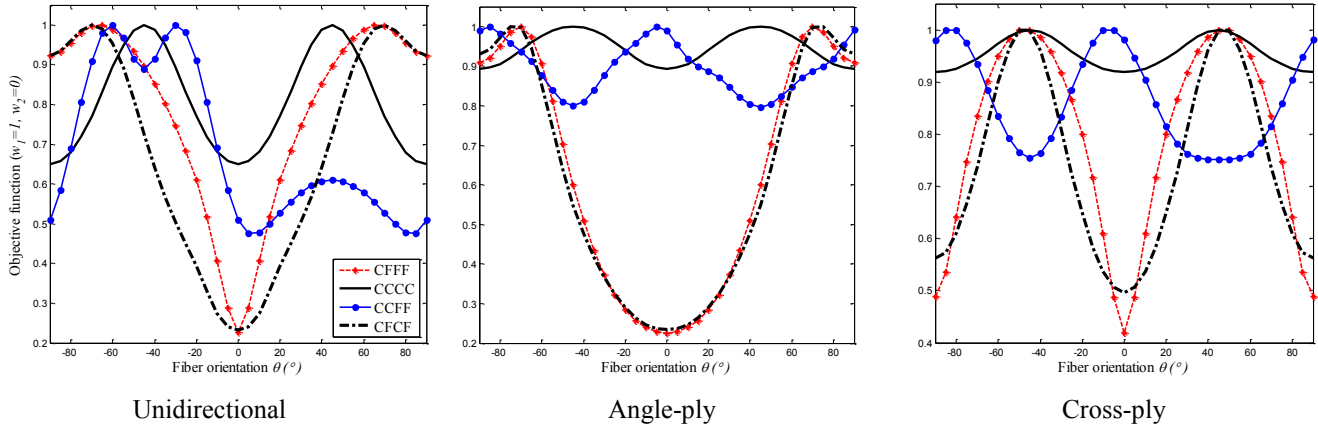


Figure 6.2. Variation of objective function ( $w_1 = 1, w_2 = 0$ ) with fiber orientation for 12-ply laminates under combination of clamped and free boundary conditions.

In the case of CFFF and CFCF boundary conditions, the trends of fundamental loss factor are quite close and similar for angle-ply laminates. However, the magnitude of loss factor for a fiber angle from  $0^\circ$  to about  $70^\circ$  is higher for unidirectional plates under CFFF boundary condition, compared with CFCF boundary condition.

In the case of CCCC boundary condition, the optimum angle for maximum damping is always at  $\pm 45^\circ$ . While other optimal angles for maximum modal loss factor are not the same as those typically adopted from a manufacturing point of view, except for unidirectional laminates under CCFF boundary condition. Table 6.1 presents the optimum fiber angles and their associated maximum fundamental loss factor for different 12-ply laminate sequences and boundary conditions.

Since the results shown in Figure 6.2 are normalized, the variation of the modal loss factor for a given fiber angle can be qualitatively observed. For a quantitative comparison, the values of the loss factor are also presented in Figure 6.3, where  $\eta_1$  represents the first modal loss factor of a plate structure.

Table 6.1. Optimum fiber orientation and maximum loss factors obtained for laminates under mixed clamped and free boundary conditions.

Layup	Parameter	CFFF	CCCC	CCFF	CFCF
Unidirectional	Loss factor (%)	1.115	0.560	1.038	1.116
	Fiber angle (°)	±65	±45	-30 and -60	±70
Angle-ply	Loss factor (%)	1.130	0.416	0.558	1.106
	Fiber angle (°)	±70	±45	-10 and -80	±75
Cross-ply	Loss factor (%)	0.700	0.416	0.596	0.626
	Fiber angle (°)	±50	±45	-10 and -80	±50

As can be seen from Figure 6.3, CCCC boundary condition provides a smaller amount of fundamental loss factor, while the fiber orientation is changed within the wide range of 30° to 75° for the laminates. It is also noticed that CCFF boundary condition always provide a greater loss factor, compared with CCCC boundary condition. Moreover, all laminates under CFFF, CCCC, and CFCF boundary conditions exhibit the maximum damping performance at two optimum points, where one is in the positive side and the other exists in the negative side of the fiber orientation array. On the other hand, both optimal solutions for the highest damping are in the negative side of the ply angle array, where a laminate is under CCFF boundary condition. Thus, it is easy to notice from the results of numerical simulations that the optimum loss factors are obtained at different optimal fiber orientations under dissimilar vibration modes of deformation.

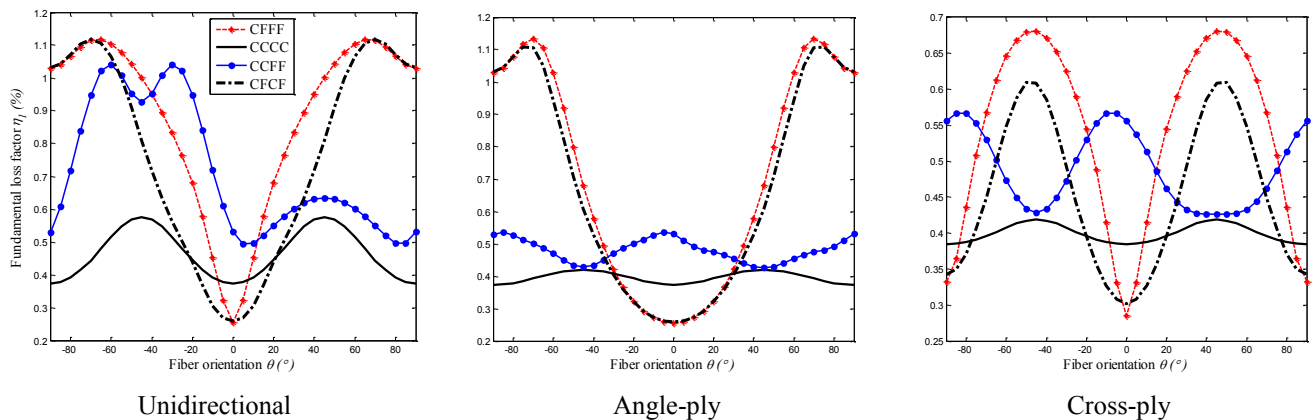


Figure 6.3. Variation of fundamental loss factor with fiber orientation for 12-ply laminates under combination of clamped and free boundary conditions.

### 6.3.1.2 Optimal fiber orientation for maximum frequency

To discuss the effect of a boundary condition on the resonance frequency, laminates with the total number of 12 layers are considered under four sets of boundary conditions. The variation of



resonance frequency with the fiber angle is plotted in Figures 6.4 and 6.5. By comparing Figures 6.2 and 6.4, it can be easily observed that the maximum frequency is obtainable at the fiber orientation yielding the minimum loss factor regardless of the lamination sequence and boundary condition. Comparing Figures 6.3 and 6.5, one can also find that the effect of boundary condition on the modal loss factor is more pronounced than the frequency. As shown in Figure 6.4, laminated plates subjected to CFFF and CFCF boundary conditions show the largest variation in the frequency regardless of lamination sequence.

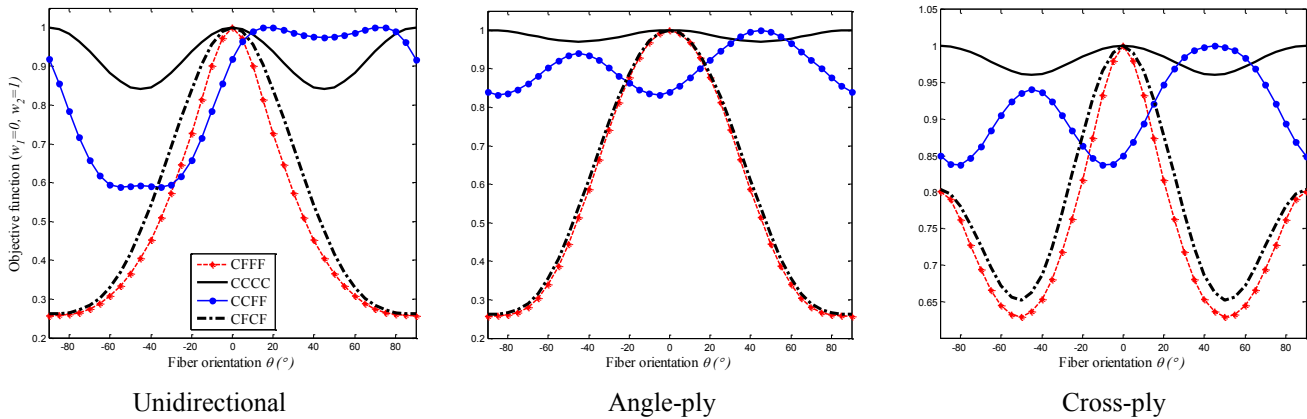


Figure 6.4. Variation of objective function ( $w_1 = 0, w_2 = 1$ ) with fiber orientation for 12-ply laminates under combination of clamped and free boundary conditions.

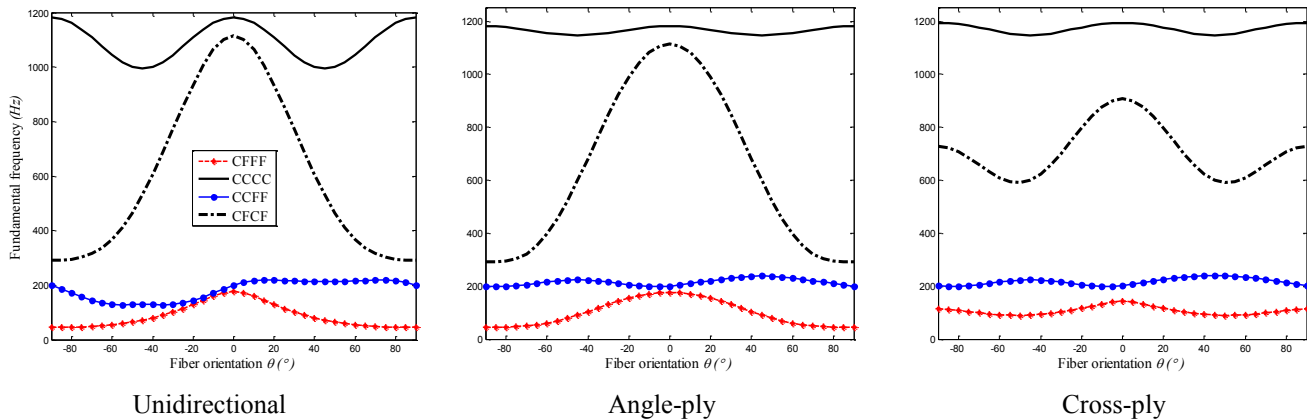


Figure 6.5. Variation of fundamental frequency with fiber orientation for 12-ply laminates under combination of clamped and free boundary conditions.

As expected, the strictest boundary condition always results in the highest frequency, regardless of the fiber angle and lamination sequence. Figure 6.5 also shows that CCCC constraint yields the largest frequency in the whole range of fiber orientation, followed by CFCF, CCFF, and CFFF for

the considered laminates. However as mentioned before, both CFFF and CFCF constraints provide the largest range of the objective (35% -75%) in the frequency.

Table 6.2 presents the optimal ply angle for the maximum frequency associated with the fundamental vibration mode. Except for a unidirectional laminate under CCFF boundary condition, it is noted that the optimal angle for the maximum frequency is the same for all laminated components under the same boundary condition. Concerning CFFF and CFCF boundary conditions, the maximum frequency is achievable at the fiber orientation of 0° for all laminate configurations. In addition, the value of the maximum frequency is the same for unidirectional and angle-ply laminates under CFFF, CCCC, and CFCF boundary conditions. While, CCFF constraint yields an identical optimum frequency for angle-ply and cross-ply laminated components.

Table 6.2. Optimum fiber orientation and maximum frequencies obtained for laminates under mixed clamped and free boundary conditions.

Layup	Parameter	CFFF	CCCC	CCFF	CFCF
Unidirectional	Frequency (Hz)	176.97	1182.13	218.35	1114.31
	Fiber angle (°)	0	0 and ±90	15 and 75	0
Angle-ply	Frequency (Hz)	176.97	1182.13	239.00	1114.31
	Fiber angle (°)	0	0 and ±90	±45	0
Cross-ply	Frequency (Hz)	142.83	1194.67	239.00	907.68
	Fiber angle (°)	0	0 and ±90	±45	0

### 6.3.1.3 Optimal fiber orientation for maximum mixed damping and frequency

With a view to designing composites with a useful combination of stiffness and damping, this section focuses on the third objective which is a combination of both stiffness and damping with equal weighting ( $w_1 = 0.5, w_2 = 0.5$ ). Results for the variation of the objective function versus the fiber angle for different lamination sequence and boundary condition are shown in Figure 6.6. As it can be realized, laminated plates with CCCC boundary condition reveal the highest objective value (83% -98%), followed by CCFF constraint (70% -92%).

Table 6.3 also provides the summary of optimum solutions in terms of the fiber angle for all sets of objectives established. It is noticed that the optimum ply angles for the first and third objectives remain almost the same, where the laminates are subjected to CCCC, CCFF, and CFCF constraints, while it differs for CFFF boundary condition.

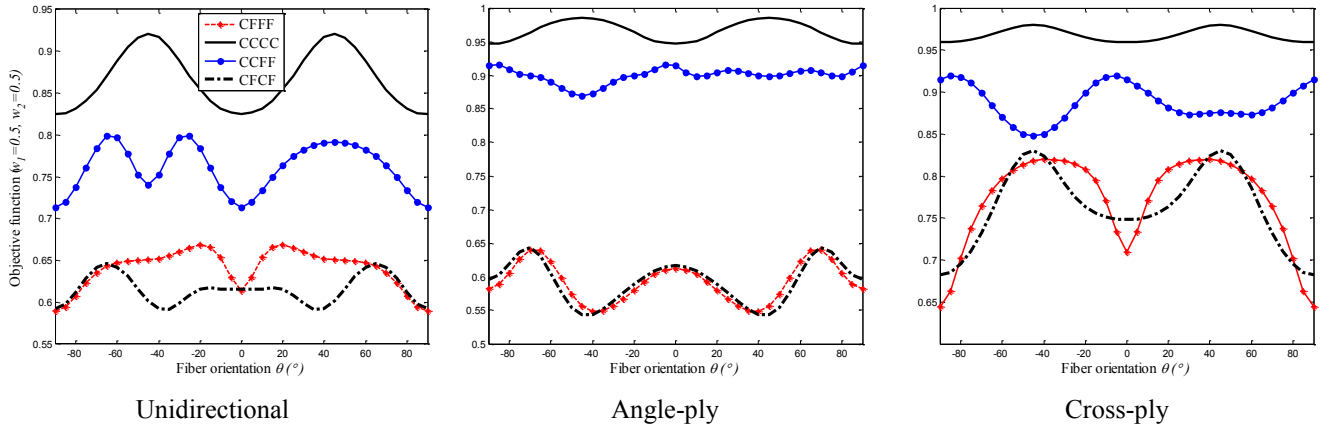


Figure 6.6. Variation of objective function ( $w_1 = 0.5, w_2 = 0.5$ ) with fiber orientation for 12-ply laminates under combination of clamped and free boundary conditions.

Table 6.3. Optimum fiber orientation and maximum objectives obtained for laminates under mixed clamped and free boundary conditions.

Layup	Parameter	CFFF	CCCC	CCFE	CFCF
Unidirectional	1 <sup>st</sup> Objective	1.115	0.560	1.038	1.116
	Loss factor (%)				
	Fiber angle (°)	$\pm 65$	$\pm 45$	$-30$ and $-60$	$\pm 70$
	2 <sup>nd</sup> Objective	176.97	1182.13	218.35	1114.31
	Frequency (Hz)				
	Fiber angle (°)	0	0 and $\pm 90$	15 and 75	0
Angle-ply	3 <sup>rd</sup> Objective (%)	67.0	92.0	80.0	65.0
	Fiber angle (°)	$\pm 20$	$\pm 45$	$-25$ and $-65$	$\pm 65$
	1 <sup>st</sup> Objective	1.130	0.416	0.558	1.106
	Loss factor (%)				
	Fiber angle (°)	$\pm 70$	$\pm 45$	$-10$ and $-80$	$\pm 75$
	2 <sup>nd</sup> Objective	176.97	1182.13	239.00	1114.31
Cross-ply	Frequency (Hz)				
	Fiber angle (°)	0	0 and $\pm 90$	$\pm 45$	0
	3 <sup>rd</sup> Objective (%)	64.0	98.5	91.6	64.3
	Fiber angle (°)	$\pm 70$	$\pm 45$	$-5$ and $-85$	$\pm 70$
	1 <sup>st</sup> Objective	0.700	0.416	0.596	0.626
	Loss factor (%)				
Cross-ply	Fiber angle (°)	$\pm 50$	$\pm 45$	$-10$ and $-80$	$\pm 50$
	2 <sup>nd</sup> Objective	142.83	1194.67	239.00	907.68
	Frequency (Hz)				
	Fiber angle (°)	0	0 and $\pm 90$	$\pm 45$	0
	3 <sup>rd</sup> Objective (%)	82.0	98.0	91.9	83.0
	Fiber angle (°)	$\pm 35$ or $\pm 40$	$\pm 45$	$-5$ and $-85$	$\pm 45$

### 6.3.2 Effect of lamination sequence

The second study is concerned with variation of fundamental loss factor and frequency versus the fiber orientation for different layups under the same boundary conditions studied before. The dimension and laminate configurations of the 12-ply laminates are also the same as the previous investigation. Thus, the results are identical to those presented earlier, while comparing the effect of the lamination sequence under a given boundary condition.

#### 6.3.2.1 Optimal fiber orientation for maximum damping

The variation in fundamental loss factors of three given stacking sequences under each boundary condition is presented in Figure 6.7. It should be noted that for all configurations, the variation of modal loss factors are symmetric with respect to the fibre angle  $0^\circ$  (same behaviour for  $0^\circ$  to either  $+90^\circ$  or  $-90^\circ$ ), except the plots associated with CCFF boundary condition. Therefore, for CFFF, CCCC and CFCF boundary conditions, the graphs are only presented for the ply angle from  $0^\circ$  to  $90^\circ$ . In addition to CCFF constraint, the graphs associated with CCCC boundary condition are also symmetric with respect to the orientations of  $\pm 45^\circ$  since the directions are the other lines of symmetry.

The results clearly present that a unidirectional square laminate yields the greatest loss factor in a broad range of fiber angle. This is attributed to the coupling effects, which become dominant in a symmetric structures, depending on the mode of deformation. The trend of variation in loss factor is the same for unidirectional and angle-ply laminates subjected to CFFF and CFCF constraints, while the magnitude is higher for a unidirectional component within the range of angle from  $5^\circ$  to  $65^\circ$ . It is further observed that both unidirectional and angle-ply laminates provide an identical maximum loss factor, where CFFF and CFCF boundary conditions are applied. As mentioned earlier, the loss factor becomes smaller under CCCC boundary condition, yet the unidirectional plate provides a significant loss factor at the optimum angle of  $45^\circ$ , compared to angle- and cross-ply structures.

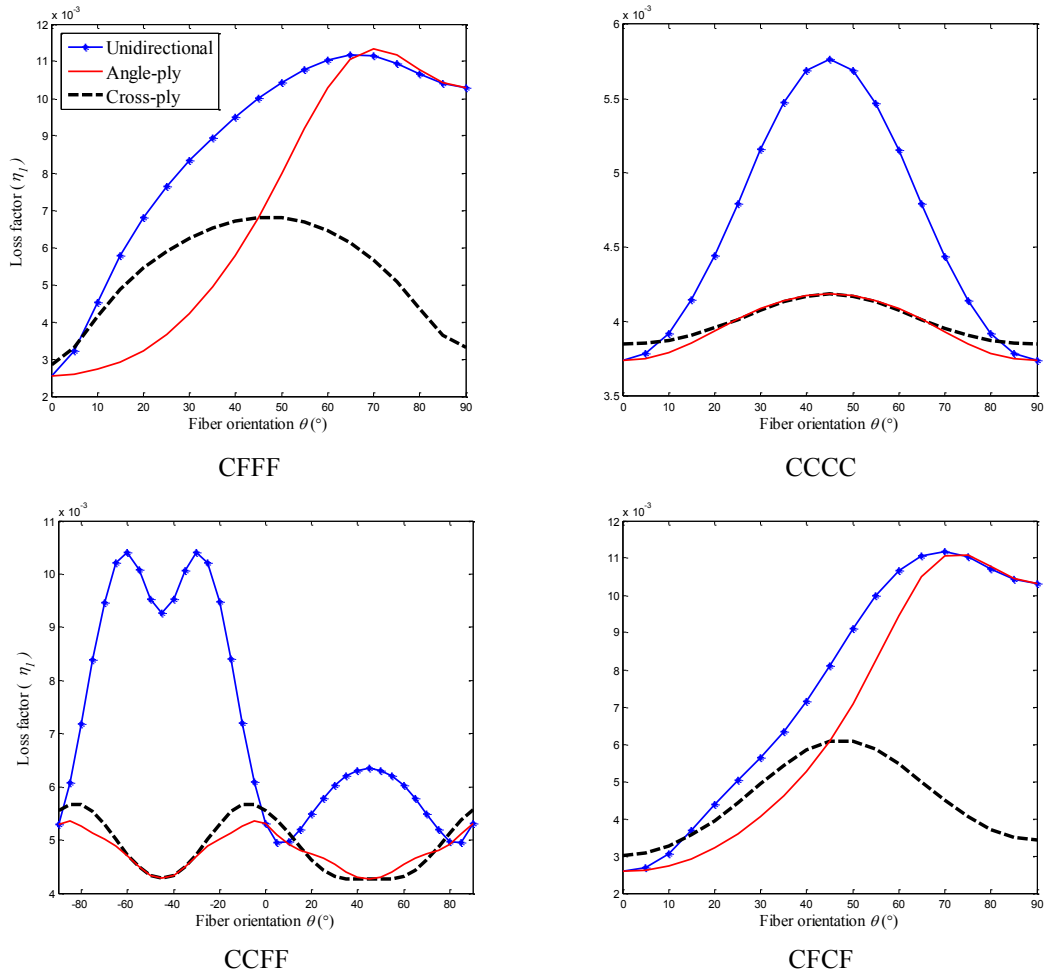


Figure 6.7. Variation of fundamental loss factor with fiber orientation for 12-ply laminates under combination of clamped and free boundary conditions.

It is also apparent that a cross-ply component under CFFF and CFCF constraints results in higher loss factor by changing the angle of the outermost layer from  $0^\circ$  to  $45^\circ$ , compared with the angle-ply laminate.

### 6.3.2.2 Optimal fiber orientation for maximum frequency

Here the variation in fundamental frequency for three stacking sequences under each boundary condition is presented in Figure 6.8. As expected, the extreme value of frequency occurs at fiber orientations yielding the minimum loss factor. For instance, the laminated plates give the minimum frequency at an angle of  $45^\circ$ , leading to the maximum loss factor. As it can be seen from Figure 6.8, laminates under CFFF and CFCF boundary conditions demonstrate the same trend of change with respect to the fiber angle, although, the magnitude of frequency is higher in the case of CFCF constraint.

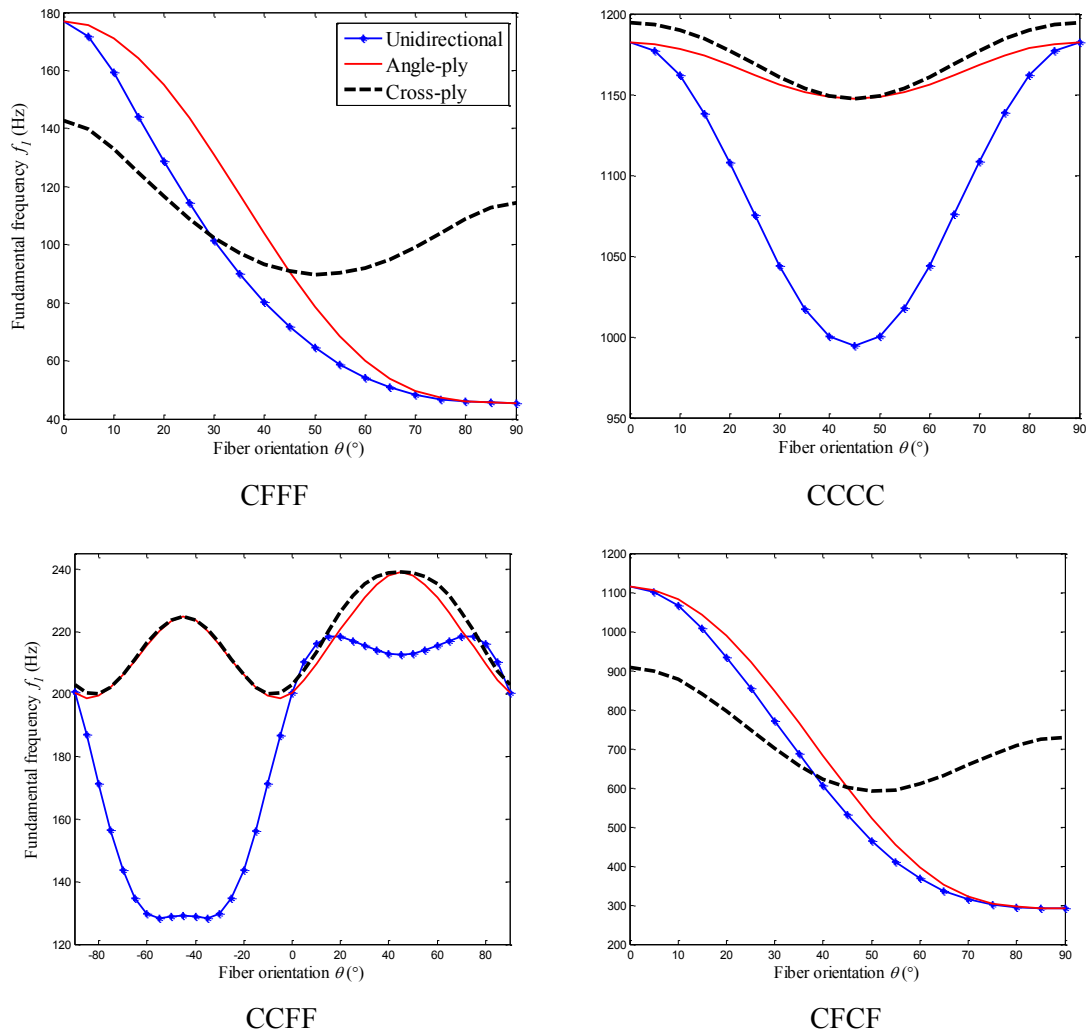


Figure 6.8. Variation of fundamental frequency with fiber orientation for 12-ply laminates under combination of clamped and free boundary conditions.

Furthermore, unidirectional and angle-ply components provide the largest variation in frequency with respect to the ply angle under CFFF and CFCF constraints. The angle- and cross-ply laminates almost provide identical frequency within the range of the fiber angle under CCCC and CCFF boundary conditions.

### 6.3.3 Effect of laminate thickness

The effect of laminate thickness on the first modal loss factor and frequency of square laminates under CFFF, CCCC, CCFF, and CFCF boundary conditions in the predefined range of fiber angle is investigated in this section. The results for the optimum fiber orientation leading to the maximum fundamental modal parameters are obtained for a 6-, 12-, and 24-ply laminates

subjected to the boundary conditions under consideration. The variation of the first modal loss factor of laminates are presented in Figures 6.9- 6.11 which correspond to unidirectional, cross-ply and angle-ply layup configurations, respectively. The influence of fiber angle and the number of layers on frequency predictions are also provided graphically in Figures 6.12-6.14 for different layup configurations.

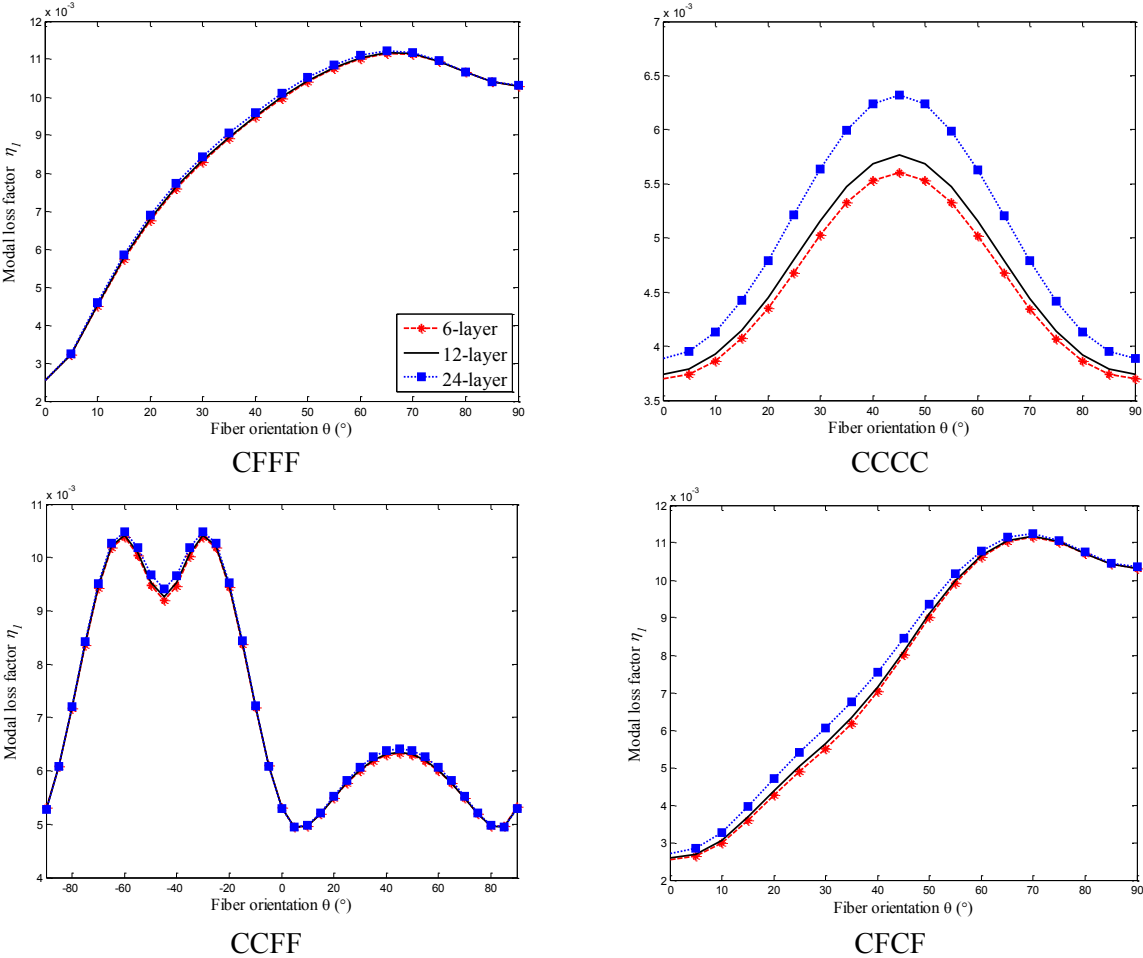


Figure 6.9. Variation of fundamental loss factor with fiber orientation for unidirectional laminates with different thicknesses under mixed free and clamped boundary conditions.

From the presented results for unidirectional laminates, it is apparent that the maximum loss factor is obtained at optimum fiber orientations of  $\pm 65^\circ$ ,  $\pm 70^\circ$ , and  $\pm 45^\circ$  under CFFF, CFCF, and CCCC boundary conditions, respectively, regardless of the number of layers. For the CCFF boundary condition, the maximum loss factor occurs at both  $-30^\circ$  and  $-60^\circ$ , considering the same laminate configuration. Note that the identical fiber orientations were also observed earlier, where 12-ply symmetric laminates were investigated in terms of the maximum loss factor.

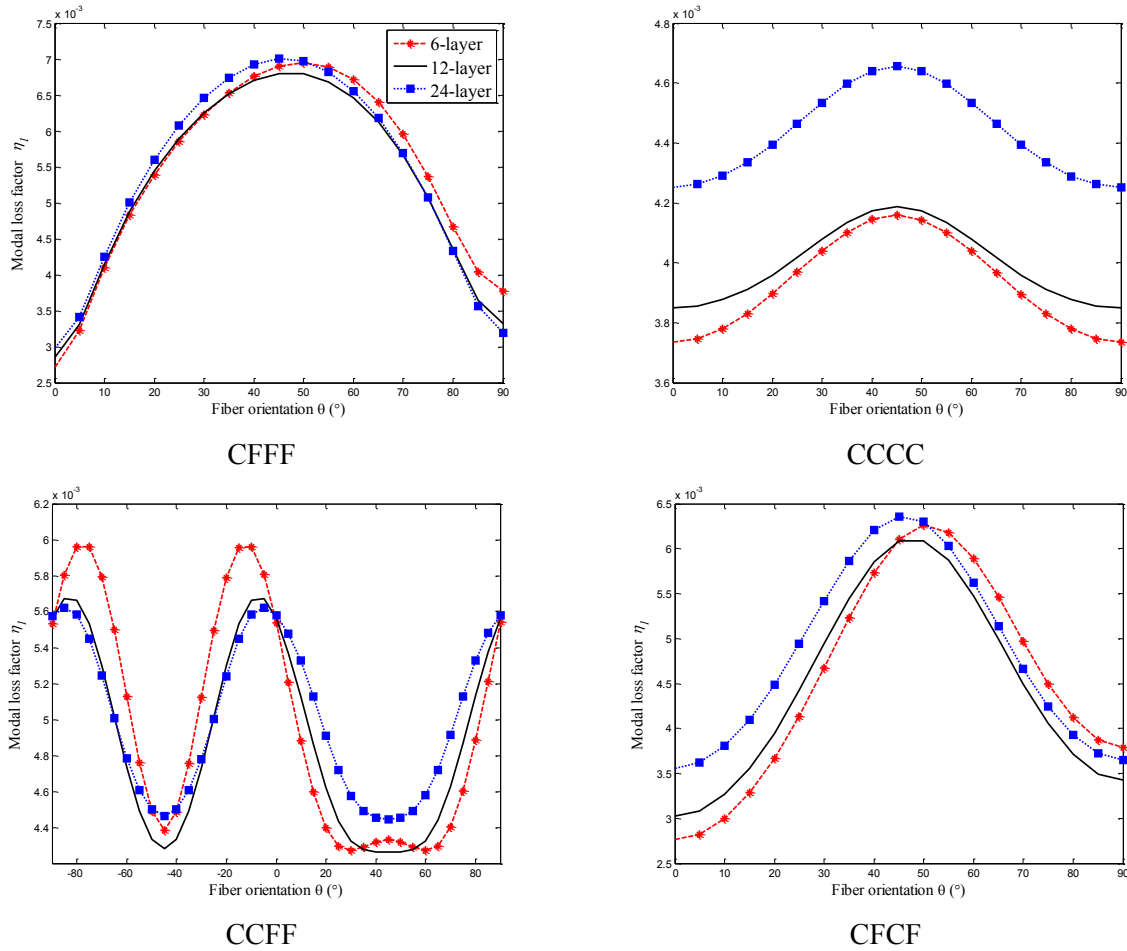


Figure 6.10. Variation of fundamental loss factor with fiber orientation for cross-ply laminates with different thicknesses under mixed free and clamped boundary conditions.

As shown in Figure 6.10, the cross-ply laminated plates with different numbers of layers provide the maximum loss factor at fiber angles with a slight deviation of  $5^\circ$ , where the components are subjected to CFFF and CFCF constraints. The optimal fiber orientations can reach to an identical value, providing that the angle increment is reduced. Therefore, the thickness has insignificant influence on alteration of the optimal fiber angle, with the exception of CCFF boundary condition. For cross-ply and angle ply laminates, it is also interesting to note that the maximum loss factor decreases with an increase in the thickness for CCFF boundary condition. Additionally, the increase in loss factor is negligible with the laminate thickness for CFFF, CCFF, and CFCF constraints at a given fiber angle. As to CCCC boundary condition, the significant change in the loss factor is, although, observed at the optimum ply angle with the thickness. Thus, it appears that the rate of change in total loss factor with the thickness depends on conditions which correspond to the structural boundaries.



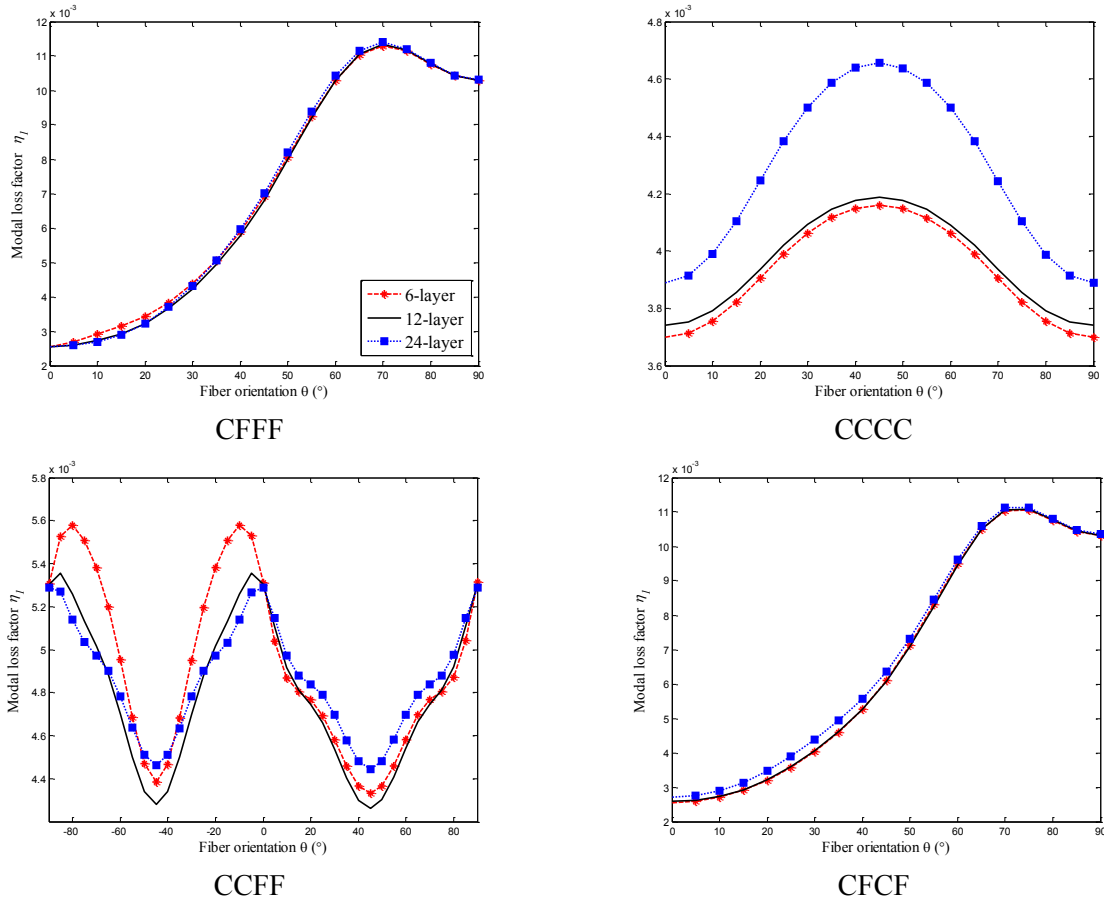


Figure 6.11. Variation of fundamental loss factor with fiber orientation for angle-ply laminates with different thicknesses under mixed free and clamped boundary conditions.

The results show that the maximum variation in total loss factor (12.5%) with thickness occurs at the optimal angle under CCCC boundary condition, when the number of layers is varied of the order of 4 (from 6 to 24). However, CCCC boundary condition yields the minimum magnitude of damping performance. With regard to frequency, a significant variation, although, is noticed for all treated laminates under four boundary conditions. By changing the number of layers from 6 to 24, the maximum frequency is increased approximately between 650% and 700% at the corresponding optimal angle. Also, the rate of variation in frequency is almost identical at a given fiber angle, where the number of layers is doubled. The effect of thickness on the frequency is, therefore, far more pronounced compared to the loss factor. Moreover, the more consistency in terms of the optimal ply angle and variation of frequency with thickness is observed from Figures 6.12-6.14, compared with predictions related to the loss factor, as illustrated in Figures 6.9-6.11.

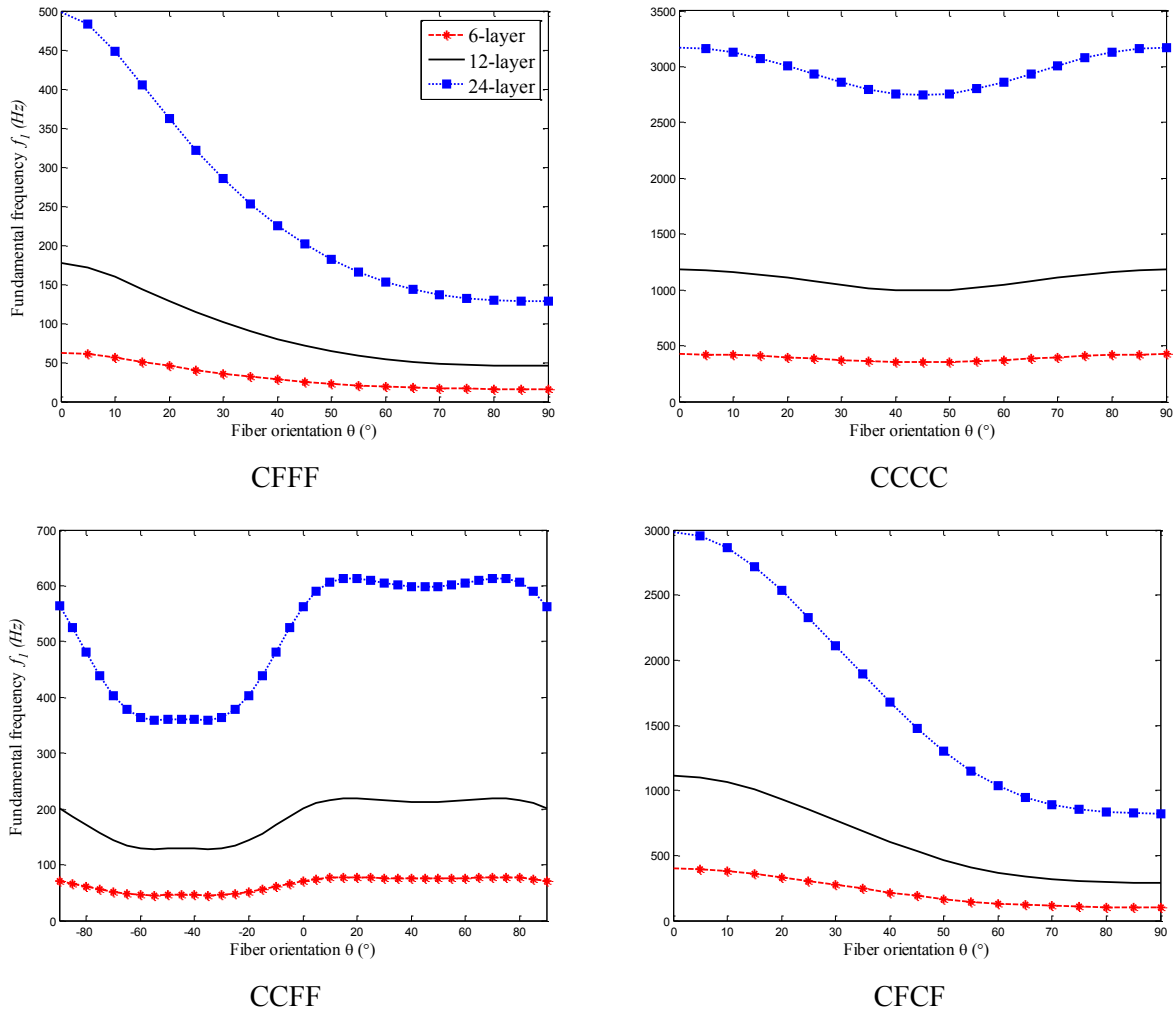


Figure 6.12. Variation of fundamental frequency with fiber orientation for unidirectional laminates with different thicknesses under mixed free and clamped boundary conditions.

Table 6.4. Maximum loss factors (%) and frequencies (Hz) of square plates with different thicknesses under combination of clamped and free boundary conditions.

Parameter	No. of Layers	CFFF	CCCC	CCFF		CFCF
				( $-90 \leq \theta \leq 0$ )	( $0 \leq \theta \leq 90$ )	
Max. Loss Factor	6	1.13	0.56	1.038	0.633	1.116
	12	1.13	0.58	1.041	0.635	1.118
	24	1.14	0.63	1.049	0.642	1.123
Corresponding Frequency	6	17.51	UD @ $\pm 45$	46.06	UD @ 45	UD @ $\pm 70$
	12	49.66	353.90	129.80	75.31	111.60
	24	140.30	994.30	363.80	212.60	315.40
Max. Frequency	6	62.66	425.01	74.76	84.88	399.86
	12	176.97	Cross-ply @ 0 & 90	224.70	Cross- & Angle-ply @ 45	1114.31
	24	497.74	3296.70	641.31	661.60	2981.83

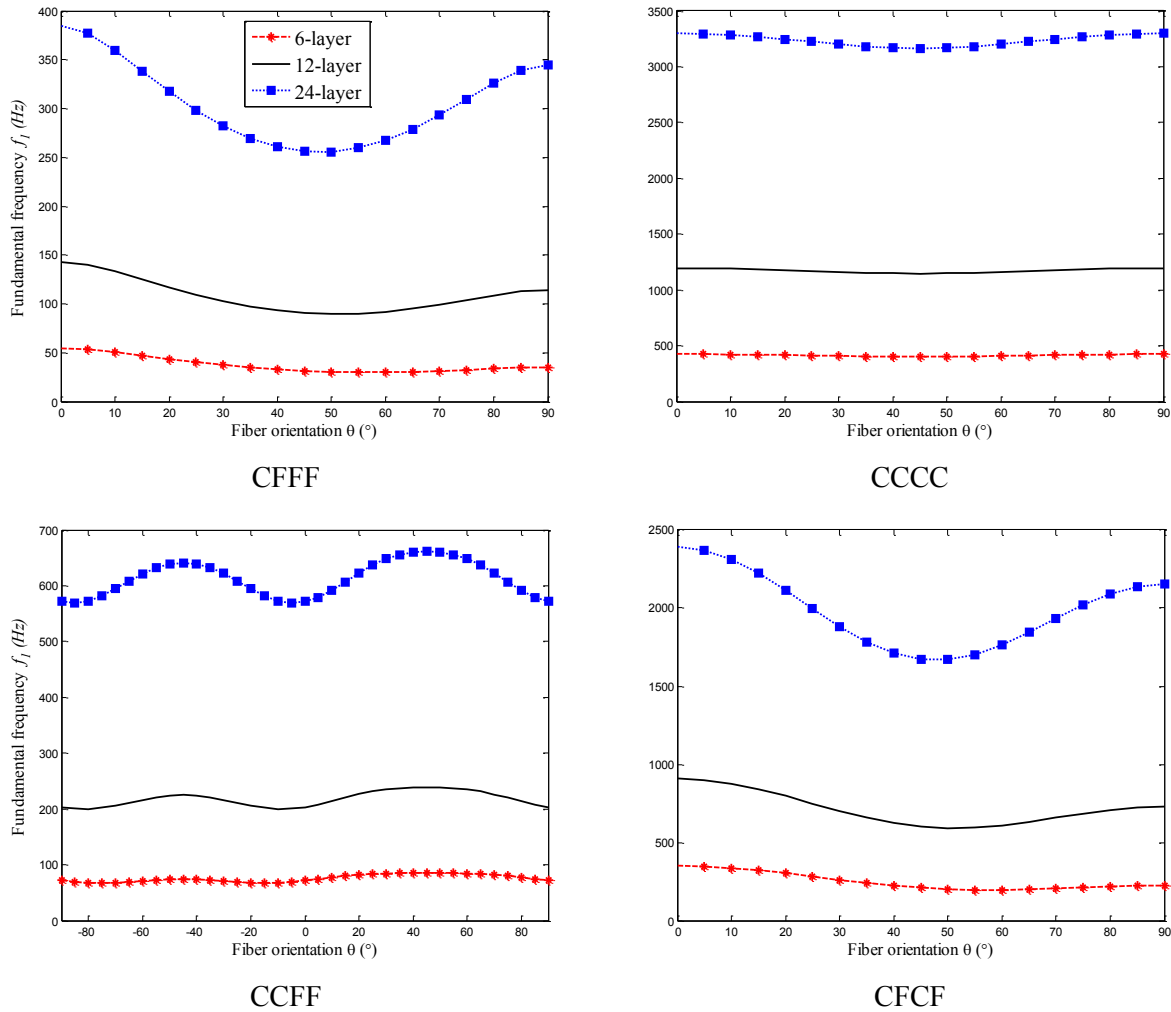


Figure 6.13. Variation of fundamental frequency with fiber orientation for cross-ply laminates with different thicknesses under mixed free and clamped boundary conditions.

As presented in Table 6.4, it is noticed that not much variation in the modal loss factor of the plates is generally reflected due to the thickness of laminates, while the natural frequency is directly proportional to that and is changed with a high order.

### 6.3.4 Effect of laminate aspect ratio

For a further investigation on maximum modal parameters (loss factor and frequency) and optimal fiber orientation, in this section, the effect of the aspect ratio  $\alpha$  (length-to-width) of cantilevered unidirectional laminated components is studied. The aforementioned boundary condition and lamination sequence have been chosen because they generally return the highest modal loss factor. The results for the fundamental frequency and modal loss factor are obtained in

a wide range of ply angle varied from  $0^\circ$  to  $90^\circ$ . The length ( $a$ ) of components is kept as a constant of 120 mm, while the widths ( $b$ ) of the laminates are set as 12, 24, 48, and 120 mm. It is assumed that a laminated component has a thickness of 12 plies. Therefore, the investigation is undertaken for the aspect ratios of 10 (beam), 5 and 2.5 (rectangular), as well as 1 (square).

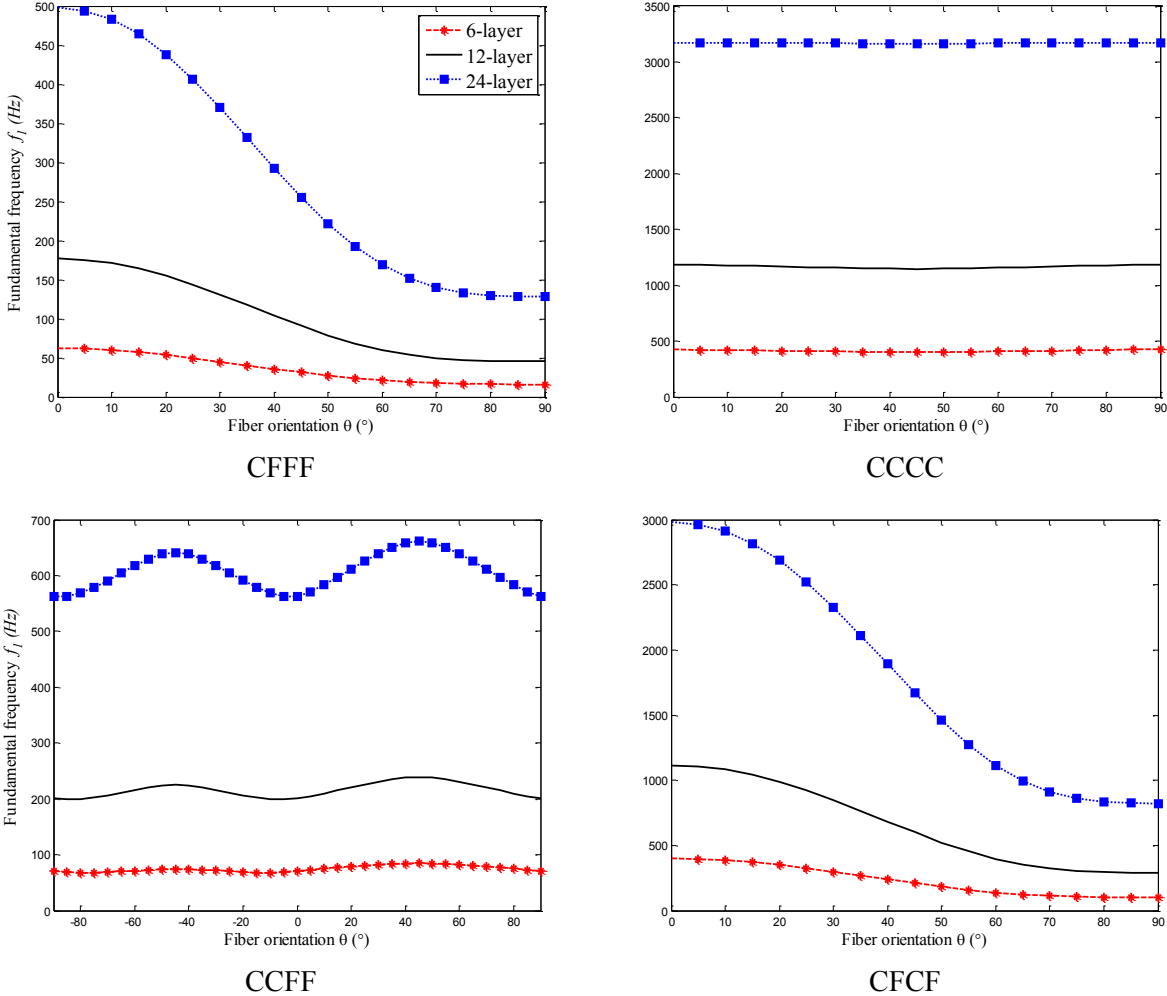


Figure 6.14. Variation of fundamental frequency with fiber orientation for angle-ply laminates with different thicknesses under mixed free and clamped boundary conditions.

The variation of loss factor and frequency with the fiber angle of the cantilevered laminates (beam and plates) are plotted in Figures 6.15a and 6.15b, respectively. From Figures 6.15a, the results clearly show that the loss factor is decreased with a decrease in the aspect ratio (or with an increase in width-to-thickness ratio at a constant length). This observation is in accordance with those reported in Ref. [134]. Moreover, one can find that the effect of the fiber orientation on the loss factor is different for various aspect ratios. For instance, the maximum loss factors are

obtained at the angles of 35°, 40°, 50°, and 65° for the aspect ratios of 10, 5, 2.5, and 1, respectively.

With respect to the frequency, it is noticed that the maximum resonance frequency occurs at the angle of 0° for all cantilevered components, irrespective of the aspect ratio. The maximum loss factor is, however, attainable at different optimal fiber orientations attributed to the associated aspect ratio. As a result, the effect of the aspect ratio on variation of the optimal fiber angle for the maximum loss factor is more dominant than that for the greatest frequency.

Table 6.5. Influence of the length on frequency and loss factor for beams with the aspect ratio of  $\alpha = 10$  at selective fiber angles.

Ply angle	Frequency (Hz)			Loss factor (%)		
	200 mm	120 mm	Difference (%)	200 mm	120 mm	Difference (%)
0°	63.74	144.60	130.0	0.251	0.252	0.4
30°	27.71	61.69	126.0	1.450	1.402	-3.3
45°	20.76	46.86	130.0	1.430	1.395	-2.45
60°	17.58	40.32	135.3	1.267	1.264	-0.24
90°	15.88	37.20	146.7	1.000	1.027	2.7

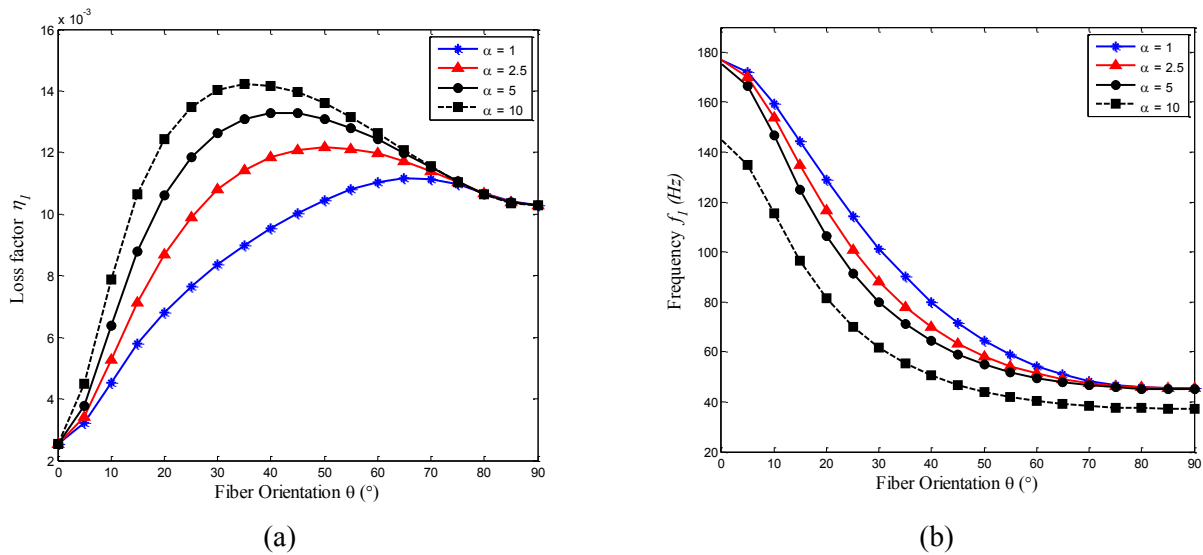


Figure 6.15. (a) Loss factors, (b) frequencies of cantilevered unidirectional laminates with various aspect ratios ( $\alpha$ ) versus the fiber orientation.

The value of frequency is also highly dependent on the length of the structure for a given aspect ratio. To demonstrate this, let us consider laminated beams with dimensions of 120 mm × 12 mm and 200 mm × 20 mm, both having aspect ratio of 10 and a thickness of 12 plies. Results for the fundamental frequency (see Figures 6.15b and 5.16) are provided in Table 6.5. As it can be

realized, for a given fiber angle, the frequency is increased in a range of about 125% to 145%, where the length is decreased from 200 mm to 120 mm. While, for the same aspect ratio, the magnitude of the modal loss factor is almost unchanged.

## 6.4 Summary and conclusions

The parametric study presented here was carried out to compare the effect of boundary conditions, fiber orientation, laminate thickness, and laminate sequence on modal frequency and damping characteristics of various laminated components. The geometrical effect, i.e. the ratio of length to width, was also investigated for clamped unidirectional components with the same length, while the width was changed.

The frequency and modal loss factor corresponding to the first mode, which is the most prominent mode in practical terms, were calculated by the developed finite element modeling. On the structural level, modal damping is analyzed with application of VED method integrated with the numerical (FE) modeling to predict damping capacity. The fundamental properties are treated separately or in a combined manner by defining different weights for the non-dimensional terms.

The numerical results showed that the damping loss factors and resonance frequencies are affected by changing the design variables taken into consideration. Observations indicated that the boundary condition and laminate configuration can significantly alter the frequency and damping properties of the structures due to noticeable coupling deformation modes. This is due to the fact that the loss factor or damping parameter increases when the mode shapes causes the highest energy dissipation or shearing (transverse and/or in-plane) in matrix due to the specific deformation mode associated with an individual boundary condition. The maximum loss factors observed by unidirectional and angle-ply layups are around two times higher than that perceived by a cross-ply layup under all boundary conditions, with the exception of CCCC constraint (see Figure 6.7). For a weak boundary condition, it was further observed that the loss factor of laminates can be well improved using optimal fiber angle.

Further, the optimal fiber angle for the maximum frequency inversely affects damping. The maximum loss factor over the given range of fiber orientation is achieved when the respective fundamental frequency is minimum. Therefore, an increase in damping occurs at the expense of a decrease in frequency. Observations also indicated that the maximum fundamental frequency and

the optimal loss factor are not obtained at the same fiber orientation and lamination sequence under the same boundary condition.

With respect to the geometry, it was shown that the loss factor is not considerably affected by the variation in thickness, compared with the frequency. Moreover, the aspect ratio plays a more decisive role on the variation of fiber angle influencing the loss factor for a given laminate sequence and boundary condition.

It can be concluded that the effect of damping of fiber-reinforced composites on the loss factor of the composite structures is essentially concerned with the fiber orientation, aspect ratio, and mode shapes, which results in a more effective dissipative capacity or maximized shear deformation.

## CHAPTER 7

### CONTRIBUTION, CONCLUSIONS, AND FUTURE WORK

#### 7.1 Major contributions

This study presents a comprehensive investigation on methods of characterization of viscoelastic properties of high-modulus fiber-reinforced polymer composite materials, systematic examination of dynamic mechanical analysis, and an optimal parametric study of laminated plates. The development in theoretical modeling and experimental methods for characterization and validation of viscoelastic properties were presented through extensive review of reported studies on fiber-reinforced composites. The review covered different static and dynamic characterization methodologies, theoretical damping formulations and modeling, and effective material and structural parameters in damping mechanism. Also, the effect of various micromechanical, macromechanical, operational, and structural parameters on the structural damping of fiber-reinforced composites addressed in earlier studies were thoroughly discussed.

The major contributions of the research work are summarized as follows:

1. An experimental characterization method, i.e. the dynamic mechanical analysis (DMA) was employed to identify three in-plane elastic and damping properties of a high-performance carbon fiber/epoxy prepreg system at room temperature. Furthermore, the complexities associated with the experimental characterization and disagreements between static and DMA experimental results from reported studies were addressed. The complex moduli and loss factors were characterized using unidirectional beams with different length-to-thickness ratios. Two distinct DMA clamps were also utilized to study the effect of clamp configurations on the accuracy of findings. To demonstrate validity of the elastic and damping properties from the DMA approach, an integrated experimental and numerical modal analysis was subsequently conducted on beam components with preferential fiber orientations. Considering this, a finite element model on the basis of DMA input data was developed to compare the measured and predicted structure responses, namely the natural frequencies and/or the modal damping factors.



2. Numerical models of beam and plate components based on the finite element method were developed for free vibration analysis under different boundary conditions. The effect of variation in the fiber angle, structural geometry, and lamination layups on the resulting vibration properties were investigated numerically, given laminates subjected to different boundary conditions. The vibration characteristics of the structures were explored in terms of the loss factor and frequency individually and their weighting combination. Finally, a number of parametric studies were performed to identify optimal fiber orientations so as to maximize the frequency and loss factor associated with the first mode shape for different lamination sequence, thickness, and boundary conditions.

## 7.2 Major conclusions

The major conclusions extracted from the present dissertation research are summarized below:

- Although direct and indirect characterization techniques either static or dynamic have been widely used to characterize material properties of composite systems, the dynamic mechanical analysis (DMA) ensured accurate characterization of dynamic properties of fiber-reinforced composites under relatively small vibration amplitudes.
- All the in-plane properties (longitudinal and transverse damping and Young's moduli) were identified with sufficient accuracy through DMA testing on beam specimens cut from a unidirectional laminate, given a proper selection of clamp configuration as well as sample aspect ratio.
- The substantial discrepancy was noticed between the storage modulus in the fiber direction and its counterpart obtained from a static test, where an incorrect aspect ratio and inappropriate DMA clamp was used.
- The remarkable improvement in accuracy of DMA findings is achieved by utilizing the proper DMA clamp arrangement, compared to the aspect ratio.
- For a high-performance or modulus fiber-reinforced composite, beam coupons with the aspect ratio of about 30 yielded the most accurate characteristics, using the three-point bending fixture.

- The in-plane shear modulus and loss factor were characterized with a quite accuracy, using beam coupons in flexure rather than employing cylindrical or rectangular specimens examined in torsion.
- Using measured flexural elastic properties from the DMA testing returned reliable and reasonable results in terms of modal frequency parameters obtained computationally, which were quite comparable with those achieved experimentally for cantilevered laminated beams and plates.
- The viscoelastic damping (VED) model reasonably provided accurate modal damping results for beam components fabricated out of slightly-damped composite materials and oscillating with small vibration amplitudes under cantilever boundary condition.
- Experimental and computational modal analyses showed that the fiber angle could significantly alter the stiffness and damping properties of the unidirectional beam structures, while the highest loss factor resulted at the expense of the natural frequency or the bending strength.
- Application of the material in a form of unidirectional beams experimentally demonstrated and that the maximal loss factor was achieved at a fiber angle of about  $35^\circ$  as opposed to the frequency, which reached the maximum at the expected fiber angle of  $0^\circ$ .
- The parametric problems aimed at maximizing the fundamental vibration properties in a mixed or separate fashion. The optimal solutions converged to fiber angles which resulted in relatively higher shear strains under the applied structural conditions and geometry.
- The careful consideration of the structural constraint, lamination sequence, and geometry was found to be important and effective for the optimal fiber orientations lending itself to the maximum loss factor and/or frequency.
- The structural damping performance was greatly affected by the mode of deformation, which stimulated the highest contribution of strain energies in a system due to bending-stretching-twisting coupling terms.
- Although, fully clamped laminates provided superior structural stiffness, CFFF and CFCF constraints generally yielded greater damping property, considering the unidirectional and angle-ply laminates in particular, and CCFF boundary condition functioned in between.

- Considering the antisymmetric boundary condition (CCFF), the maximum loss factor was achieved at two negative fiber orientation, while the loss factor was maximized at  $\pm\theta_{opt}$  in the case of other boundary conditions.
- The effect of laminate thickness on damping property was negligible for all boundary conditions, with the exception of CCCC constraint.
- The maximum loss factors were achieved at different optimal fiber orientations for cantilevered unidirectional components with different length-to-width ratios.

### 7.3 Recommendation for the future works

In this research work, viscoelastic properties of a high-performance prepreg composite material were systematically identified using the DMA approach. The fundamental vibration characteristics of laminated beam and plate structures were also investigated experimentally and numerically based on the input data obtained by the DMA method. Further, the objective vibration parameters were fully investigated by models formulated to study the effects of different factors, which provide important design perspectives for composite structures. The DMA method, however, needs to be further studied so as to study the effect of frequency and temperature on viscoelastic properties, based on which one can estimate structural properties under various operational conditions. In particular, further efforts in design optimization of complex structures are highly desirable. The work done in this thesis can be extended in the following directions:

- Examine higher deformation modes of laminated beam components so as to compare the correlations of experimental modal damping properties with predicted counterparts, which can be calculated based on the DMA results at various frequencies.
- Study on the thermal effect in DMA testing and investigate the compatibility between experimental modal damping and numerical ones, which are resulted on the basis of input data from the DMA approach at elevated temperatures.
- Investigate the effect of damping in the forced vibration analysis of laminated composite plates under different boundary conditions.

- Determine the optimal fiber angle and geometry parameters in composite laminates with more complexity such as stiffened panels to maximize vibration objectives in terms of combined frequency and damping, using optimization methods.
- Investigate the contributions and effects of coupling terms to strain energies in a mode of deformation for plates with different lamination sequences as subjected to different boundary conditions.
- Examine moduli  $G_{LT}$  and  $G_{L\hat{T}}$  together with the corresponding damping values through the DMA method, using a  $0^\circ$  beam subjected to torsional deformation, for the purpose of comparison with results obtained in this study. Likewise, determine complex modulus  $G_{T\hat{f}}^*$  by testing a  $90^\circ$  beam in torsion.
- Conduct further experimental verification and characterizations in vacuo and air in order to distinguish the damping from the material and the structure at higher vibration amplitudes.

## References

- [1] Treviso A, Van Genechten B, Mundo D, Tournour M. Damping in composite materials: Properties and models. *Compos Part B Eng* 2015; 78: 144-52.
- [2] Chandra R, Singh SP, Gupta K. Damping studies in fiber-reinforced composites – a review. *Compos Struct* 1999; 46 (1): 41-51.
- [3] Latheswary S, Valsarajan K, Rao Y. Free vibration analysis of laminated plates using higher-order shear deformation theory. *IE (I) Journal-AS* 2004; 85: 18-24.
- [4] Wang W, Kam T. Material characterization of laminated composite plates via static testing. *Compos Struct* 2000; 50 (4): 347-52.
- [5] Carlsson LA, Adams DF, Pipes RB. *Experimental characterization of advanced composite materials*. CRC press, 2014.
- [6] Tarnopol'skii Y, Kincis T. *Static Test Methods for Composites*. 1984.
- [7] Hodgkinson JM. *Mechanical testing of advanced fibre composites*. Elsevier, 2000.
- [8] Pendleton R, Tuttle M. *Manual on experimental methods for mechanical testing of composites*. Springer Science & Business Media, 2012.
- [9] Araujo A, Soares CM, de Freitas MM. Characterization of material parameters of composite plate specimens using optimization and experimental vibrational data. *Compos Part B Eng* 1996; 27 (2): 185-91.
- [10] Rikards R, Chate A, Gailis G. Identification of elastic properties of laminates based on experiment design. *Int J Solids Struct* 2001; 38 (30): 5097-115.
- [11] Hwang SF, Chang CS. Determination of elastic constants of materials by vibration testing. *Compos Struct* 2000; 49 (2): 183-90.
- [12] Berthelot JM, Angoulvant F. Measuring the bending stiffnesses of orthotropic and symmetric laminates from flexural vibrations. *J Compos Mater* 2002; 36 (4): 443-75.
- [13] Frederiksen PS. Parameter uncertainty and design of optimal experiments for the estimation of elastic constants. *Int J Solids Struct* 1998; 35 (12): 1241-60.
- [14] Rikards R, Chate A, Steinchen W, Kessler A, Bledzki A. Method for identification of elastic properties of laminates based on experiment design. *Compos Part B Eng* 1999; 30 (3): 279-89.
- [15] Bledzki A, Kessler A, Rikards R, Chate A. Determination of elastic constants of glass/epoxy unidirectional laminates by the vibration testing of plates. *Compos Sci Technol* 1999; 59 (13): 2015-24.
- [16] Ragauskas P, Belevičius R. Identification of material properties of composite materials. *Aviation* 2009; 13 (4): 109-15.
- [17] Chowdhury FH, Hosur MV, Jeelani S. Investigations on the thermal and flexural properties of plain weave carbon/epoxy-nanoclay composites by hand-layup technique. *J Mater Sci* 2007; 42 (8): 2690-700.

- [18] Chowdhury F, Hosur M, Jeelani S. Studies on the flexural and thermomechanical properties of woven carbon/nanoclay-epoxy laminates. *Mater Sci Eng A* 2006; 421 (1): 298-306.
- [19] Swaminathan G, Shivakumar KN, Russell LC. Anomalies, influencing factors, and guidelines for DMA testing of fiber reinforced composites. *Polym Compos* 2009; 30 (7): 962-69.
- [20] Swaminathan G, Shivakumar K. A re-examination of DMA testing of polymer matrix composites. *J Reinf Plast Compos* 2009; 28 (8): 979-94.
- [21] Gibson RF, Plunkett R. Dynamic mechanical behavior of fiber-reinforced composites: measurement and analysis. *J Compos Mater* 1976; 10 (4): 325-41.
- [22] Talbot J, Woodhouse J. The vibration damping of laminated plates. *Compos Part A Appl Sci Manuf* 1997; 28 (12): 1007-12.
- [23] Lazan BJ. Damping of materials and members in structural mechanics. vol. 42: Pergamon press Oxford, 1968.
- [24] Zhang SH, Chen HL. A study on the damping characteristics of laminated composites with integral viscoelastic layers. *Compos Struct* 2006; 74 (1): 63-69.
- [25] Chandra R, Singh S, Gupta K. A study of damping in fiber-reinforced composites. *J Sound Vib* 2003; 262 (3): 475-96.
- [26] Maheri M. The effect of layup and boundary conditions on the modal damping of FRP composite panels. *J Compos Mater* 2011; 45 (13): 1411-22.
- [27] Suarez S, Gibson R, Sun C, Chaturvedi S. The influence of fiber length and fiber orientation on damping and stiffness of polymer composite materials. *Exp Mech* 1986; 26 (2): 175-84.
- [28] Berthelot J-M, Sefrani Y. Damping analysis of unidirectional glass and Kevlar fibre composites. *Compos Sci Technol* 2004; 64 (9): 1261-78.
- [29] Ni R, Adams R. A rational method for obtaining the dynamic mechanical properties of laminae for predicting the stiffness and damping of laminated plates and beams. *Composites* 1984; 15 (3): 193-99.
- [30] Hwang SJ, Gibson RF. The use of strain energy-based finite element techniques in the analysis of various aspects of damping of composite materials and structures. *J Compos Mater* 1992; 26 (17): 2585-605.
- [31] Hu B-G, Dokainish M. Damped vibrations of laminated composite plates—modeling and finite element analysis. *Finite Elem Anal Des* 1993; 15 (2): 103-24.
- [32] Adams R, Maheri M. Dynamic flexural properties of anisotropic fibrous composite beams. *Compos Sci Technol* 1994; 50 (4): 497-514.
- [33] Sefrani Y, Berthelot J-M. Temperature effect on the damping properties of unidirectional glass fibre composites. *Compos Part B Eng* 2006; 37 (4): 346-55.
- [34] Maheri M, Adams R, Gaitonde J. The effect of temperature on the dynamic characteristics of heat-resistant thermoplastic composites. *Compos Sci Technol* 1996; 56 (12): 1425-34.

- [35] Torvik PJ, Runyon B. Modifications to the method of modal strain energy for improved estimates of loss factors for damped structures. *Shock Vib* 2007; 14 (5): 339-53.
- [36] Hashin Z. Complex moduli of viscoelastic composites—II. Fiber reinforced materials. *Int J Solids Struct* 1970; 6 (6): 797-807.
- [37] Sun CT, Wu JK, Gibson RF. Prediction of material damping of laminated polymer matrix composites. *J Mater Sci* 1987; 22 (3): 1006-12.
- [38] Crane RM, Gillespie JW. Analytical model for prediction of the damping loss factor of composite materials. *Polym Compos* 1992; 13 (3): 179-90.
- [39] Yim JH. A damping analysis of composite laminates using the closed form expression for the basic damping of Poisson's ratio. *Compos Struct* 1999; 46 (4): 405-11.
- [40] Melo JDD, Radford DW. Viscoelastic characterization of transversely isotropic composite laminae. *J Compos Mater* 2003; 37 (2): 129-45.
- [41] Rikards R, Chate A, Barkanov E. Finite element analysis of damping the vibrations of laminated composites. *Comput Struct* 1993; 47 (6): 1005-15.
- [42] Ungar EE, Kerwin Jr EM. Loss factors of viscoelastic systems in terms of energy concepts. *J Acoust Soc Am* 1962; 34 (7): 954-57.
- [43] Meunier M, Shenoï R. Dynamic analysis of composite sandwich plates with damping modelled using high-order shear deformation theory. *Compos Struct* 2001; 54 (2): 243-54.
- [44] Adams R, Maheri M. Damping in advanced polymer–matrix composites. *J Alloy Compd* 2003; 355 (1): 126-30.
- [45] Adams R, Bacon D. Effect of fibre orientation and laminate geometry on the dynamic properties of CFRP. *J Compos Mater* 1973; 7 (4): 402-28.
- [46] Berthelot J-M. Damping analysis of laminated beams and plates using the Ritz method. *Compos Struct* 2006; 74 (2): 186-201.
- [47] Korontzis DT, Vellios L, Kostopoulos V. On the viscoelastic response of composite laminates. *Mech Time-depend Mater* 2000; 4 (4): 381-405.
- [48] Zhao Y, Weng G. Effective elastic moduli of ribbon-reinforced composites. *J Appl Mech* 1990; 57 (1): 158-67.
- [49] Chandra R, Singh S, Gupta K. Micromechanical damping models for fiber-reinforced composites: a comparative study. *Compos Part A Appl Sci Manuf* 2002; 33 (6): 787-96.
- [50] Gibson R, Hwang S, Kwak K. The effects of the fiber/matrix interphase on composite damping properties. *Proceedings of the 36th International SAMPE Symposium*, 1991, pp. 592-606.
- [51] Dong S, Gauvin R. Application of dynamic mechanical analysis for the study of the interfacial region in carbon fiber/epoxy composite materials. *Polym Compos* 1993; 14 (5): 414-20.
- [52] Chua PS. Dynamic mechanical analysis studies of the interphase. *Polym Compos* 1987; 8 (5): 308-13.

- [53] Crane RM, Gillespie JW. Characterization of the vibration damping loss factor of glass and graphite fiber composites. *Compos Sci Technol* 1991; 40 (4): 355-75.
- [54] Hadi A, Ashton J. Measurement and theoretical modelling of the damping properties of a unidirectional glass/epoxy composite. *Compos Struct* 1996; 34 (4): 381-85.
- [55] Hwang S, Gibson R. Micromechanical modeling of damping in discontinuous fiber composites using a strain energy/finite element approach. *Journal of engineering materials and technology* 1987; 109 (1): 47-52.
- [56] Saravanos DA, Chamis CC. Unified micromechanics of damping for unidirectional and off-axis fiber composites. 1990;
- [57] Adams RD, Bacon D. The dynamic properties of unidirectional fibre reinforced composites in flexure and torsion. *J Compos Mater* 1973; 7 (1): 53-67.
- [58] Adams R, Bacon D. Measurement of the flexural damping capacity and dynamic Young's modulus of metals and reinforced plastics. *J Phys D Appl Phys* 1973; 6 (1): 27.
- [59] Clary R. Vibration characteristics of unidirectional filamentary composite material panels. *Composite Materials: Testing and Design (Second Conference)*, 1972, pp. 415-38.
- [60] Crane RM, Gillespie Jr JW. Damping loss factor determination of glass and graphite fiber composites. DTIC Document 1989.
- [61] Maheri M, Adams R. Finite-element prediction of modal response of damped layered composite panels. *Compos Sci Technol* 1995; 55 (1): 13-23.
- [62] Billups E, Cavalli M. 2D damping predictions of fiber composite plates: Layup effects. *Compos Sci Technol* 2008; 68 (3): 727-33.
- [63] Zinoviev PA, Ermakov YN. *Energy dissipation in composite materials*. CRC Press, 1994.
- [64] Kostopoulos V, Korontzis DT. A new method for the determination of viscoelastic properties of composite laminates: a mixed analytical–experimental approach. *Compos Sci Technol* 2003; 63 (10): 1441-52.
- [65] Berthelot J-M, Assarar M, Sefrani Y, El Mahi A. Damping analysis of composite materials and structures. *Compos Struct* 2008; 85 (3): 189-204.
- [66] Melo JDD, Radford DW. Viscoelastic properties of composite laminated beams by dynamic mechanical analysis. 17th International Congress of Mechanical Engineering Sao Paulo, Brazil, 2003.
- [67] Melo JDD, Radford DW. Time and temperature dependence of the viscoelastic properties of CFRP by dynamic mechanical analysis. *Compos Struct* 2005; 70 (2): 240-53.
- [68] Finegan IC, Tibbetts GG, Gibson RF. Modeling and characterization of damping in carbon nanofiber/polypropylene composites. *Compos Sci Technol* 2003; 63 (11): 1629-35.
- [69] Chandra R, Singh S, Gupta K. Experimental evaluation of damping of fiber-reinforced composites. *J Compos Technol Res* 2003; 25 (2): 96-107.



- [70] Dalenbring M. Experimental material damping estimation for planar isotropic laminate structures. *Int J Solids Struct* 2002; 39 (19): 5053-79.
- [71] Matter M, Gmür T, Cugnoni J, Schorderet A. Numerical-experimental identification of the elastic and damping properties in composite plates. *Compos Struct* 2009; 90 (2): 180-87.
- [72] Suarez S, Gibson R, Deobald L. Random and impulse techniques for measurement of damping in composite materials. *Exp Tech* 1984; 8 (10): 19-24.
- [73] Maheri M. Vibration damping in composite/honeycomb sandwich beams. University of Bristol, 1991.
- [74] Hwang S, Gibson R. Influence of bending-twisting and extension-bending coupling on damping of laminated composites. *J Mater Sci* 1993; 28 (1): 1-8.
- [75] Bicos AS, Springer GS. Vibrational characteristics of composite panels with cutouts. *AIAA J* 1989; 27 (8): 1116-22.
- [76] Hwang SJ, Gibson RF, Singh J. Decomposition of coupling effects on damping of laminated composites under flexural vibration. *Compos Sci Technol* 1992; 43 (2): 159-69.
- [77] Zabaras N, Pervez T. Viscous damping approximation of laminated anisotropic composite plates using the finite element method. *Comput Method Appl Mech Eng* 1990; 81 (3): 291-316.
- [78] Li J, Narita Y. Analysis and optimal design for the damping property of laminated viscoelastic plates under general edge conditions. *Compos Part B Eng* 2013; 45 (1): 972-80.
- [79] Song X. Vacuum assisted resin transfer molding (VARTM): model development and verification. 2003;
- [80] Sayre JR. Vacuum-Assisted Resin Transfer Molding (VARTM) Model Development, Verification, and Process Analysis. 2000;
- [81] Advani SG, Hsiao K-T. Manufacturing techniques for polymer matrix composites (PMCs). Elsevier, 2012.
- [82] Grunenfelder L, Nutt S. Void formation in composite prepregs—effect of dissolved moisture. *Compos Sci Technol* 2010; 70 (16): 2304-09.
- [83] Cender TA, Gangloff Jr JJ, Simacek P, Advani SG. Void reduction during out-of-autoclave thermoset prepreg composite processing. SAMPE international symposium, 2014.
- [84] Centea T, Hubert P. Out-of-autoclave prepreg consolidation under deficient pressure conditions. *J Compos Mater* 2014; 48 (16): 2033-45.
- [85] Grunenfelder L, Centea T, Hubert P, Nutt S. Effect of room-temperature out-time on tow impregnation in an out-of-autoclave prepreg. *Compos Part A Appl Sci Manuf* 2013; 45: 119-26.
- [86] Hou T, Jensen B. Evaluation of Double-Vacuum-Bag Process for Composite Fabrication. Proceedings of 49 th SAMPE International Symposium & Exhibition, Long Beach, CA, 2004.
- [87] Miller SG, Lort III RD, Zimmerman TJ, Sutler J, Pelham LI, McCorkle LS, et al. Face-sheet Quality Analysis and Thermo-Physical Property Characterization of OoA and Autoclave Panels. *SAMPE J* 2012; 48 (5): 56-61.

- [88] ISO BSEN 6721–1. Plastics-Determination of dynamic mechanical properties- Part 1: General principles. ISO; 2011.
- [89] Kazakevičiūtė-Makovska R, Mogharebi S, Steeb H, Eggeler G, Neuking K. A Critical Assessment of Experimental Methods for Determining the Dynamic Mechanical Characteristics of Shape Memory Polymers. *Adv Eng Mater* 2013; 15 (8): 732-39.
- [90] Menard KP. Dynamic mechanical analysis: a practical introduction. CRC press, 2008.
- [91] Ehrenstein GW, Riedel G, Trawiel P. Thermal analysis of plastics: theory and practice. Carl Hanser Verlag GmbH Co KG, 2012.
- [92] Zhao J, Barron AR. Dynamic Mechanical Analysis. ed.
- [93] Goertzen W, Kessler M. Dynamic mechanical analysis of carbon/epoxy composites for structural pipeline repair. *Compos Part B Eng* 2007; 38 (1): 1-9.
- [94] Costa ML, Botelho EC, Paiva JMFd, Rezende MC. Characterization of cure of carbon/epoxy prepreg used in aerospace field. *J Mater Res* 2005; 8: 317-22.
- [95] Pirvu A, Gardner DJ, Lopez-Anido R. Carbon fiber-vinyl ester composite reinforcement of wood using the VARTM/SCRIMP fabrication process. *Compos Part A Appl Sci Manuf* 2004; 35 (11): 1257-65.
- [96] Abedi M, Hojjati M, Sedaghati R. Evaluation of in-plane elastic properties of out-of-autoclave carbon/epoxy composite using DMA. The Composites and Advanced Materials Conference, Dallas, TX, 2015.
- [97] Noor AK, Burton WS. Assessment of shear deformation theories for multilayered composite plates. *Appl Mech Rev* 1989; 42 (1): 1-13.
- [98] Reddy JN. Mechanics of laminated composite plates and shells: theory and analysis. CRC press, 2004.
- [99] Vidal P, Gallimard L, Polit O. Modeling of composite plates based on Reissner's Mixed Variational Theorem with variables separation. *Compos Part B Eng* 2016; 86: 229-42.
- [100] Robbins D, Reddy J. Modelling of thick composites using a layerwise laminate theory. *Int J Numer Method Eng* 1993; 36 (4): 655-77.
- [101] Carrera E. Theories and finite elements for multilayered, anisotropic, composite plates and shells. *Archives of Computational Methods in Engineering* 2002; 9 (2): 87-140.
- [102] Carrera E. On the use of the Murakami's zig-zag function in the modeling of layered plates and shells. *Comput Struct* 2004; 82 (7): 541-54.
- [103] Reissner E. On a certain mixed variational theorem and a proposed application. *Int J Numer Method Eng* 1984; 20 (7): 1366-68.
- [104] Reddy JN. A simple higher-order theory for laminated composite plates. *J Appl Mech* 1984; 51 (4): 745-52.
- [105] Stein M. Nonlinear theory for plates and shells including the effects of transverse shearing. *AIAA J* 1986; 24 (9): 1537-44.

- [106] Soldatos K. A transverse shear deformation theory for homogeneous monoclinic plates. *Acta Mechanica* 1992; 94 (3-4): 195-220.
- [107] Karama M, Afaq K, Mistou S. A new theory for laminated composite plates. *Proceedings of the Institution of Mechanical Engineers, Part L: Journal of Materials Design and Applications* 2009; 223 (2): 53-62.
- [108] Yang PC, Norris CH, Stavsky Y. Elastic wave propagation in heterogeneous plates. *Int J Solids Struct* 1966; 2 (4): 665-84.
- [109] Carrera E, Brischetto S. Analysis of thickness locking in classical, refined and mixed multilayered plate theories. *Compos Struct* 2008; 82 (4): 549-62.
- [110] Carrera E, Brischetto S. A survey with numerical assessment of classical and refined theories for the analysis of sandwich plates. *Appl Mech Rev* 2009; 62 (1): 010803.
- [111] Aydogdu M. Comparison of various shear deformation theories for bending, buckling, and vibration of rectangular symmetric cross-ply plate with simply supported edges. *J Compos Mater* 2006; 40 (23): 2143-55.
- [112] Idlbi A, Karama M, Touratier M. Comparison of various laminated plate theories. *Compos Struct* 1997; 37 (2): 173-84.
- [113] Sayyad AS, Ghugal YM. On the free vibration analysis of laminated composite and sandwich plates: A review of recent literature with some numerical results. *Compos Struct* 2015; 129: 177-201.
- [114] Zhang Y, Yang C. Recent developments in finite element analysis for laminated composite plates. *Compos Struct* 2009; 88 (1): 147-57.
- [115] Hoa SV. *Computer-aided design of polymer-matrix composite structures*. Marcel Dekker, Inc., 1995.
- [116] Petyt M. *Introduction to finite element vibration analysis*. Cambridge University Press, 1990.
- [117] Ferreira AJ. *MATLAB codes for finite element analysis: solids and structures*. vol. 157: Springer Science & Business Media, 2008.
- [118] Narita Y, Leissa A. Frequencies and mode shapes of cantilevered laminated composite plates. *J Sound Vib* 1992; 154 (1): 161-72.
- [119] Crawley EF. The natural modes of graphite/epoxy cantilever plates and shells. *J Compos Mater* 1979; 13 (3): 195-205.
- [120] Khdeir A, Reddy J. Free vibrations of laminated composite plates using second-order shear deformation theory. *Comput Struct* 1999; 71 (6): 617-26.
- [121] Khdeir A. Free vibration of antisymmetric angle-ply laminated plates including various boundary conditions. *J Sound Vib* 1988; 122 (2): 377-88.
- [122] Bert C, Chen T. Effect of shear deformation on vibration of antisymmetric angle-ply laminated rectangular plates. *Int J Solids Struct* 1978; 14 (6): 465-73.

- [123] Reddy J. Free vibration of antisymmetric, angle-ply laminated plates including transverse shear deformation by the finite element method. *J Sound Vib* 1979; 66 (4): 565-76.
- [124] Khdeir A. Comparison between shear deformable and Kirchhoff theories for bending, buckling and vibration of antisymmetric angle-ply laminated plates. *Compos Struct* 1989; 13 (3): 159-72.
- [125] Lin D, Ni R, Adams R. Prediction and measurement of the vibrational damping parameters of carbon and glass fibre-reinforced plastics plates. *J Compos Mater* 1984; 18 (2): 132-52.
- [126] Alam N, Asnani N. Vibration and damping analysis of fibre reinforced composite material plates. *J Compos Mater* 1986; 20 (1): 2-18.
- [127] Baker WE, Woolam WE, Young D. Air and internal damping of thin cantilever beams. *Int J Mech Sci* 1967; 9 (11): 743-66.
- [128] Rouhi M, Ghayoor H, Hoa SV, Hojjati M. Effect of structural parameters on design of variable-stiffness composite cylinders made by fiber steering. *Compos Struct* 2014; 118: 472-81.
- [129] Saravanos DA, Chamis CC. Multiobjective shape and material optimization of composite structures including damping. *AIAA J* 1992; 30 (3): 805-13.
- [130] Saravanos D, Chamis C. An integrated methodology for optimizing the passive damping of composite structures. *Polym Compos* 1990; 11 (6): 328-36.
- [131] White R, Abdin E. Dynamic properties of aligned short carbon fibre-reinforced plastics in flexure and torsion. *Composites* 1985; 16 (4): 293-306.
- [132] Nelson D, Hancock J. Interfacial slip and damping in fibre reinforced composites. *J Mater Sci* 1978; 13 (11): 2429-40.
- [133] Li J, Narita Y. The effect of aspect ratios and edge conditions on the optimal damping design of thin soft core sandwich plates and beams. *Journal of Vibration and Control* 2012: 1077546312463756.
- [134] Hwang SJ, Gibson RF. The effects of three-dimensional states of stress on damping of laminated composites. *Compos Sci Technol* 1991; 41 (4): 379-93.